USING 2D AND 3D BASIN MODELLING AND SEISMIC SEEPAGE INDICATORS TO INVESTIGATE CONTROLS ON HYDROCARBON MIGRATION AND ACCUMULATION IN THE VULCAN SUB-BASIN, TIMOR SEA, NORTH-WESTERN AUSTRALIA

By

Tetsuya Fujii

Bachelor of Geology, Shinshu University, Japan
Master of Geophysics, the University of Tokyo, Japan

This thesis is submitted in fulfillment of the requirements for the degree of

Master of Science

at

Australian School of Petroleum (ASP)
The University of Adelaide

September 2006

STATEMENT OF AUTHENTICITY AND AVAILABILITY

This work contains no material which has been accepted for the awards of any other degree or diploma in any university or other tertiary institution and, to the best of my knowledge and belief, contains no material previously published or written by another person, except where due reference has been made in the text.

I give consent to this copy of my thesis, when deposited in the University Library, being available for loan and photocopying.

Tetsuya Fujii

ABSTRACT

2D and 3D basin models have been constructed of the southern and central parts of the Vulcan Sub-basin, which is located in the Timor Sea, north-western Australia. This work was carried out in order to better elucidate the petroleum migration and accumulation histories and exploration potential of the region. The study area extended from the southern limit of the Swan Graben in the south-west to the northern part of the Cartier Trough in the north-east. The results from the basin modelling have been compared with the seafloor bathymetry and physiography, the spatial distributions of hydrocarbon related diagenetic zones (HRDZs) in the region, as well as the distribution of other leakage and seepage indicators. A new method for identifying potential HRDZs using seismic data has also been developed.

The 2D/3D modeling results from the Swan Graben indicate that horizontal and downward oil expulsion from the source rocks of the Late Jurassic Lower Vulcan Formation into the upper Plover Formation sandstones was active from the Early Cretaceous to the present day. Oil migration from the Lower Vulcan Formation into the Late Cretaceous Puffin Formation sands in the Puffin Field was simulated via lateral migration along the bottom of an Upper Vulcan Formation seal and by vertical migration above the seal edge. Modelling also indicates that Late Jurassic sequences over the Montara Terrace are thermally immature and did not contribute to the hydrocarbon accumulations in the region. On the other hand, 3D modelling results indicate that the Middle Jurassic Plover Formation in the Montara Terrace became thermally mature after the Pliocene and hence it could have contributed to both the specific hydrocarbon accumulations and the overall hydrocarbon inventory in the area.

In the southern Cartier Trough, the Lower Vulcan Formation is typically at a lower thermal maturity than that seen in the Swan Graben, due to a combination of a relatively recent (Pliocene) increased burial and a thinner Lower Vulcan Formation. Here, horizontal and downward oil/gas expulsion from the Lower Vulcan Formation into the Plover Formation sandstone was active from the Late Tertiary to the present day, which is significantly later than the timing of the expulsion in the Swan Graben.

In the central Cartier Trough, the areal extent of both generation and expulsion increased as a result of rapid subsidence and deposition from about 5.7 Ma to the present day. This Pliocene loading has resulted in the rapid maturation of the Early to Middle and Late Jurassic source system and expulsion of oil very recently.

Oil migration from the Lower Vulcan Formation into the Jabiru structure, via the Plover Formation carrier bed, was simulated in both the 2D and the 3D modelling. In particular, the 3D modelling simulated oil migration into the Jabiru structure, both from the southern Cartier Trough (after the Miocene) and also from the northern Swan Graben (in the Early Cretaceous). Early gas migration, and the attendant formation of a gas cap, was also simulated. Importantly, this result provides a potential alternative interpretation for the formation of at least some of the residual zones in the Timor Sea, as well as in other areas.

Traditionally, most of the residual zones within the Timor Sea have been attributed to fault seal reactivation and failure. However, the simulated early gas cap in the Jabiru structure has formed as a result of gas exsolution as the migrating hydrocarbons entered the Jabiru trap (and its shallow flanks), which was then only located a few hundred metres below the surface. The rapidly decreasing pressure allowed the gas to form a separate phase, with the result that in the Early Cretaceous, in the 3D model, the Jabiru trap was composed of a relatively large gas cap with a thinner ("black oil") oil leg. Progressive burial through the Tertiary, and the attendant increase in pressure, resulted in the gas going back into solution. The associated decrease in the bulk volume of the hydrocarbon accumulation produced a "residual" oil zone at the base of the column, purely through a change in phase, rather than through loss of hydrocarbons from fault seal failure, for example.

The processes outlined in this scenario would be essentially indistinguishable from those produced by fault seal failure when assessing traps using fluid history tools such as GOI. Such a process could be critically important in the case of shallow, low-relief traps, where only the exsolved gas could be trapped, with the "black oil" component displaced below the spill of the trap. Small, sub-commercial gas fields would thus be located around the periphery of the source depocentres - though these would be the result of an early, rather than late, gas charge. Small black oil accumulations could be developed inboard from such gas fields.

A new method to extract HRDZs from 3D seismic data has predicted the location of new HRDZs in the northern Vulcan Sub-basin. Further investigation is needed to confirm/refine the method but it has the potential to significantly aid HRDZ mapping (and seal assessment and hydrocarbon migration studies). A workflow for future studies is proposed which includes inputs from basin modelling, leakage and seepage mapping, and fault seal and fault reactivation studies. Implementation of this workflow should ultimately allow a more reliable estimation of GOR prior to drilling.

ACKNOWLEDGEMENTS

First of all, I sincerely thank Dr. Geoffrey W. O'Brien and Dr. Peter Tingate at the Australian School of Petroleum for their strong support for my study, including assistance with planning of the study and reading drafts of the thesis.

I particularly thank Dr. John Kennard of Geoscience Australia for providing his study results used for this study as input data, and for his numerous suggestions and constructive comments which improved this work. I also thank Dr. Alexander Kaiko of Curtin University of Technology for his valuable comments, particularly in regard to the heat flow calibration. I am grateful to the technical support staff in IES for contributing numerous technical comments and advice on the operation of PetroMod^{TM}. I would also like to thank Japan Oil, Gas and Metals National Corporation (former Japan National Oil Corporation), which funded this study, and the Australian School of Petroleum for general assistance.

Aspects of this work were supported by the Australian Petroleum Co-operative Research Centre (APCRC) and the APCRC Seals Consortium. I especially thank Geoscience Australia and PGS for access to some of the data used in this study.

TABLE OF CONTENTS

LIST OF FIGURES

LIST OF TABLES

APPENDICES

CHAPTER ONE

INTRODUCTION

The Vulcan Sub-basin is located in the Timor Sea and has been one of the Australia's most actively explored regions (Fig.1-1). There have been a number of commercial and non-commercial oil and gas discoveries within the sub-basin, including the Skua, Puffin, Jabiru, Challis, Oliver, Montara, Talbot, Tahbilk and Tenacious fields. This success has spurred the acquisition of many thousands of kilometers of 2D and 3D seismic data and the drilling of numerous exploration wells. Numerous studies relating to the processes of petroleum generation, migration, accumulation, leakage and seepage have been carried out to better understand the key characteristics of the petroleum systems in the region (Lisk and Eadington, 1994; Beardsmore and O'Sullivan, 1995; O'Brien et al, 1996b, 1999a; Baxter et al, 1997, 1999; Lowry, 1998; Lisk et al, 1998, 1999; Kennard et al, 1999; Chen et al, 2001, 2002). In spite of this effort, there is still significant debate about the location of the mature source kitchens, the timing of petroleum expulsion from the source rocks and the dominant factors controlling the distribution of oil and gas, and particularly, the gas-to-oil ratio, in the region.

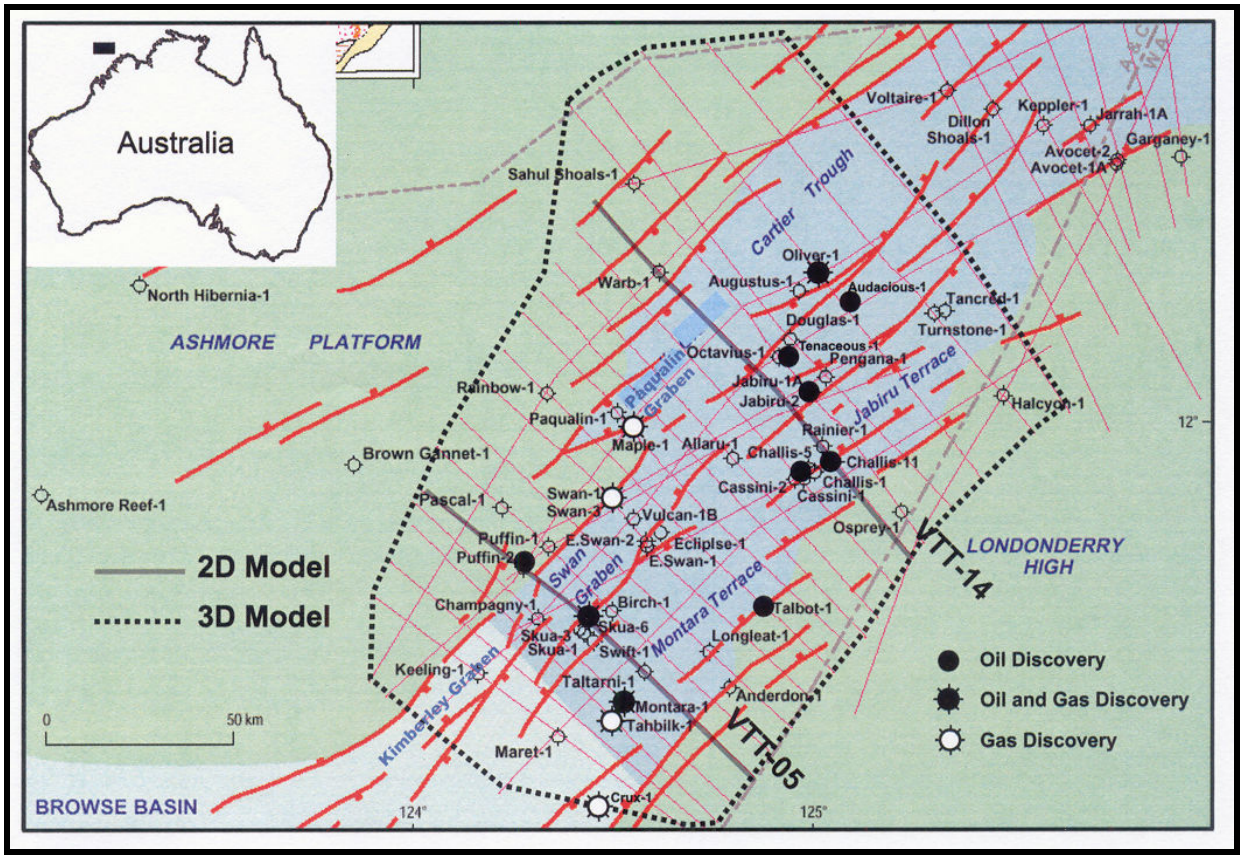

Figure 1-1. Vulcan Sub-basin map showing basin elements, oil and gas discoveries and distribution of modelled 2D sections and 3D region. Modified after Kennard and Deighton (2000)

There are different interpretations on the timing of petroleum generation and migration in the Swan Graben (Fig. 1-1), which is thought to be one of the main kitchen areas of the region (Patillo and Nichols, 1990). Lisk et al (1998, 1999) and Kennard et al (1999) proposed that the principal oil migration in the graben, and attendant accumulation along the migration fairways took place in the Tertiary, whereas Baxter et al (1997) postulated that charging was early, perhaps during the Cretaceous. If the latter interpretation is correct, then the main oil charge had already occurred by the Late Cretaceous and the relative timing of oil generation and formation trap (structural development and seal deposition) were very close together, perhaps too close together to allow accumulation in some plays. Under an “early charge” scenario, much of the oil expelled from the source rock could have been lost, rather than trapped. In contrast, if the timing of expulsion were late, then the situation is much more favourable for preservation of the hydrocarbon charge. Determining which of these models is correct, or at least the more likely, is clearly important if this area is to be successfully explored in the future.

Another issue facing exploration is that the principal kitchen area which has sourced the large oil and gas accumulations at the Jabiru, Challis and Oliver Fields has not yet been identified conclusively. For example, there are two different interpretations of the location of the effective kitchen area in the Cartier Trough. Kennard et al (1999) proposed that the main oil expulsion event which contributed to the accumulation in the Oliver structure took place in the southern Cartier Trough, whereas Chen et al (2002) interpreted it to have been located in the central Cartier Trough.

Another important issue within the region relates to the relative timing of hydrocarbon charge and structural reactivation events which led to trap breaching in the area. In the Late Miocene to Early Pliocene, the progressive convergence and ultimate collision of the Australian and Eurasian plates resulted in structural reactivation of many Mesozoic extensional faults (Woods, 1992; O’Brien and Woods, 1995; O’Brien et al, 1996a, 1999a, 2002a). This fault reactivation resulted in the breaching of many of the charged traps in the area, probably beginning at about 5.7 Ma (O’Brien et al, 2004). As such, if generation and expulsion in the region were truly early, then there would seem to be little opportunity for recharging of these breached traps. In contrast, if expulsion were very late, such as in the Pliocene for example, then the opportunity for recharge exists.

Finally, there are few studies focused on the controlling factors of petroleum accumulation with respect to GOR. O’Brien et al. (1996, 1998) described the

importance of trap integrity in relation to the distribution of oil and gas in the Vulcan Sub-basin, but did not focus on the influence of source facies and maturity. Quite recently, Edwards et al. (2004) proposed that the source facies influenced the oil and gas distribution, though they did not consider the influence of trap integrity on hydrocarbon distribution. Integrated studies that focus on the determining the relative balance between, and the individual importance of, of each of these factors are clearly necessary.

Several basin modelling studies have been carried out on the Vulcan Sub-basin. These include 2D structural restoration modelling to clarify the hydrocarbon generation history (Baxter et al 1997), multi 1D maturation and expulsion modelling (of 62 wells) to clarify generation and expulsion history (Kennard et al 1999) and 3D structural restoration modelling to clarify hydrocarbon migration pathways (Chen et al 2002). To date, however, no 2D/3D hydrocarbon generation, migration and accumulation modelling, using fluid flow simulation software, has been published for this region.

This study aims to address some of the uncertainties associated with processes of petroleum migration, accumulation and preservation-destruction within the Vulcan Sub-basin and thereby provide an improved framework within which to better understand the exploration potential of this area. The modelling results presented here represent the results of relatively simple models, the aim of which is to understand the main elements of generation, migration and accumulation in the study area. 2D and 3D basin simulations have been carried out using PetroMod^{TM} 2D/3D.

The study investigated the similarities and differences in the results obtained from 2D and 3D basin modelling. Moreover, it compared and contrasted the generation and migration histories obtained from the modelling with two contrasting source rock scenarios, one using only the proven Late Jurassic Lower Vulcan Formation and the other using both the Lower Vulcan Formation and the Early to Middle Jurassic Plover Formation.

Finally, these modelling results have been compared, in a preliminary manner, with hydrocarbon leakage indicators derived principally from the seismic data. These data include seafloor bathymetry, seismic amplitude at and immediately below sea floor, fault distribution and the distribution of Hydrocarbon-Related Diagenetic Zones or HRDZs (O'Brien and Woods, 1995).

CHAPTER TWO

GEOLOGY OF THE VULCAN SUB-BASIN

2.1 STRATIGRAPHY AND STRUCTURAL GEOLOGY

The Vulcan Sub-basin is a Middle to Late Jurassic rift basin located in Australia's Timor Sea.

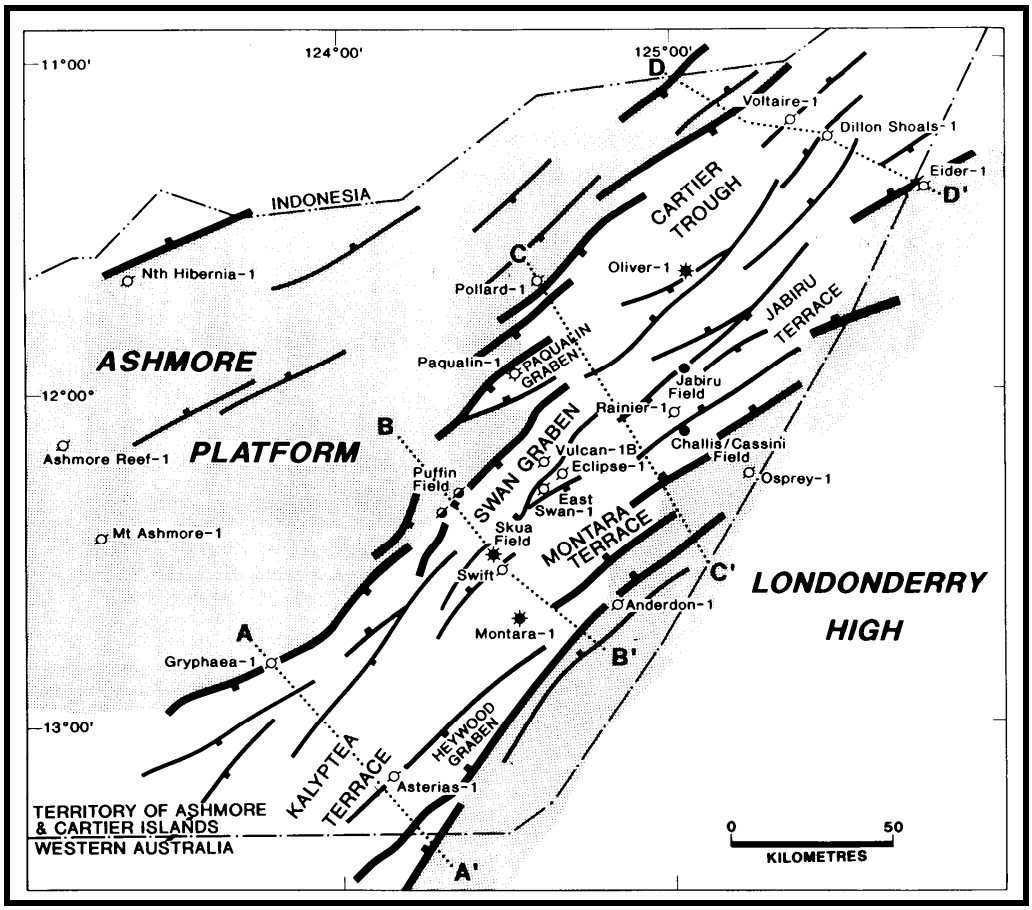

Figure 2-1. Structural elements of the Vulcan Sub-basin (from Pattillo and Nicholls, 1990)

North-east and east-northeast trending horst and platform areas, such as the Montara Terrace and the Jabiru Terrace, are located to the south-east of the Swan Graben and the Cartier Trough, respectively. The Londonderry High and the Ashmore Platform, which are principally comprised of Triassic sediments sealed by Cretaceous shales, are located to the south-east and the north-west of the sub-basin (Fig. 1-1, 2-1).

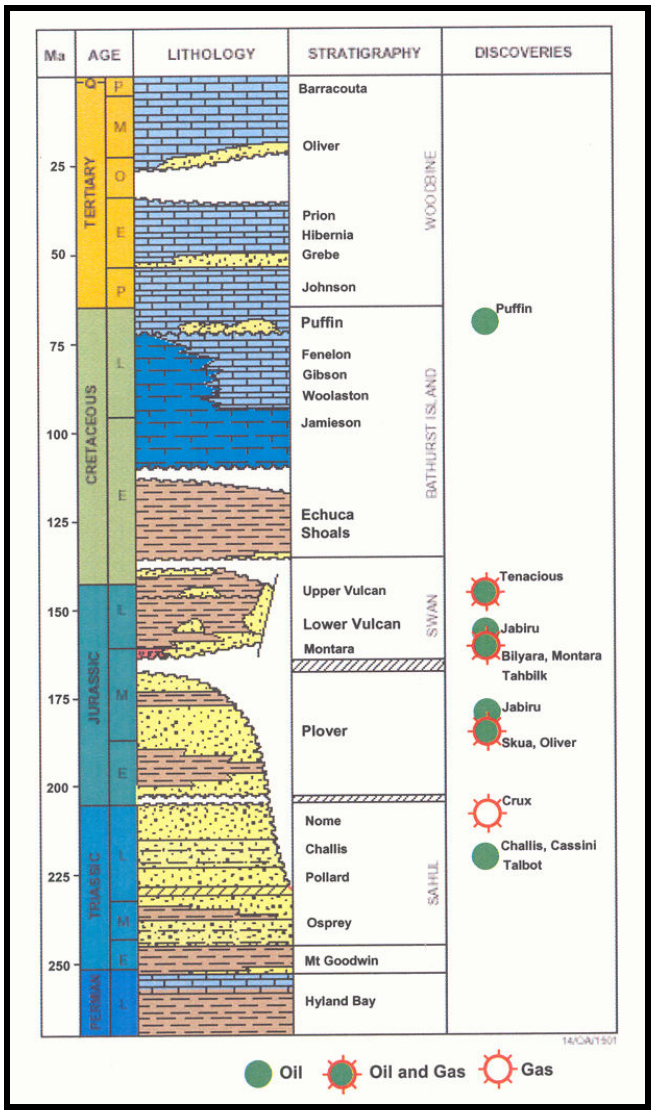

Figure 2-2. Stratigraphy of the Vulcan Sub-basin (Kennard and Deighton, 2000)

2.2 PETROLEUM GEOLOGY

In this region, there are more than 20 oil and gas discoveries including the Skua, Puffin, Jabiru, Challis, Oliver, Montara, Talbot, Tahbilk and Tenacious fields (Fig. 1-1, Fig. 2-1, Table 2-1).

Almost all of the hydrocarbon fields discovered in the region consist of Triassic and/or Jurassic sandstone reservoirs that are sealed by Late Jurassic to Early Cretaceous marine shales (Fig. 2-2). The Vulcan Sub-basin has a northeast-southwest structural grain (Fig. 1-1, 2-1), with several major Late Jurassic source rock depocentres such as the Swan and the Paqualin Grabens (Patillo and Nichols, 1990). These grabens are located in the southern and central parts of the sub-basin respectively (Fig. 1-1). The Cartier Trough is a major Jurassic and Neogene depocentre and is located in the

central and northern parts of the sub-basin (Fig. 1-1).

The Lower Vulcan Formation, an organic-rich, Late Jurassic marine succession, is thought to be the principal working source rock for the majority of petroleum accumulations in the area (Fig. 2-2; Kennard et al, 1999; Edwards et al, 2004). Another, but subsidiary, source rock is thought to be provided by coal-rich layers within the Plover Formation, which consists of Early to Middle Jurassic marine to terrestrial sediments (Edwards et al, 2004). The Lower Vulcan Formation is thought to be thick within the Swan Graben, the Paqualin Graben and the Cartier Trough, although it is thin on the Montara and the Jabiru terraces (AGSO, 1996).

The main petroleum reservoir in the Vulcan Sub-basin is the Plover Formation, which consists principally of Early to Middle Jurassic fluvial to deltaic sandstones. Interpreted deep marine fan sediments in the Late Jurassic (Tithonian-Berriasian) Vulcan Formation and the Late Cretaceous Puffin Formation can locally also be important reservoir facies. The Puffin Formation sandstones are thought to be distributed in the southern parts of the Vulcan Sub-basin and in the northern Browse Basin (O'Brien et al, 1999; O'Brien et al, 2004).

The principal sealing units are the post-rift, Early Cretaceous marine sediments of the Echuca Shoals Formation and Jamieson Formation, though the Upper Vulcan Formation can occasionally act as a seal (Kivior, 2002).

Most oil and gas accumulations discovered in the region are trapped within faulted traps and horsts, which formed during Jurassic rifting (Woods, 1992). To date, significant petroleum accumulations have not been discovered on the flanking Permo-Triassic platform areas, perhaps because of an absence of charge, or because the top seal facies are poorer.

In the Late Miocene to Early Pliocene, the progressive convergence and the collision of the Australian and Eurasian plates resulted in structural reactivation and breaching of many of the petroleum accumulations in this region (Woods, 1992; O'Brien and Woods, 1995; O'Brien et al, 1996a; O'Brien et al, 1999a, 2002, 2004; Shuster et al, 1998). In this region, as a result of this tectonism, the principal exploration risk is thought to relate to fault seal integrity,

Table 2-1. Oil and gas fields in the Vulcan Sub-basin (Data source: Database from IHS Energy ProbE ™, 2002).

Field Name	Discovery Date	Field Type	Latitude	Longitude	Reservoir Unit Name	Reservoir Top Depth	Fluid System	Max Oil Density	Max GOR	Oil Type	Gas Type
			(deg)	(deg)		(m)		(API)	(cuft/bbl)		
Audacious	Feb-01	Oil	-11.72	125.11	Plover Fm.	1981		55		Unspecified	
Bluff	Jul-98	Oil	-10.83	126.20	Montara Beds	3292	Single phase oil reservoir	40		Unspecified	
Buffalo	Oct-96	Oil and gas	-10.67	126.10	Elang Fm.	3307	Single phase oil reservoir	53	120	Unspecified	
Cassini	Jul-88	Oil and gas	-12.15	124.97	Challis Fm.	1404	Two phase reservoir	42	213	Paraffinic	Wet
Challis	Oct-84	Oil and gas	-12.12	125.00	Challis Fm.	1320	Single phase oil reservoir	40	350	Paraffinic	Wet
Crux	May-00	Gas and cond.	-12.94	124.45	Nome Fm.	3853		52		cond.	
Halcyon	Jul-91	Gas	-11.94	125.47	Flamingo Group	1283	Single phase gas reservoir				Dry
Jabiru	Sep-83	Oil and gas	-11.93	125.00	Plover and Lower Vulcan Fm.	1560	Single phase oil reservoir	43	449	Paraffinic	Wet
Keeling	Jan-90	Gas	-12.62	124.17		3014	Single phase gas reservoir				Dry
Maple	Feb-90	Gas and cond.	-12.02	124.54	Challis Fm.	3666	Dew-point reservoir	50		cond.	Wet
Montara	May-88	Oil and gas	-12.69	124.53	Lower Vulcan Fm.	2667	Single phase oil reservoir	36	3612	Unspecified	Wet
Oliver	Feb-88	Oil, gas and cond.	-11.64	125.01	Plover Fm.	2930	Two phase reservoir	50		cond.	
Padthaway	Apr-00	Gas and cond.	-12.68	124.49	Lower Vulcan Fm.	2591		50		cond.	Wet
Paqualin	Feb-89	Gas	-11.98	124.51	Upper Vulcan Fm.	2850	Single phase gas reservoir				
Puffin	Jul-74	Oil	-12.36	124.28	Puffin Fm.	2014	Single phase oil reservoir	48		Paraffinic	
Skua	Jan-86	Oil and gas	-12.51	124.40	Plover Fm.	2259	Two phase reservoir	45	930	Paraffinic	Wet
Swan	Sep-91	Gas and cond.	-12.19	124.49	Puffin Fm.	2255	Dew-point reservoir	41		cond.	Wet
Swift	Jan-85	Oil	-12.54	124.45	Lower Vulcan Fm.	2384	Single phase oil reservoir	42		Unspecified	Wet
Tahbilk	Dec-90	Gas and cond.	-12.73	124.50	Montara Fm.	2598	Dew-point reservoir	50		cond.	Wet
Talbot	Dec-89	Oil and gas	-12.45	124.88	Challis Fm.	1490	Two phase reservoir	54	768	Unspecified	Wet
Tenacious	Jul-97	Oil, gas and cond.	-11.86	124.90	Plover Fm.	2764	Single phase oil reservoir	50		cond.	

cond. - condensate, Fm. - Formation

CHAPTER THREE

REVIEW OF METHODOLOGIES

3.1 BASIN MODELLING

Basin modelling is a numerical analysis technique that is used to simulate geological processes in sedimentary basins. In petroleum exploration, basin modelling is generally taken to involve the numerical simulation of geological and geochemical processes such as petroleum generation, migration and accumulation. Basin modelling is increasingly recognized as a powerful approach for both the evaluation of the timing of hydrocarbon generation and also for understanding the distribution of hydrocarbon pools within a basin.

There is, however, still debate regarding the effectiveness of its application in actual petroleum exploration. In particular, within frontier areas, where the input and calibration data often have large uncertainties, modelling must be undertaken and interpreted carefully if meaningful results are to be obtained. On the other hand, areas such as the Vulcan Sub-basin have had an active exploration history, and hence an abundance of input and calibration data exist to test and refine the models produced. Consequently, in such regions, high-resolution basin simulations can be carried out in order to help better understand petroleum systems and evaluate untested exploration prospectivity. Moreover, the lessons learnt from such studies can then be applied to frontier basin systems, thereby improving our ability to evaluate the potential of such regions.

3.2 STUDY PROCEDURE

3.2.1 Basin modelling

3D basin modelling provides a much more accurate analysis of the migration pathways and the actual volumes of accumulated hydrocarbons than does 2D modelling. However, in 3D modeling, the preparation of the input data and the calculation time are more time-consuming than is the case with 2D modelling. In the present study, both 2D and 3D modelling have been carried out. 2D modelling was used to help constrain the timing of generation and expulsion, as well as the key geological processes and events important to the generation/migration cycle. 3D basin modelling was then used to examine the extent of the effective source kitchen

and the migration pathways. Finally, by comparing the results obtained by both the 2D and the 3D modelling, the relative benefits and limitations of each approach to actual petroleum exploration were assessed.

3.2.2 Seepage indicators

The 3D seismic mapping component of the study aimed principally to constrain a leakage and seepage model of hydrocarbon migration and accumulation through the mapping of bathymetry, seismic amplitude at sea floor, fault distribution and HRDZs. This mapping aimed to complement the 3D generation/migration work which was also undertaken.

The work-flow for the leakage and seepage study is listed below.

a. Mapping of seafloor faults, chemo-synthetic communities, mounds and pockmarks via the use of bathymetry data, which potentially leads to the detection of active, present day hydrocarbon seeps.
b. Mapping of seafloor seismic amplitude anomalies, especially those resulting from enhanced carbonate cementation caused by hydrocarbon seepage and oxidation processes.
c. Construction of an isochron map of the Top Paleocene to Base Miocene horizons, which facilitated the mapping of HRDZs in the region.
d. Mapping of the Jurassic (rift) and Neogene (reactivation) fault trends using coherency slicing, time dip of the Top Paleocene etc, to determine any linkages, or lack thereof, between rift and reactivation faults.

All mapping work has been done using the mapping software in IESX (Basemap in GeoFrame 4.0.4).

3.2.3 Integration

This seismic mapping was integrated with 2D and 3D PetroMod™ basin (generation/migration) modelling to determine what correlations exist. This work then provided a holistic understanding of the processes of hydrocarbon leakage and seepage in this prospective region.

3.3 PETROMOD™

3.3.1 Overview

Integrated Exploration Systems (Julich, Germany) PetroMod™ 2D/3D software package was used for the modelling in this study. PetroMod™ 2D/3D is a finite element basin simulator which can model 2D and 3D hydrocarbon generation, migration and accumulation in sedimentary basins. This software can simulate 3-phase fluid flow (oil, gas and water) and multi-component PVT-relationships and can take into account dissolution and exsolution between each phase. It has also a unique petroleum migration (Hybrid) model which can integrate the benefits of Darcy flow and flow-path modelling. This feature enables the user to conduct high-resolution migration and accumulation analyses in relatively short calculation times (Hantschel et al, 2000).

3.3.2 Principles used in PetroMod™ simulations

The basic theoretical principles involved in basin modelling using PetroMod™ are described below. Figure 3-1 shows the summary of equations used in PetroMod™ 2D/3D.

3.3.2.1 Basic equation

In PetroMod™, a mass balance equation (Eq. 3-1) is used for the petroleum generation, migration and accumulation (PetroMod™ users manual: simulation /migration, 2004; Aziz & Settari, 1979; Huyakorn & Pinder, 1983; Bethke, 1985).

$$\partial_t(\rho_f v_f) + S_f \partial_t(\rho_f \phi) + \phi \partial_t(\rho_f S_f) = -\phi \partial_t(\rho_f S_{add}) \quad \text{(f ... water, oil, gas)} \qquad \text{... Equation 3-1}$$

Flow terms — Compaction — Petroleum Generation

where v_f = fluid velocity, ρ_f = fluid density, ϕ = porosity, S_f = fluid saturation, and S_{add} = additional saturation due to oil and gas generation.

The first two terms of the equation are flow terms (general fluid mechanics), whereas the other two terms represent special basin modelling factors. These effects are compaction (i.e. porosity change) and petroleum generation (from hydrocarbon sources). In this model, the mass balance of fluid flow in porous media requires that the average density of a volume element changes if fluids, as mass fluxes, stream through the element (the second term in the flow terms). The average density change can be related to porosity or saturation changes if special flow mechanisms and fluid

properties are assumed. In the models constructed, it is assumed that the solid (rock) material is ideally rigid and that the fluids are immiscible and incompressible. These assumptions imply that porosity changes and compaction can only occur due to the outflow of fluids from the element.

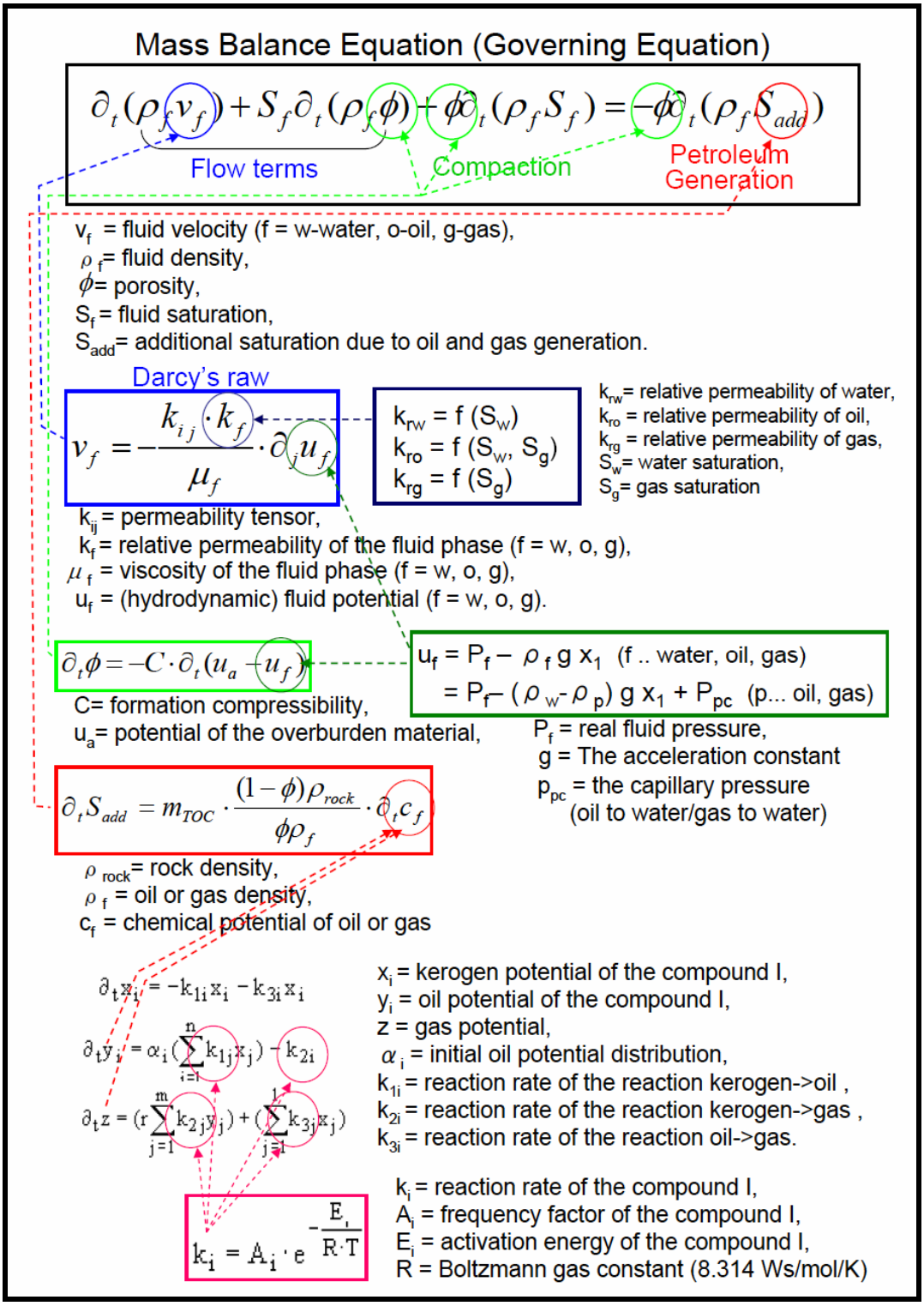

Figure 3-1. A summary of equations used in PetroMod™ 2D/3D.

3.3.2.2 Sediment compaction

In general, porosity change, the third term of equation 3-1, is driven by the change of the overburden load potential due to subsequent sedimentation. In PetroMod^{TM}, this process is described by the following compaction law (PetroMod^{TM} users manual: simulation/migration). Porosity is given as a function of effective stress.

$$\partial_t \phi = -C \cdot \partial_t (u_a - u_f) \quad \text{... Equation 3-2}$$

Effective Stress

where ϕ = porosity, C= formation compressibility, u_a= potential of the overburden material, and u_f=average fluid potential. The difference between the overburden and the fluid potential is the effective stress. The sedimentation rate directly affects the overburden potential, and therefore both overpressuring and compaction processes are strongly influenced by depositional rates.

3.3.2.3 Petroleum generation

The source term for petroleum generation shown in Equation 3-1 contains the additional or generated petroleum (oil or gas) saturation. The representative values for the petroleum kinetics are the chemical petroleum potentials (mass of hydrocarbons per TOC mass) and the relationship between the chemical potentials and the generated saturations are the following (PetroMod^{TM} users manual: simulation/migration).

$$\partial_t S_{add} = m_{TOC} \cdot \frac{(1-\phi)\rho_{rock}}{\phi \rho_f} \cdot \partial_t c_f \quad \text{... Equation 3-3}$$

where m_{TOC} = TOC mass, ϕ = porosity, ρ_{rock} = rock density, ρ_f = oil or gas density, and c_f = chemical potential of oil or gas. The chemical potential c_f indicates mass ratio of the oil or gas to the mass of the total organic carbon content.

In these equations, every set of petroleum kinetics contains the definition and description of three different reactions (PetroMod^{TM} users manual: simulation /generation; Tissot and Welte, 1978):

kerogen -> oil, kerogen -> gas, oil -> gas.

Consequently, every reaction is described by a set of activation energies, frequency factors, and initial amounts of the materials or corresponding distributions of these

values. It is assumed that kerogen and oil, as the initial products in these reactions, can consist of different components that react with different reaction rates. All possible sub-reactions can thus be represented in the following manner:

	kerogen -> oil	kerogen -> gas	oil -> gas
Reaction rate	k1	k3	k2
	$X_1 \xrightarrow{k_{11}} Y$	$X_1 \xrightarrow{k_{31}} Z$	$Y_1 \xrightarrow{k_{21}} Z$
	$X_2 \xrightarrow{k_{12}} Y$	$X_2 \xrightarrow{k_{32}} Z$	$Y_2 \xrightarrow{k_{22}} Z$
	…………………	…………………	…………………
	$X_n \xrightarrow{k_{1n}} Y$	$X_l \xrightarrow{k_{3l}} Z$	$Y_m \xrightarrow{k_{2m}} Z$

(X: Kerogen, Y: Oil, Z: Gas)

.... Equation 3-4

These equations are defined with different reaction parameters for the different kerogen types. For kerogen Types I and II, the kerogen->oil->gas reaction is the main process, while for kerogen Type III an important part of the gas is obtained from the kerogen->gas reaction.

For the mass balance considerations, the chemical potentials of the kerogen components x_i, for the oil components y_i (=c_f) and the gas z (=c_f) are introduced. The mass balance for the reaction system in Equation 3-4 yields to the following equations.

$\partial_t x_i = -k_{1i} x_i - k_{3i} x_i$ for kerogen components ... Equation 3-5

$\partial_t y_i = \alpha_i (\sum_{j=1}^{n} k_{1j} x_j) - k_{2i}$ for oil components ... Equation 3-6

$\partial_t z = (r \sum_{j=1}^{m} k_{2j} y_j) + (\sum_{j=1}^{1} k_{3j} x_j)$ for gas ... Equation 3-7

where x_i = kerogen potential of the compound I, y_i = oil potential of the compound I, z = gas potential, α_i = initial oil potential distribution, k_{1i} = reaction rate of the reaction

kerogen -> oil , k_{2i} = reaction rate of the reaction kerogen -> gas , k_{3i} = reaction rate of the reaction oil -> gas.

As with most chemical processes, the petroleum generation process is a function of time and temperature. While time dependency is obvious when the differential equation system of the mass balances are integrated, temperature dependency is connected to the reaction parameter. This exponential dependency is described with the Arrhenius law.

$$k_i = A_i \cdot e^{-\frac{E_i}{R \cdot T}} \qquad \text{... Equation 3-8}$$

where k_i=reaction rate of the compound I, A_i = frequency factor of the compound I, E_i = activation energy of the compound I, R =Boltzmann gas constant (8.314 Ws/mol/K).

For the solution of the kinetic problem, the definition of initial values for the chemical potentials is necessary. In the case of the kerogen and oil potentials, the initial values can be given for every component or their activation energy.

3.3.2.4 Petroleum migration and expulsion

In PetroMod™, Darcy's law for multi-phase is used for the modelling of fluid flow (PetroMod™ users manual: simulation/migration):

$$v_f = -\frac{k_{ij} \cdot k_f}{\mu_f} \cdot \partial_j u_f \qquad \text{... Equation 3-9}$$

where v_f = velocity of the fluid phase (f = w-water, o-oil, g-gas), k_{ij} = permeability tensor, k_f = relative permeability of the fluid phase (f = w, o, g), μ_f = viscosity of the fluid phase (f = w, o, g), u_f=(hydrodynamic) fluid potential of the phase (f = w, o, g).
This gives the first term in Equation 3-1.

Whereas the fluid potentials can be regarded as the driving forces of migration, the transport properties depend on the permeability and viscosity values. As the fluid velocities approach zero when the concentration is reduced, the relative permeability is assumed to depend strongly on saturation.

The relative permeability of oil is assumed to be a function of both the water and the gas saturation and is calculated as follows.

$k_{rw} = f(S_w)$ $k_{ro} = f(S_w, S_g)$ $k_{rg} = f(S_g)$

and $$k_{ro} = k_{row} \cdot k_{rog}$$ ... Equation 3-10

where k_{rw}= relative permeability of water, k_{ro} = relative permeability of oil, k_{rg} = relative permeability of gas, k_{row} = relative permeability of oil in a oil water system, k_{rog}= relative permeability of oil in a oil gas system, S_w = water saturation, S_g = gas saturation.

Figure 3-2 shows the typical example of the relative permeability function for a water-oil system. The oil saturation threshold value, from which oil began to flow out of cell due to its saturation increase, is called critical oil saturation (residual saturation). This parameter is important to evaluate hydrocarbon expulsion timing from the source rock or fluid flow pattern. In PetroMod™, the user can set this value.

In the migration and expulsion model, the cell must be filled to the saturation value before flow can continue into the next cell. After flow has occurred, the cell must be filled again before migration from the cell can continue. This value is termed the “residual saturation” in migration modelling through the carrier bed, whereas it is called the “critical saturation” in expulsion modelling. Saturation values of approximately 20% will therefore result in 'pulsed' migration and large differences in saturation values along the migration path. Lower saturation values, for example 3 to 5%, which more closely approximate bulk values for thicker layers, can result in higher mean flow velocities as the cells only have to wait for a smaller amount of petroleum before flow can continue.

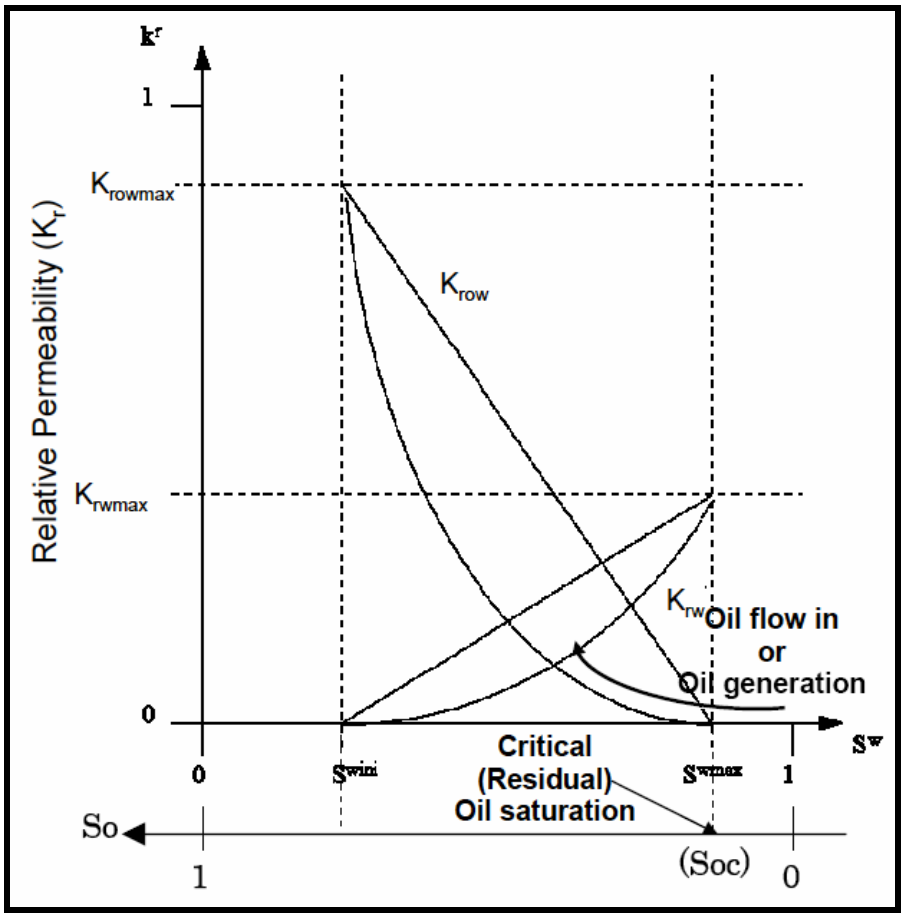

Figure 3-2. Relative permeability function for water-oil system (Helander, 1983).

The fluid potential (or overpressure of the fluid) is derived from the real pore pressure field under consideration of the buoyancy potential:

$u_f = P_f - \rho_f g x_1$ (f .. water, oil, gas) ... Equation 3-11

where u_f = fluid potential, P_f = real fluid pressure, and ρ_f = fluid density. Fluid potential is the mechanical energy contained in a unit volume fluid. Just as heat moves from high to low temperature, fluid flows from high to low fluid potential.

The x_1 axis is directed vertically downwards and g is the acceleration constant. The difference of the pore pressures of the two fluids is the capillary pressure. It is generated due to the fact that the adhesive attractive forces of two immiscible fluids are essentially greater than the cohesive repulsive forces. In pore systems, this capillary pressure is influenced by the pore geometry, mainly by the pore throat sizes.

It ranges from 0.01MPa (sandstone) to 5MPa (tight shales) with an interfacial tension of 0.03N/m (Hubbert, 1953; Hunt, 1996).

Finally, the fluid potentials can be written in the following form:

$u^f = P^f – (\rho^w - \rho^p) g x_1 + P^{pc}$ (p... oil, gas) ... Equation 3-12

Therein, P^{pc} is the capillary pressure of the oil to water or gas to water respectively.

These potential definitions produce the following petroleum driving forces:

- The petroleum moves from high pore pressure regions, produced for example by high sedimentation rates, to low pore pressure regions.
- Due to the lower density, petroleum tends to migrate vertically upward.
- Petroleum migrates from regions of high capillary pressure to regions of low pressure; obstacles such as cap rocks with high capillary pressure levels inhibit migration. This can lead to changes of the flow direction and migration paths, or to accumulations.

3.3.2.5 Phase behavior

In PetroMod^{TM}, phase composition models are used for the handling of the generated hydrocarbon components. These models enable different approaches to relate components to phases depending on the prevailing PT conditions (Fig. 3-3). In PetroMod^{TM}, three models for the petroleum phase and one model for the water phase are available:

1. Simple Ratio Model
2. Symmetrical Black Oil Model (SBO)
3. Flash Calculations

1./ Simple Ratio Model: This assumes two phases (liquid and vapor) consisting of just two components (*liquid* component "oil" and *vapor* component "gas"). Some components may occur in both phases simultaneously in a certain PT dependent ratio. The simplest approach of such a model would be to assign all components to either the liquid or the vapor phase. This is applied to the basic kerogen => oil => gas reaction.

2./ Symmetrical Black Oil Model (SBO): In this type of model, the components generated during simulation are divided into two classes: a pseudo-component gas (e.g. CO_2, N_2, C_2-C_4) and a pseudo-component oil (e.g. C_5-C_6, C_7-C_{13}, C_{13+}). Depending on their respective bubble- and dew-point curves (Fig. 3-3), the

components can occur as both gas and oil components in the vapor phase, as well as in the liquid phase. This model is based on simple look-up tables, which contain generalized PT curves, i.e. the bubble- and dew-point curves for the two pseudo-components. The bubble- and dew-point curves of the two-component system define the component-ratio in the respective phase. This is calculated dynamically for each time-step during the simulation. However, once a curve is selected, it will be used throughout the entire simulation. The ratio of the individual components within the pseudo-component remains fixed.

3./ Flash Calculations : The algorithm on which the flash calculation is based allows the fast and accurate calculations of generalized PT curves. These can subsequently be used in e.g. the Symmetrical Black Oil model. It is especially suited to deal with multi-component models, since fundamental properties (e.g. critical points, PVT) can be assigned to the individual pure components instead of using pre-defined bubble- and dew-point curves. The exact dissolution of each individual component into the existing phases is thus enabled. A combination of components into a pseudo-component or a static pre-assignment of components to a specific phase is not necessary. If the components and PT conditions are known, Flash Calculations determine the resulting phases and phase compositions dynamically. Changes in phase/component behavior are taken into account over time and with respect to the changing PT conditions during HC generation and petroleum evolution.

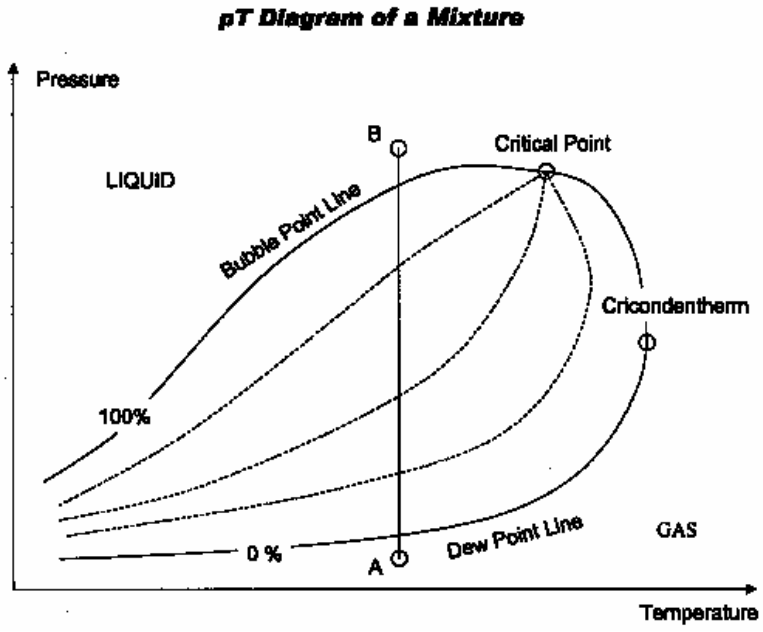

Figure 3-3. Schematic diagram of phase behavior of a gas-liquid mixture (Calhoun, 1976).

3.3.2.6 Fault Model

In PetroMod^{TM}, all faults assigned by the user can have changing transmissibility with time. Faults can be assigned different transmissibility values for three different time periods (Period 1 to 3) along and/or across the fault. The transmissibility value of faults consists of two components, namely transmissibility along, and across, faults. These values are assigned as relative values compared to the transmissibility value of the original host rock.

In PetroMod^{TM}, fault juxtaposition, that is the actual displacement of formations across faults, is not treated precisely. Figure 3-4 is an example of fault assignment in PetroMod^{TM} 2D (VTT-05 section). On the actual 2D seismic data, the Lower Vulcan Formation is juxtaposed next to the Middle to Lower Plover Formation through faulting (left of Fig. 3-4a). In the model, however, the Lower Vulcan Formation is obliged to connect to the uppermost parts of Plover Formation due to a gridding limitation. This is a limitation of PetroMod^{TM} similar to most existing 2D/3D numerical basin simulators. This gridding limitation makes it difficult to simulate direct hydrocarbon migration from the Lower Vulcan Formation to the middle and lower parts of the Plover Formation across the fault.

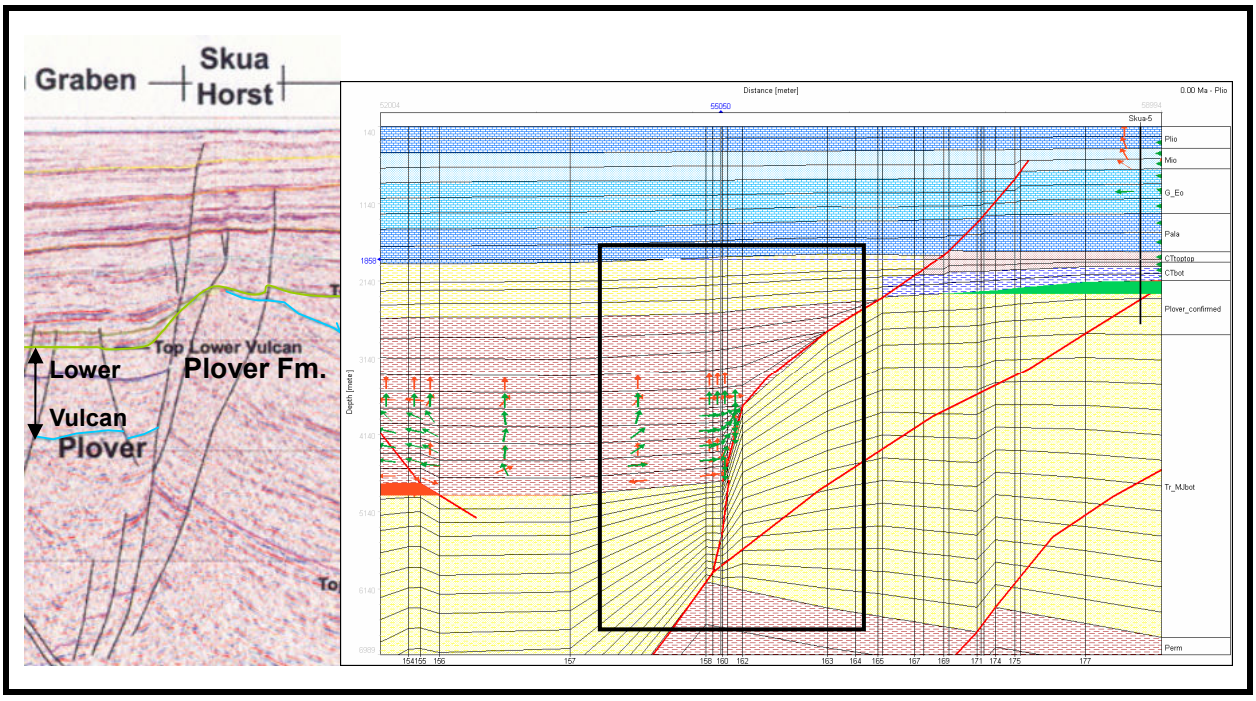

Figure 3-4a. Example of fault assignment in PetroMod^{TM} 2D (VTT-05). Area in rectangle shows main field in Fig. 3-4b.

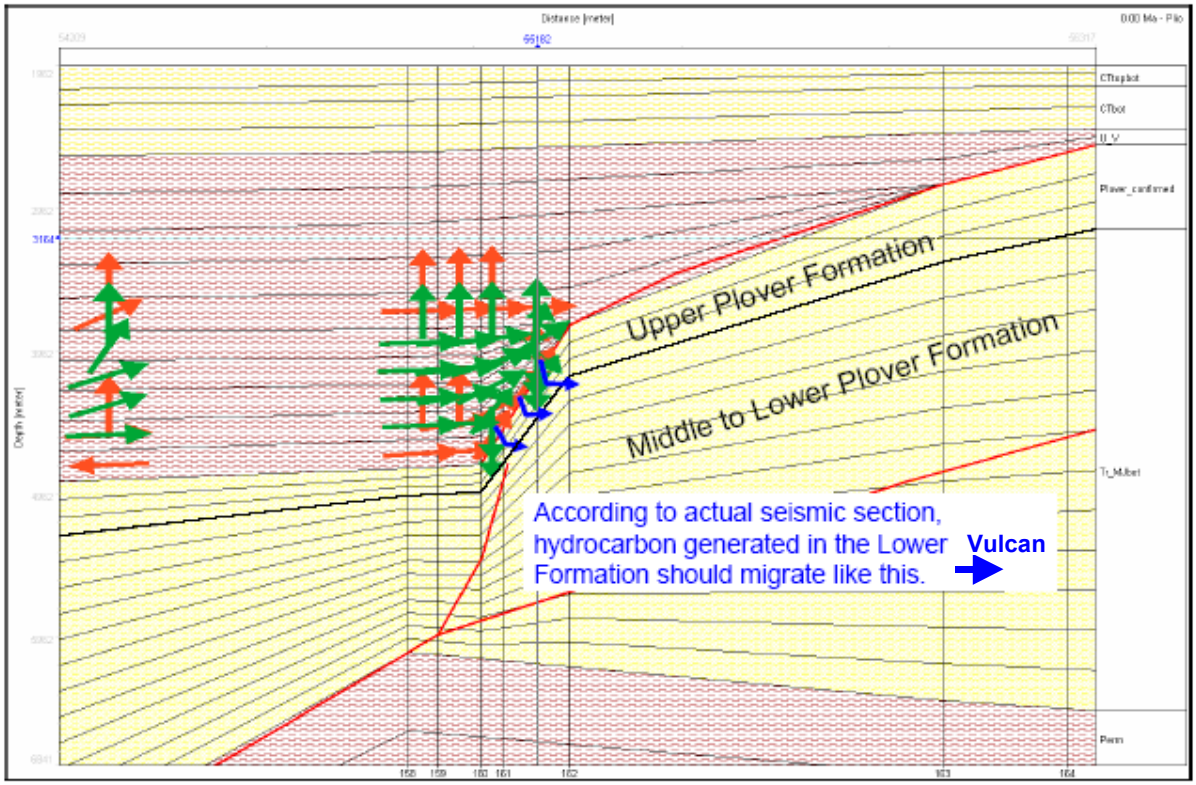

Figure 3-4b. Example of fault assignment in PetroMod^{TM} 2D (VTT-05) - Close up.

3.2.2.7 Hybrid Simulation

The Darcy flow model is used in modelling hydrocarbon expulsion from source rocks and hydrocarbon accumulation in traps under the seal - including leakage through the seal - whereas simple flow-path modelling is used for modelling secondary migration within the carrier beds (Figure 3-5). This “hybrid simulation” is a useful petroleum migration modelling facility within PetroMod^{TM}, which combines the benefits of flow-path simulation with those of Darcy flow simulation (Hantschel et al, 2000). This simplification of modelling enables the user to undertake much more rapid simulations compared with the more typical Darcy flow simulation.

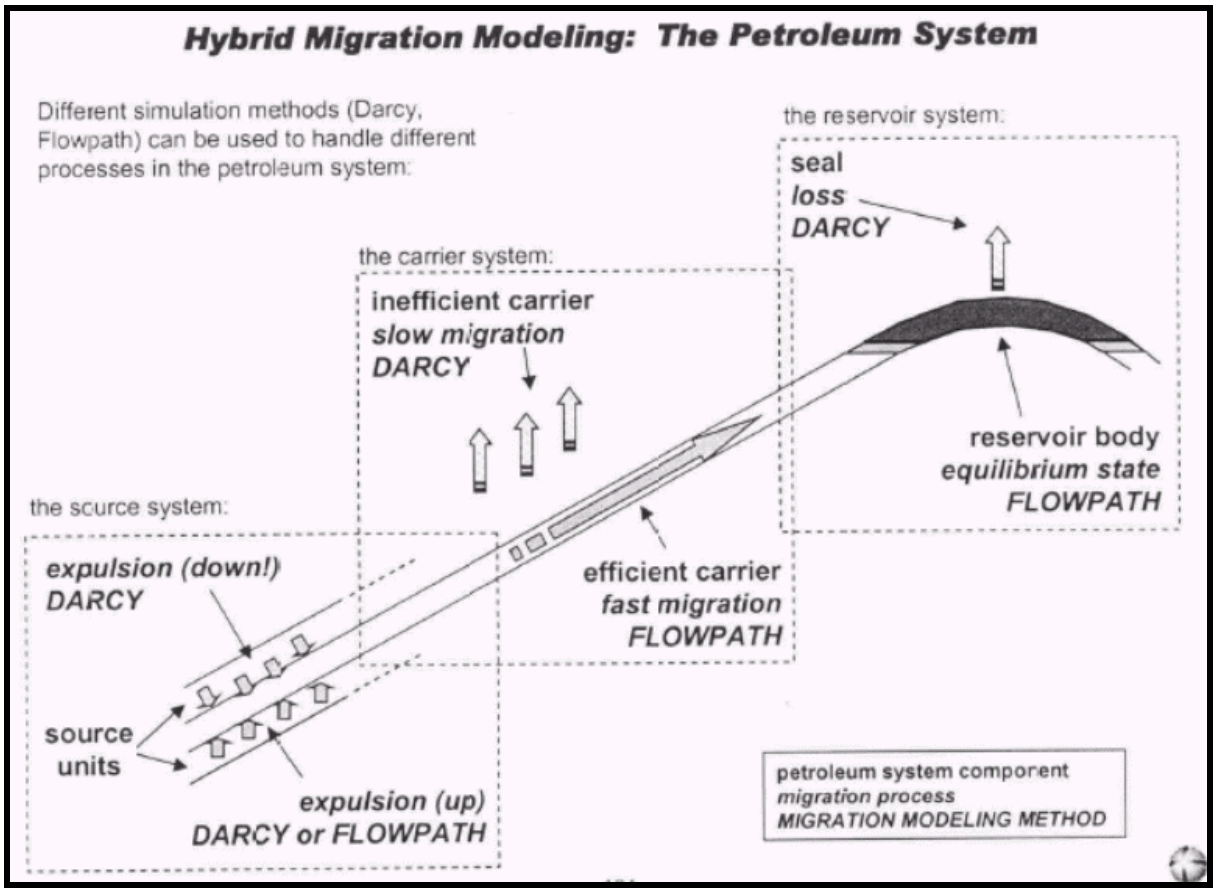

Figure 3-5. Schematic diagram showing the basic principles of hybrid simulation (IES, 2002).

3.4 LEAKAGE AND SEEPAGE INDICATORS

3.4.1 Overview

Petroleum seeps are surface occurrences of thermogenic hydrocarbons that have been generated in the sub-surface. A good definition of a seep is "the surface expression of a migration pathway, along which petroleum is currently flowing, driven by buoyancy from a sub-surface origin" (Clarke and Cleverly, 1990). The presence of seeps indicates that a source system is, or has been, active in a basin.

Seepage information, such as oil and gas shows on the surface, has been utilised in petroleum exploration as a key indicator for petroleum accumulation beneath the surface. Work published by BP and others in the early 1990's (Clarke and Cleverly, 1990) demonstrated that over 75% of the world's petroliferous basins contain surface seeps, the exceptions being those with an unbroken regional evaporitic seals, such as the Hith Anhydrite in the Arabian-Iranian foreland basin. The results of their study clearly indicate the importance of seeps and seepage in petroleum exploration.

However, there have been many difficulties associated with the actual application of seep investigations in petroleum exploration. Specifically, some of the key questions that need addressing include:

1. Does the seep come from a charged, but leaking structure or directly from an active source rock?
2. If the seepage is coming from a leaking structure, how big is the trap and how full is it?
3. Does the presence of seepage associated with a trap imply that the seal has failed and, therefore, that the trap is completely breached?
4. Does the absence of seepage simply indicate the presence of a good regional seal, or merely the absence of a working source system?

Regarding question 1, the actual source of the seepage (trap versus source rock) is distinguishable, at least to some extent, by combining investigations of the trap using seismic data (e.g., the location of chimneys - chaotic patterns caused by the existence of gas and seeps in relation to deeper structures) with the outputs from regional basin modelling (although there are often large uncertainties associated with the thermal history and burial depth in source rock).

With regard to the second question, the research is still on going, although numerous efforts are being made with relation to quantitative estimation of the amounts of hydrocarbon leakage and seepage using seismic techniques (Hunt, 1996).

The solutions to the third and fourth questions can be resolved, to some extent, by combining an evaluation of the seal rock properties and with an evaluation of fault seal integrity using geo-mechanical techniques.

The most effective way to apply hydrocarbon leakage and seepage information to petroleum exploration is to integrate it with other geological, geochemical and geophysical data via basin modelling and seal rock evaluation, rather than using it in isolation.

3.4.2 Bathymetry

Bathymetry data have often been neglected in petroleum and basin prospect evaluation, in spite of the fact that bathymetry data can potentially provide important insights into the processes of petroleum leakage and seepage. Hovland et al (1994) suggested, after analysis of 2D seismic data in the Porcupine Basin off western

Ireland and the Vulcan Sub-basin off north-west Australia, that an important, causal relationship existed between the locations of seabed mounds and underlying hydrocarbon seeps. On the other hand, Bailey et al (2003) reported a negative relationship between spatial fault distribution and deep-sea carbonate mounds in the Porcupine Basin, offshore Ireland. Recently, O'Brien et al (2002b) described an apparent relationship between the distribution of seafloor carbonate mounds and fault distributions and orientations in the Nancar Trough in Australia's Timor Sea.

In the present study, a new bathymetry grid was produced for part of the Timor Sea using a PGS data-set; the seafloor horizon was produced by auto-tracking the seafloor over the whole 3D seismic volume. Subsequent importation of the bathymetry grid into GeoViz (IESX) allowed the following images and maps to be produced.

a. Seafloor faults.
b. Chemo-synthetic communities.
c. Pockmarks.
d. Hard-grounds.

3.4.3 Seafloor amplitude

Areas of active hydrocarbon seepage at the seafloor can have relatively higher seismic amplitudes due to localised carbonate cementation (Hovland, 1988), which is the result of bacterial oxidation of the seeping hydrocarbons. Typically, a 16 to 32 millisecond seismic window at the seafloor is exported and the geographic location of any anomalous amplitudes analyzed. Mapping these features can potentially provide a representation of the areal distribution of present day related seepage, and hence by implication, the location of deeper, failing seals. Such features also provide an indication of where active charge systems are located.

3.4.4 Hydrocarbon Related Diagenetic Zones (HRDZs)

In the Timor Sea region, hydrocarbons (both methane and heavier hydrocarbons) which have leaked, or are leaking, up faults arrays or through failing top seals from Mesozoic traps have been progressively oxidised by bacteria within shallow (Eocene) aquifer sands to produce carbonate-cemented zones which have anomalously high seismic velocities. These cemented areas have been termed Hydrocarbon-Related Diagenetic Zones or HRDZs (O'Brien & Woods, 1995). The HRDZs in the Eocene Grebe Sandstone (Fig. 3-5) produce time pull-up on seismic data and can be used to

map the extent of leaky fault segments that overlie deeper, charged traps (O'Brien et al., 1999a). HRDZs in the Timor Sea are characteristically large (3,000-5,000m long) over completely breached accumulations, but are typically much smaller (100-1,500m long) or absent over commercial oil fields in the area.

The mapping of HRDZs in the Timor Sea is a quick and effective method for mapping palaeo-, and perhaps present day, hydrocarbon leakage and seepage. If one is using 3D seismic data, then HRDZs can be mapped by producing (by auto-picking both horizons) an isochron map of the Top Paleocene to Base Miocene interval. In such an approach, the anomalous high velocity zones will appear as time "thins" – which effectively define ovoid to (more usually) lenticular zones. On time maps of the Top Paleocene horizon, the HRDZs often produce moderate to strong pull-up, with the absolute amount of pull-up being directly proportional to the amount of hydrocarbons that have leaked from the underlying traps. The Top Paleocene time highs also mimic the leaking fault arrays. The presence of HRDZs over a given structure, or within a given area, has important implications. Their presence can high-grade areas from a charge point of view, as HRDZs rely upon leaking hydrocarbons to form. The location and extent of the HRDZs with respect to the underlying structure can provide important information on the fault seal integrity of the underlying trap. The ability to map HRDZs seismically provides an empirical, predictive (i.e. pre-drill) capability to assess trap integrity, but also has afforded significant insights into the actual processes which have controlled trap leakage and breaching. These include the exact lengths of the leaky fault segments in assorted trap types, the dip and azimuth of the leaky faults, their spatial relationships to the sealing facies within and around the traps, and the location of seafloor seeps.

In this study the 3D seismic data sets acquired by PGS (Chapter 4.2) were analysed using above mapping methodology. New methodology developed in this process and preliminary application results are discussed in detail in Chapter 5.7.

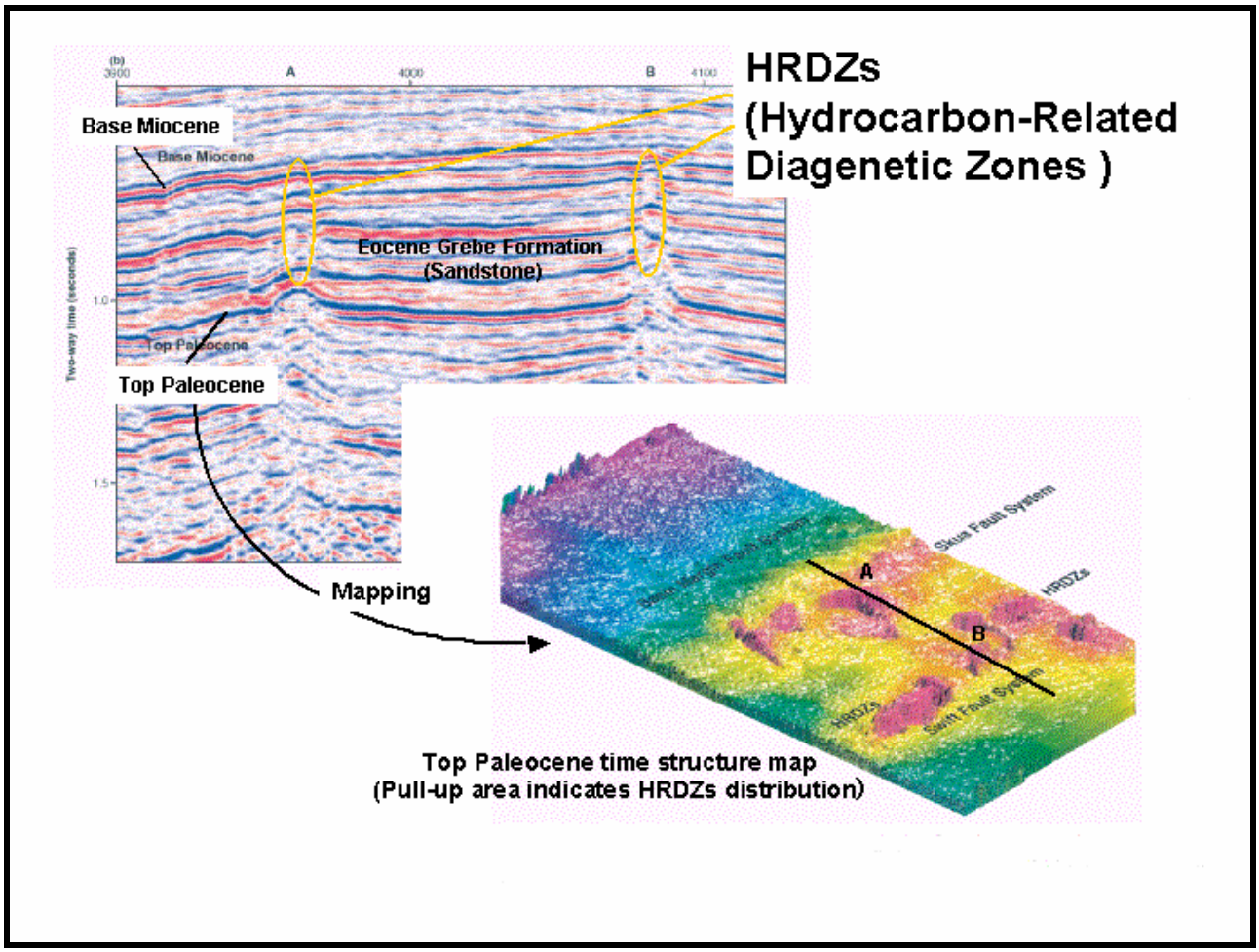

Figure 3-6. Example of HRDZs (O'Brien et al. 1999a).

CHAPTER FOUR

GEOLOGICAL DATA SET

4.1 BASIN MODELLING INPUT

4.1.1 Modelling section and area

The 2D VTT seismic survey data acquired by the Australian Geological Survey Organization (AGSO; now Geoscience Australia) in 1995 were used as the basis for both the 2D and 3D modelling (Fig. 1-1). This survey is composed of 27 lines, including 19 northwest-southeast dip lines and 8 southwest-northeast strike lines. The survey has a line spacing of approximately 5-10 km for dip lines and 20 km for strike lines. Total survey length is approximately 5,000 line kilometres.

2D modelling was carried using two seismic dip lines, VTT-05 and VTT-14 (Fig. 1-1 and 4-1). The southernmost of these lines (VTT-05) extended across the Montara Terrace and Swan Graben to the Ashmore Platform. Line VTT-05 intersects the Puffin oil accumulation and the Skua oil/gas field. The Swan Graben has been interpreted to contain the main source rock system for these fields (Pattilo & Nichols, 1990; Kennard et al., 1999; Edwards et al., 2004).

This line was selected because it provided an opportunity to assess the characteristics of petroleum generation and expulsion in the Swan Graben source depocentre and the dominant controls on hydrocarbon migration and accumulation in the Puffin and Skua structures. The northernmost line (VTT-14) extended across the Jabiru Terrace and the southern Cartier Trough (just to the north of the Paqualin Graben) to the Ashmore Platform, south of the Oliver-1 oil and gas field. The line intersects the southern extension of the Jabiru oil field, the Challis oil/gas field and the southern Cartier Trough, which is a potential source rock kitchen for these fields (Edwards et al., 2004). This line was selected to help clarify the characteristics of petroleum generation and expulsion in the southern Cartier Trough and to determine the possible first-order controls on hydrocarbon migration and accumulation in the Tenaceous, Jabiru and Challis structures.

3D modelling was conducted using 3D surfaces derived from the interpretation of the depth-converted 2D VTT seismic lines, as published in Chen et al (2002). The area covered by these data extended over much of the Vulcan Sub-basin (approximately 219 km east-west and 239 km north-south) and the major petroleum accumulations

and source rock kitchens in the area (Fig. 1-1).

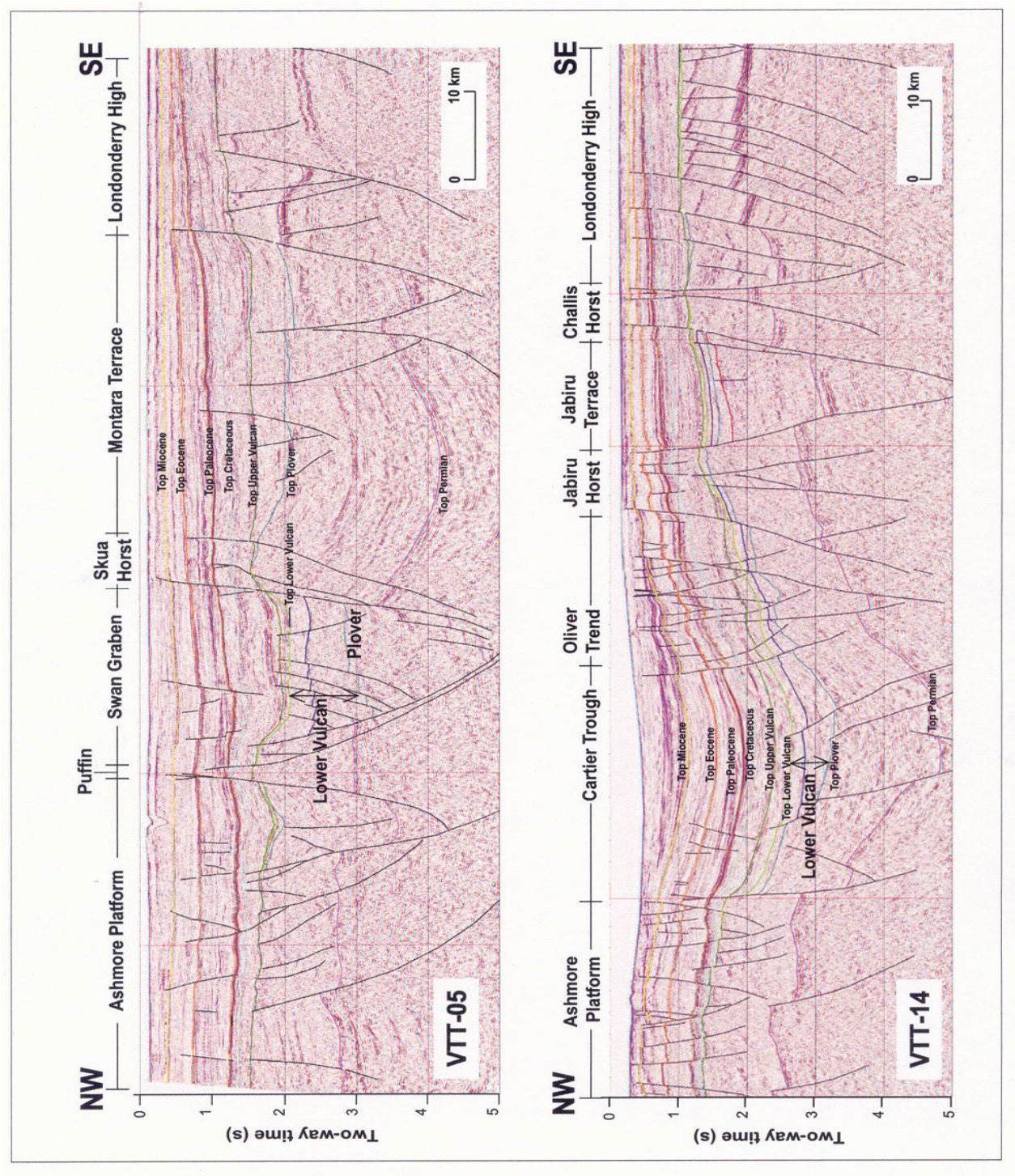

Figure 4-1. Seismic time sections used for modelling (VTT-05, 14).

4.1.2 Stratigraphy

Seismic horizons and faults interpreted by Chen et al (2002) were used for the modelling. A total of 10 horizons were interpreted by these authors; these horizons are

shown in Table 4-1. Well control for these horizons was established using biostratigraphic data and the depth-TWT curves from 42 wells in this basin. The Top Triassic horizon was not interpreted due to the poor resolution within the available seismic data. On the other hand, interpretation of the deeper, near-Top Permian horizon, which typically produces a strong seismic reflector, was carried out. Geological ages for each horizon (formation boundaries) were assigned based on general stratigraphic data from the Vulcan Sub-basin (Table 4-1).

A total of 12 layers were used in the basin modeling, as two additional, essentially "dummy" formations/units were added to the original 10 horizons described by Chen et al (2002). The first added horizon was within the Cretaceous succession which was divided into two units in order to incorporate the Puffin Formation sandstones within the modelling. The second horizon was created by subdividing the Late Jurassic and the Triassic units (10:90) in order to take into account the source rock potential of the Plover Formation. The upper part (top 10%) of this unit was assigned to the Plover Formation. This approximate assignation was based on the thickness of the Plover Formation intersected in the Skua-1 well (600m). As a result, the assigned thicknesses of the Plover Formation in the Swan Graben, the southern Cartier Trough and the Cartier Trough were 500m, 450m and 320m respectively.

Table 4-1. Age and lithology assigned for each formation units used in the modelling.

<table>
<tr><th>Age</th><th>AGSO (1996), Chen et al (2002) Interpretation (Top)</th><th>Formation unit used in this modeling</th><th>Age (Ma)</th><th>Rock Type (%)</th></tr>
<tr><td rowspan="4">Tertiary</td><td colspan="2">Pliocene</td><td>7-0</td><td>Limestone 100</td></tr>
<tr><td colspan="2">Miocene</td><td>34 -7</td><td>Limestone 80 Sandstone 20</td></tr>
<tr><td colspan="2">Eocene</td><td>56-34</td><td>Limestone 70 Sandstone 30</td></tr>
<tr><td colspan="2">Paleocene</td><td>65-56</td><td>Limestone 100</td></tr>
<tr><td rowspan="3">Cretaceous</td><td rowspan="2">Cretaceous</td><td>Upper Cretaceous (Top 50%)</td><td>100-65</td><td>Shale 50 Marl 50 (Pascal-Puffin-Skua-Montara-Tahbilk: Sandstone 50-75)</td></tr>
<tr><td>Lower Cretaceous (Bottom 50%)</td><td>136-100</td><td>Shale 50 Marl 50 (Puffin-1,2 Sandstone 50 Shale 25 Marl 25)</td></tr>
<tr><td colspan="2">Upper Vulcan</td><td>144-136</td><td>Sandstone 20 Shale 80</td></tr>
<tr><td rowspan="4">Jurassic</td><td colspan="2">Lower Vulcan (Upper)</td><td>150-144</td><td>Sandstone 10 Shale 90</td></tr>
<tr><td colspan="2">Lower Vulcan (Lower)</td><td>163-150</td><td>Sandstone 20 Shale 80</td></tr>
<tr><td rowspan="3">Middle Jurassic and Triassic</td><td>Plover (Top 10%)</td><td>172-163</td><td>Sandstone (Shaly) (PetroMod™ default)</td></tr>
<tr><td rowspan="2">Middle Jurassic and Triassic (Bottom 90%)</td><td>250-172</td><td rowspan="2">Sandstone 50 Shale 50</td></tr>
<tr><td>Triassic</td></tr>
<tr><td>Permian</td><td colspan="2">Upper Permian</td><td>270-250</td><td>Shale 70 Limestone 30</td></tr>
</table>

Depth conversion was carried out by Chen et al (2002) using the “layer cake” method of Marsden (1989). Seismic two-way time (TWT) curves from 42 wells in the Vulcan Sub-basin were used in order to refine the seismic interval velocities. The modelled depth conversion was adjusted until there was a less than 3% difference between the converted depth and the actual depth seen in the exploration wells.

4.1.3 Lithologies, rock properties and grid assignment

Figures 4-2 and 4-3 show the depth-converted seismic section, lithologies and source rock distributions used in the 2D modelling of VTT-05 and VTT-14 respectively. The depth structure map of the Top Plover Formation used for the 3D modeling is shown in Figure 4-4.

Details of these horizon and fault data (format and loading procedure) are described in Appendix 4-1-1.

The lithologies for each formation unit and sub-unit, shown in Table 4-1, were based on well composite logs for about 50 wells in the basin (AGSO, 1999; Appendix 4-1-2). Lithologies in each unit are assumed to be relatively uniform across the sub-basin. The exception was the sand-rich Puffin Formation, which was assumed, based upon well data, to be distributed asymmetrically in the southern part of the Vulcan Sub-basin (Fig. 4-5). When building the model, the Puffin Formation was considered to be deposited as a turbidite fan supplied from the Londonderry High south-east of the basin, probably through the palaeo-equivalent of the Penguin Deep (O’Brien et al, 1999b; de Boer, 2004). A compressibility model, the default model in PetroMod^{TM}, was used for modelling sediment compaction (Table 4-2, Chapter 3.2.2.2).

In the 2D basin modelling, all of the faults interpreted by Chen et al (2002) were represented (Figs 4-2 and 4-3). Grid intervals for the horizontal direction were assigned so that these faults could be modelled: finer grid intervals were assigned around the faults and steep culminations. These faults were anticipated to be a barrier to petroleum migration, particularly in the modelled section on line VTT-14 (Fig. 4-3), which has the down-to-the-southeast fault between southern Cartier Trough and the Jabiru Horst.

On the other hand, in the 3D modelling, all faults interpreted by Chen et al (2002) were imported (shown as brown lines on Figure 4-4), but only major faults which were assumed to have a potentially large influence on petroleum migration (shown as

green lines) were designated to be “effective” faults with respect to migration and given vertical and horizontal flow properties (Fig. 4-4). In addition, the number (i.e. the density) of the faults interpreted by Chen et al (2002) and used in our 3D model was much smaller or lower than that present on 2D seismic lines VTT-05 and -14. The horizontal grid interval used for the simulation was about 2.4 km, a value which was established by considering the width of the 2D seismic survey lines (5–20 km) used to create this 3D surface, balanced against the need to keep simulation times to a reasonable (approximately one day) period.

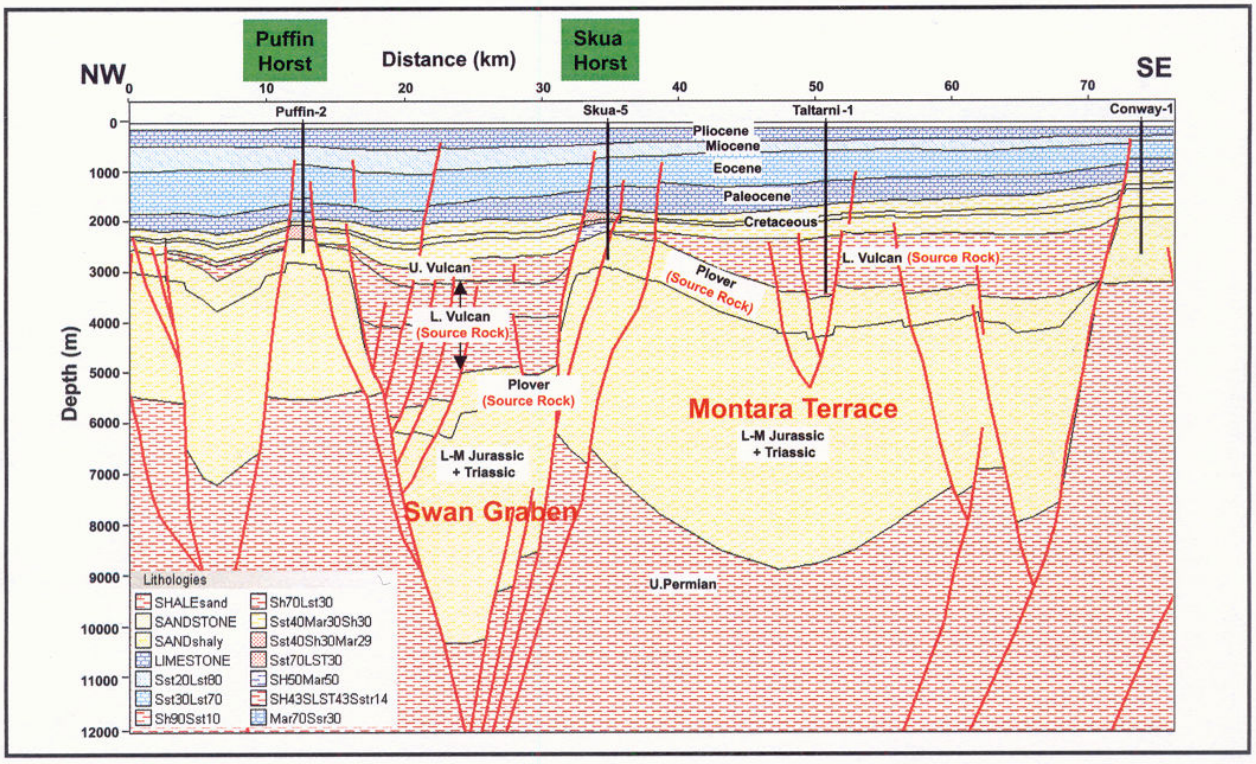

Figure 4-2. Seismic depth section used for 2D modelling (VTT-05).

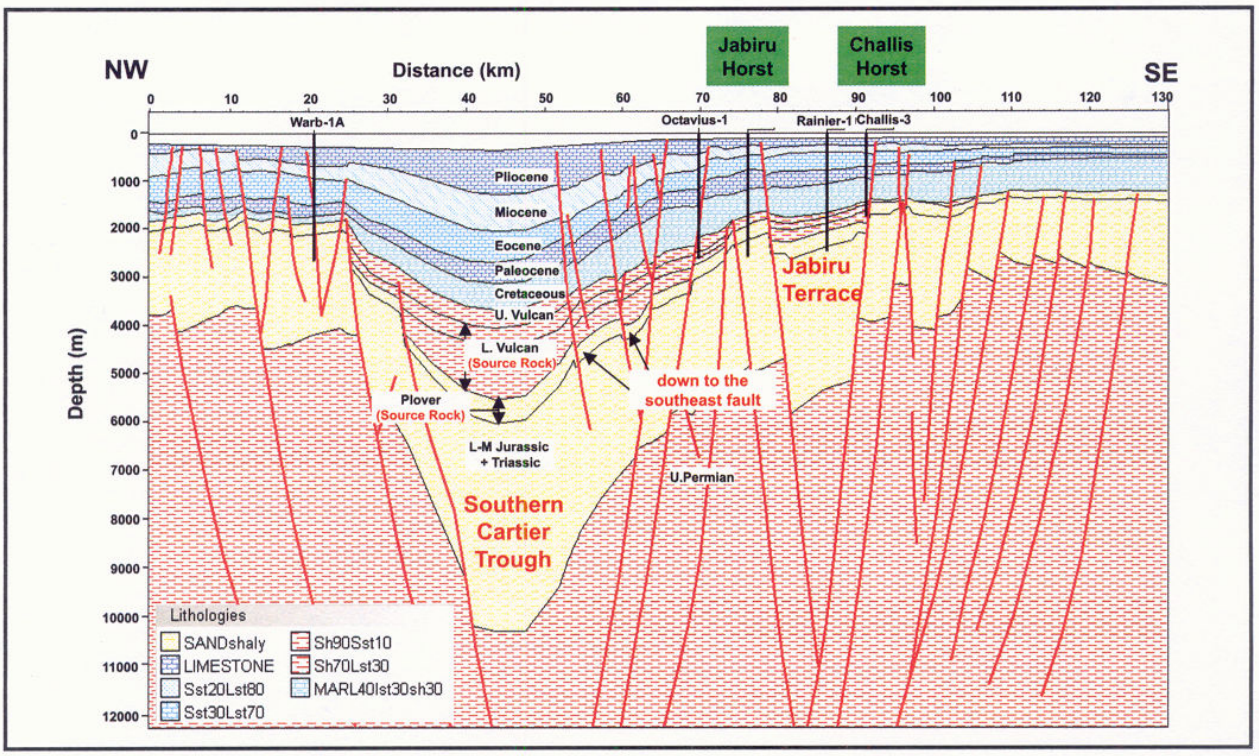

Figure 4-3. Seismic depth section used for 2D modelling (VTT-14).

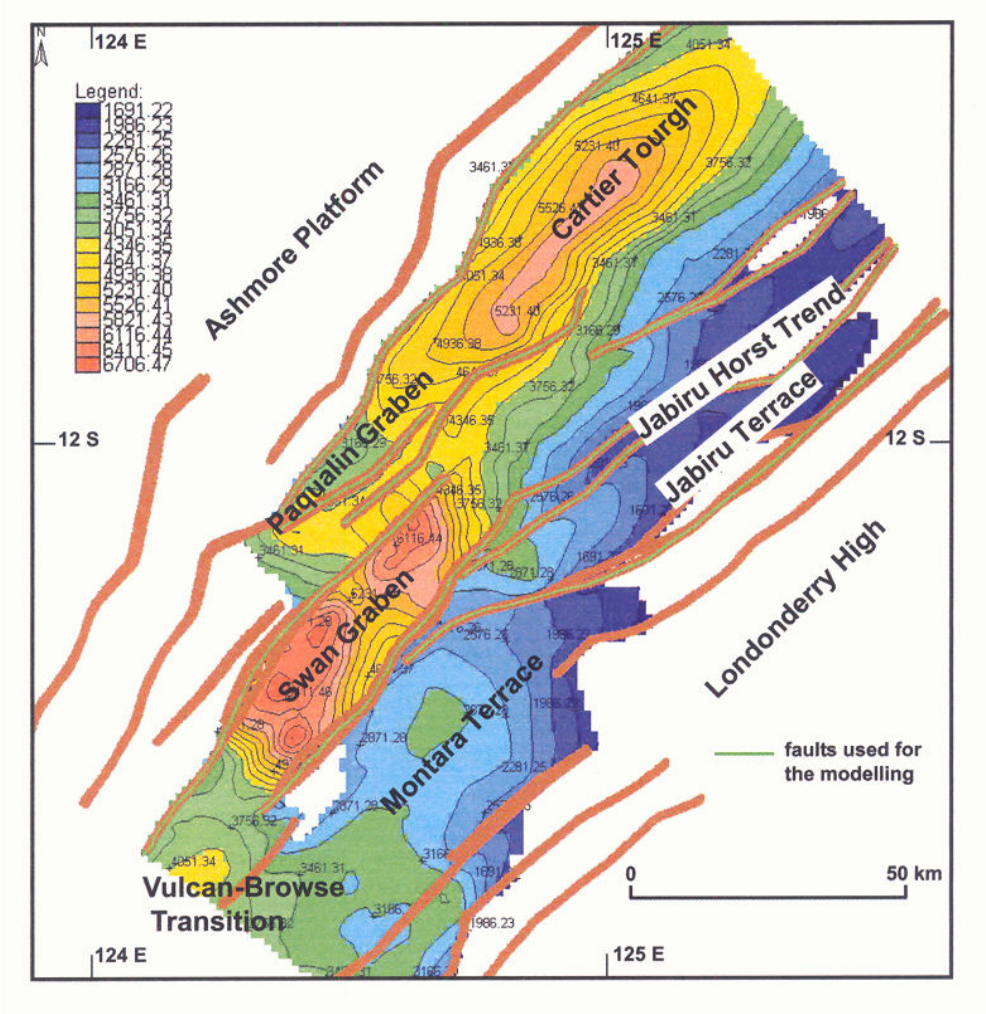

Figure 4-4. Top Plover Formation depth map and fault distribution used for the 3D modelling. A total of nine broad structural provinces are noted.

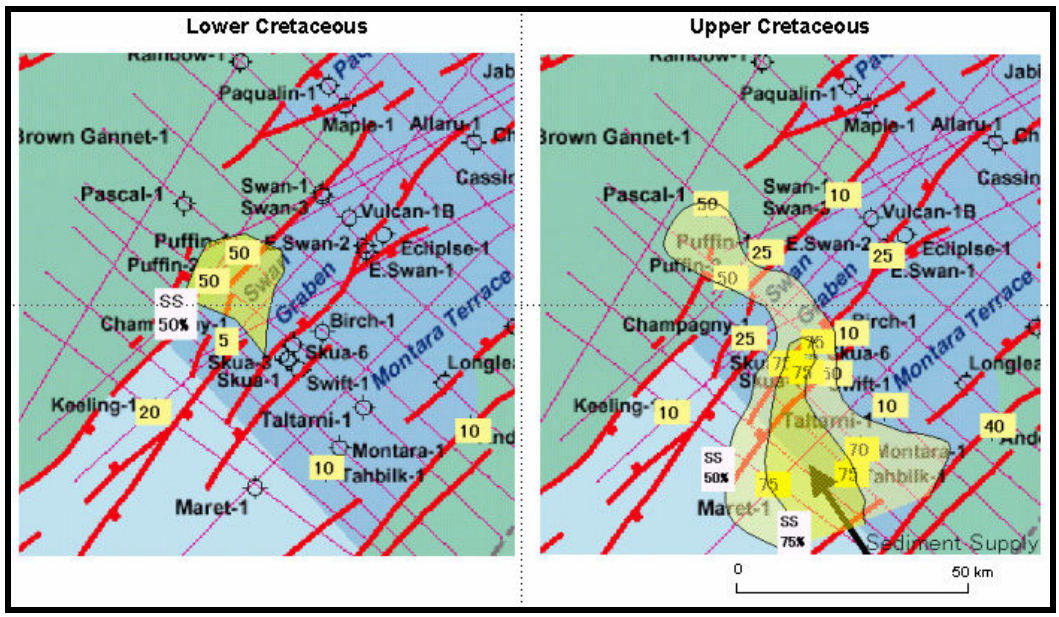

Figure 4-5. Thickness and distribution of the Late Cretaceous Puffin Formation sandstone as used in the modelling.

Table 4-2. Rock properties related to compaction used in modelling.

Name in PetroMod™	Applied Formation unit	Density (kg/m3)	Initial Porosity (unitless)	Minimum Porosity (unitless)	Compaction Model	Comp. Max (1E-7/lPa)	Comp. Min (1E-7/lPa)
SANDSTONE	-	2660.0	0.42	0.05	Comp. Model (3.3.2.2)	500.0	10.0
SANDsilty	Plover Fm.	2664.0	0.46	0.05		1200.0	10.0
SS75SH13MR12	*1	2665.8	0.46	0.05		1005.0	10.0
SS50SH25MR25	*2	2671.8	0.49	0.05		1937.8	10.0
SS65SH35	*1	2667.0	0.50	0.05		2671.1	10.0
SS50SH50	Middle Jurassic and Triassic	2670.0	0.53	0.05		5477.2	10.0
Shale100	-	2680.0	0.65	0.05		60000.0	10.0
SH50MR50	L. Cretaceous	2683.5	0.56	0.05		7510.0	10.0
SH80SS20	L. Vulcan lower Upper Vulcan	2676.0	0.60	0.05		23031.1	10.0
SH90SS10	L. Vulcan upper	2678.0	0.63	0.05		37173.5	10.0
SH70LM30	Upper Permian	2689.0	0.53	0.05		9943.4	10.0
LIMESTONE	Pliocene Paleocene	2710.0	0.24	0.05		150.0	10.0
LM80SS20	Miocene	2700.0	0.28	0.05		190.8	10.0
LM70SS30	Eocene	2695.0	0.29	0.05		215.3	10.0

Comp. – Compressibility

*1 – Upper Cretaceous around Pascal-Puffin-Skua-Montara-Tahbilk

*2 – Lower Cretaceous around Puffin-1, 2

In this modelling, it was considered important to simulate petroleum migration across faults from the Lower Vulcan Formation to the Plover Formation. In this case, no fluid barrier was assigned to the permeability across the boundary for all faults. In contrast, fluid flow along faults was not allowed (refer to Chapter 3.3.2.6).

A regionally extensive unconformity is recognized in the Oligocene in the Vulcan Sub-basin. Kennard et al (1999) proposed that erosion associated with this unconformity probably does not exceed 100m, because they could find no evidence of significant erosion in their seismic and stratigraphic data. Consequently, these workers did not include erosion in the 1D modeling that they undertook, As a consequence of the work of Kennard et al (1999), no erosion of the Oligocene sediments has been incorporated into the modelling.

4.1.4 Source rock properties

Representative Total Organic Carbon (TOC) concentrations and Hydrogen Index (HI) values were determined for each unit/formation, based on the combination of Rock-Eval analysis and net thickness obtained from well data (Table 4-3, Fig. 4-6 and 4-7). TOC values were assumed to be relatively higher than the analyzed average value, based on the concept that generally the original TOC in a given immature source rock is higher than the values obtained from otherwise identical rocks that are

thermally mature and have expelled hydrocarbons. The source rocks are assumed to be distributed uniformly within each formation. For the Plover Formation, which is not penetrated completely in most of the wells, the distributions are inferred mainly from the Rock-Eval analyses in Skua-1, in which more than 600 m of Plover Formation were intersected.

Table 4-3. Source rock parameters used in modelling.

Unit Name	TOC (%)	Kerogen Kinetics (Kennard et al. 1999)		HI (mg/g)	Distribution
		Primary Reaction	Secondary Cracking		
Upper Vulcan	1.5	Paqualine-1(sq 4c) Bulk kinetic data	Cracking of Light Oil	250	Uniform
Lower Vulcan (Upper)	2.5	Vulcan-1B(sq 4b) Bulk kinetic data		300	Uniform
Lower Vulcan (Lower)	2.5	East Swan-2(sq 4a) Bulk kinetic data		300	Uniform
Plover	4	Skua-1(sq 3) Bulk kinetic data		300	Uniform

Sq 3 - Plover, Sq 4a - Lower Vulcan (Lower), Sq 4b - Lower Vulcan (Upper), Sq 4c- Upper Vulcan

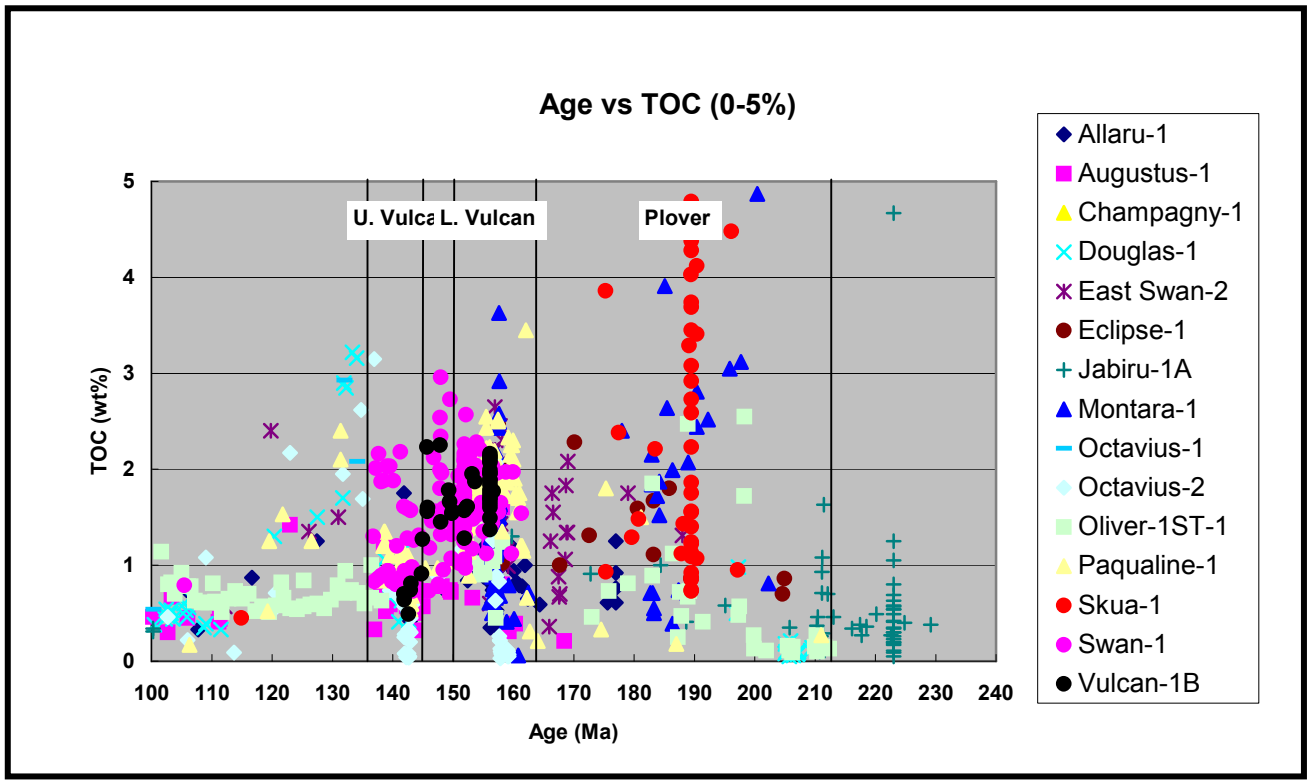

Figure 4-6a. Rock-Eval analysis data of TOC used for modelling input (0 – 5 %).

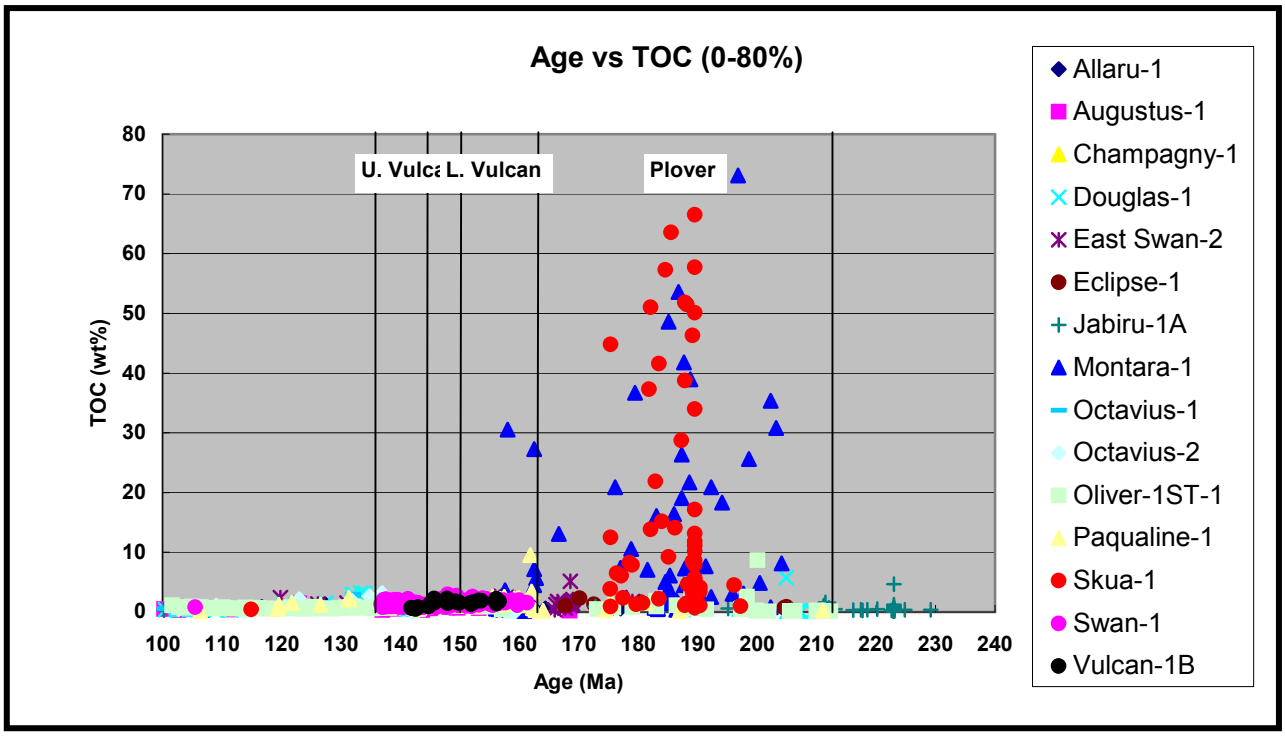

Figure 4-6b. Rock-Eval analysis data of TOC used for modelling input (0-80%).

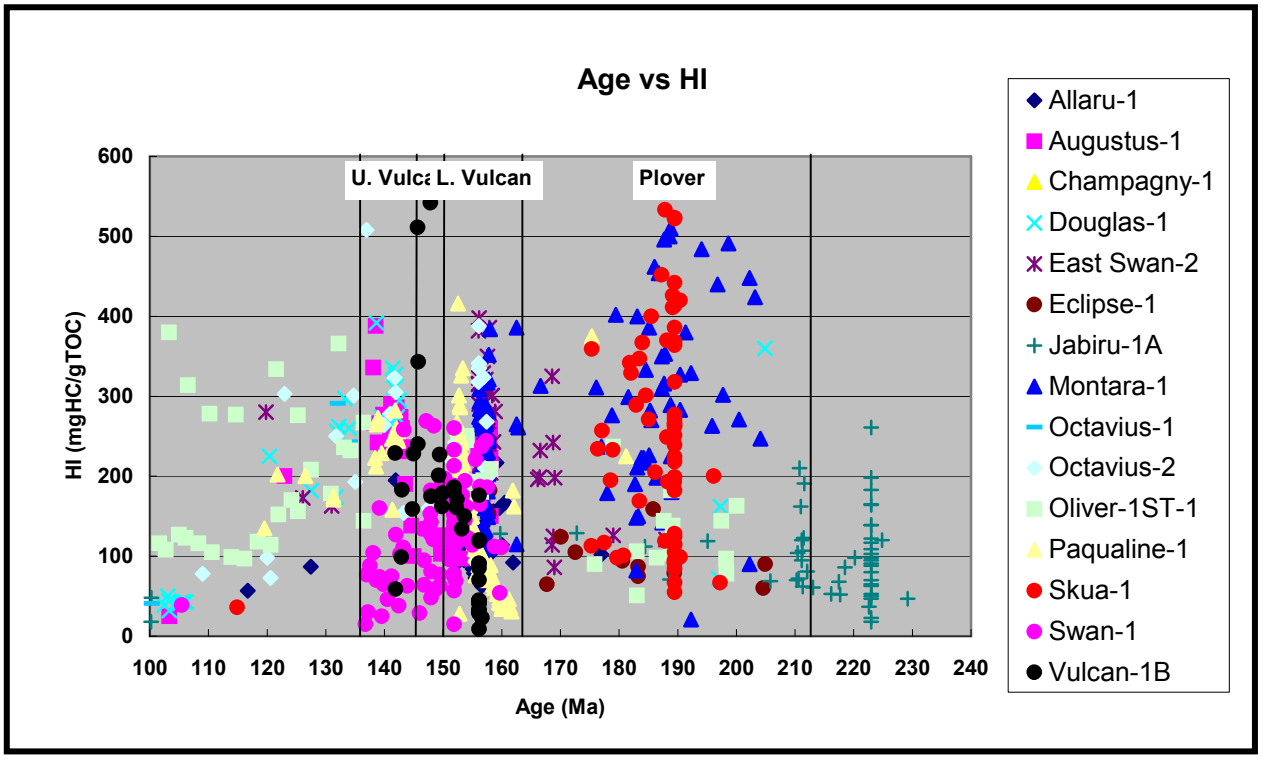

Figure 4-7. Rock-Eval analysis data of HI used for modelling input.

Kerogen-oil-gas reactions were used for the petroleum generation model. Kerogen kinetic data were obtained from geochemical analyses published by Kennard et al (1999) (Table 4-3, Fig. 4-8, Appendix 4-1-3). The kerogen kinetics were determined on

selected, immature, potential source units from open-system pyrolysis studies and estimated using the method of parallel first-order reactions. At the time of peak generation, this generation model is similar to the Type 'J' kinetic parameters determined by Lowry (1998).

Kerogen Primary Reaction (Kerogen to Oil)

L. Vulcan_L (sq 4a)
–East Swan-2 (sq 4a) Bulk kinetic data

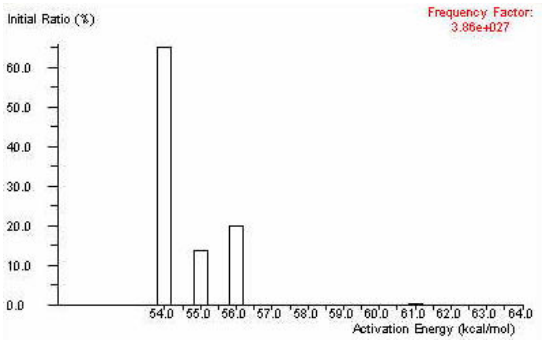

L. Vulcan_U (sq 4b)
–Vulcan-1B (sq 4b) Bulk kinetic data

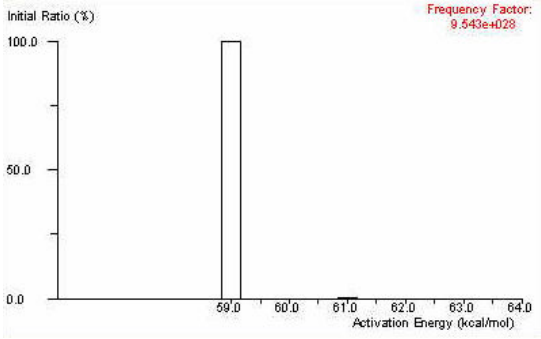

Plover (sq 3)
–Skua-1 (sq 3) Bulk kinetic data

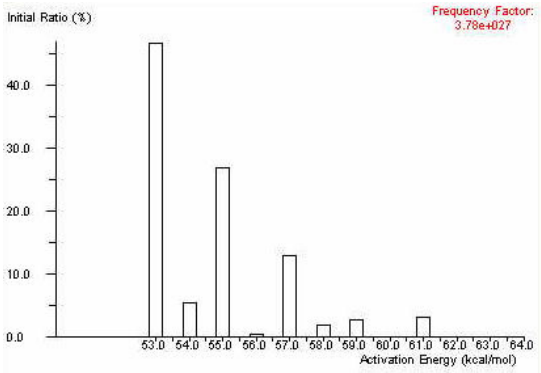

Kerogen Secondary Cracking (Oil to Gas)

L. Vulcan_L (sq 4a),
L. Vulcan_U(sq 4b),
Plover (sq 3)
–Kinetic Parameters for the Cracking of Light Oil from Kennard et al (1999)

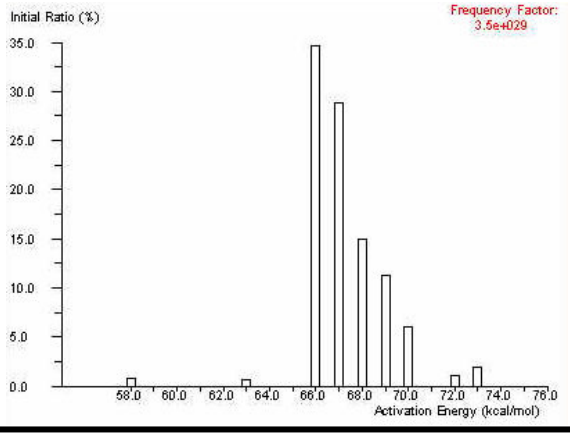

Figure 4-8. Kerogen kinetic data used for the modeling undertaken in this study.

4.1.5 Palaeo-water depths and palaeo-surface temperatures

Palaeo water depths estimated by Kennard and Deighton (2000) using biostratigraphic analysis were used for the estimation and input of palaeo-water depths in our modelling (Fig. 4-9). In the models presented in this thesis, it is assumed that water depths were greater than 300m within the Swan Graben during the Late Cretaceous, when deep marine sediments were deposited (Kennard and Deighton (2000). Large spatial variations are recognized in water depth, particularly in the Late Jurassic, Late Cretaceous, and also at the present day. It was thought these variations would affect the results of the modelling, particularly in regards to the assessment of migration pathways. For this reason, a different palaeo water depth model (Figure 4-9) was used for each of the nine geological regions or structural provinces shown in Figure 4-4.

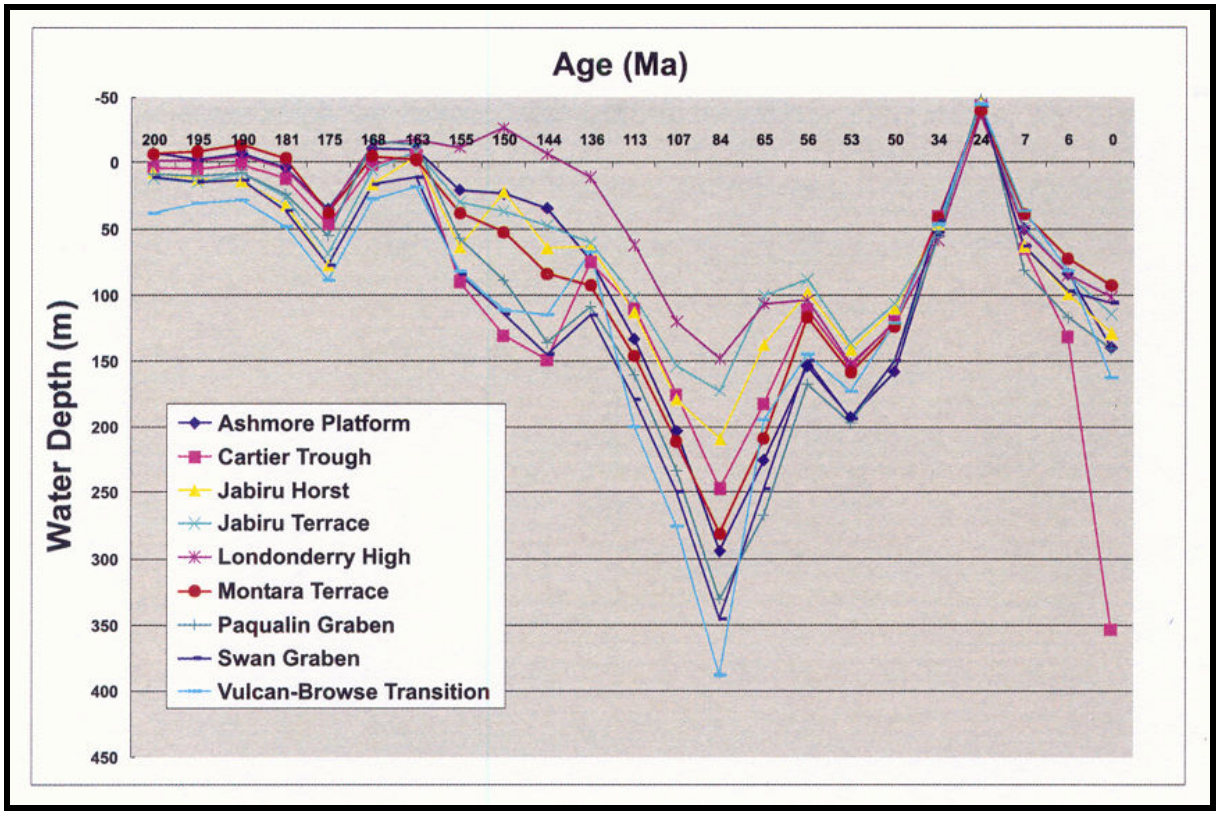

Figure 4-9. Palaeo water depth used for modelling (from Kennard and Deighton, 2000).

The palaeo-surface temperature analyses undertaken by Kennard et al (1999) and Kennard and Deighton (2000) were used for inputting the palaeo-sea bottom temperatures. Their data from the southern Cartier Trough showed that the variations in palaeo-temperatures are typically small, both temporally (10-25^{o}C) and spatially (5-10^{o}C). Such variations have only a minor effect on the results of the simulations.

4.1.6 Heat flow model

Heat flow models, developed by Kennard et al (1999) via sediment burial and thermal history analysis using the WinBury^{TM} 1D software suite, were used as the fundamental basis for the heat flow used in the modelling. A variation on Kennard et al.'s work was that an essentially constant heat flow of 60 mW/m^2 was used for the (post-rift) Tertiary (Fig. 4-10). In the thermal history analysis, Kennard et al (1999) used a model obtained by modifying the simple extension model of McKenzie (1978) via incorporation of the flexural isostatic model developed by Baxter et al (1997, 1998). Moreover, the model of Kennard et al (1999) was calibrated using observation data such as bottom hole temperature, vitrinite reflectance and fluorescence, apatite fission track analysis (AFTA) and fluid inclusion palaeo-temperature data.

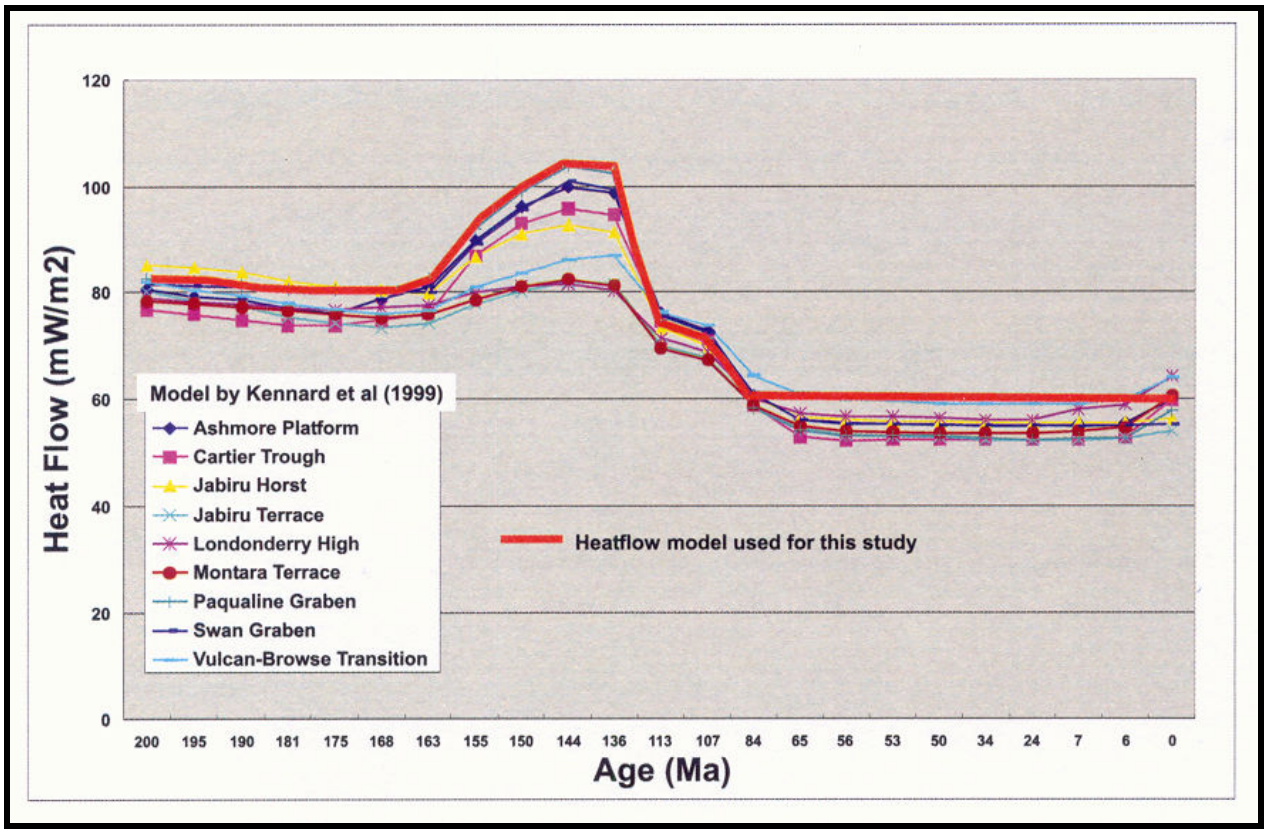

Figure 4-10. Palaeo heat flow used for modelling.

In the model used in this study, increases of heat flow up to 20 mW/m^2 were interpreted to have accompanied the crustal rifting in the Late Jurassic. A single heat flow model (Fig. 4-10: sold thick red line) was assigned for all of the nine geological segments (Fig. 4-4) in order to keep the modeling reasonably simple.

4.1.7 Petroleum expulsion, secondary migration and phase model

In PetroMod™, a saturation-based model is used for petroleum expulsion. This model assumes that generated hydrocarbons must fill a certain percentage of the pore space in a finite-element cell before they are expelled.

In the modelling of Kennard et al (1999), the authors used a 5% porosity saturation for the gas expulsion threshold and 40% for the oil expulsion threshold. The 40% saturation value for oil seems to be too high compared to the results of other studies, such as those by Rullkotter et al (1988), Pepper and Corvi (1995) and Okui et al (1998), where values of 10-30% seem more typical. In my model, an oil expulsion threshold of 10% was used, based on the relationship between TOC and saturation threshold obtained empirically by Waples (1997). In the Waples (1997) model, both pore-space saturation and saturation of adsorptive sites on kerogen are taken into account. On the other hand, a saturation value of 5% was used as the gas expulsion threshold, the same as used by Kennard et al (1999).

A petroleum secondary migration model, a Hybrid model with Darcy flow in source rocks and flow path in reservoirs, was used for the 2D and 3D modelling. A 3% hydrocarbon saturation was used for the migration threshold in the carrier bed, which is the default value in the PetroMod™. This default value was set considering the saturation values are a property of the entire finite-element cell.

The Flash Calculation module, which is the most sophisticated phase model in PetroMod™ 2D/3D, was used in the modelling.

4.2 PGS 3D SEISMIC DATA SET (ONNIA 3D)

4.2.1 Overview

Fair-quality 3D seismic data (the Onnia Survey) acquired by PGS were used for the leakage and seepage analysis in this study. The Onnia 3D survey covers more than 18,000 km^2 of the Timor Sea and provides coverage of the major oil and gas fields (Fig. 4-11). Total amount of data was extremely large, up to about 1.5 TB; at 32 bit, the 137 million traces (bin size = 9.375 m (inline) x 14.0625 m (xline)) equate to approximately 150 x 3590 tapes. Each square kilometre of data roughly uses 0.08 GB of space.

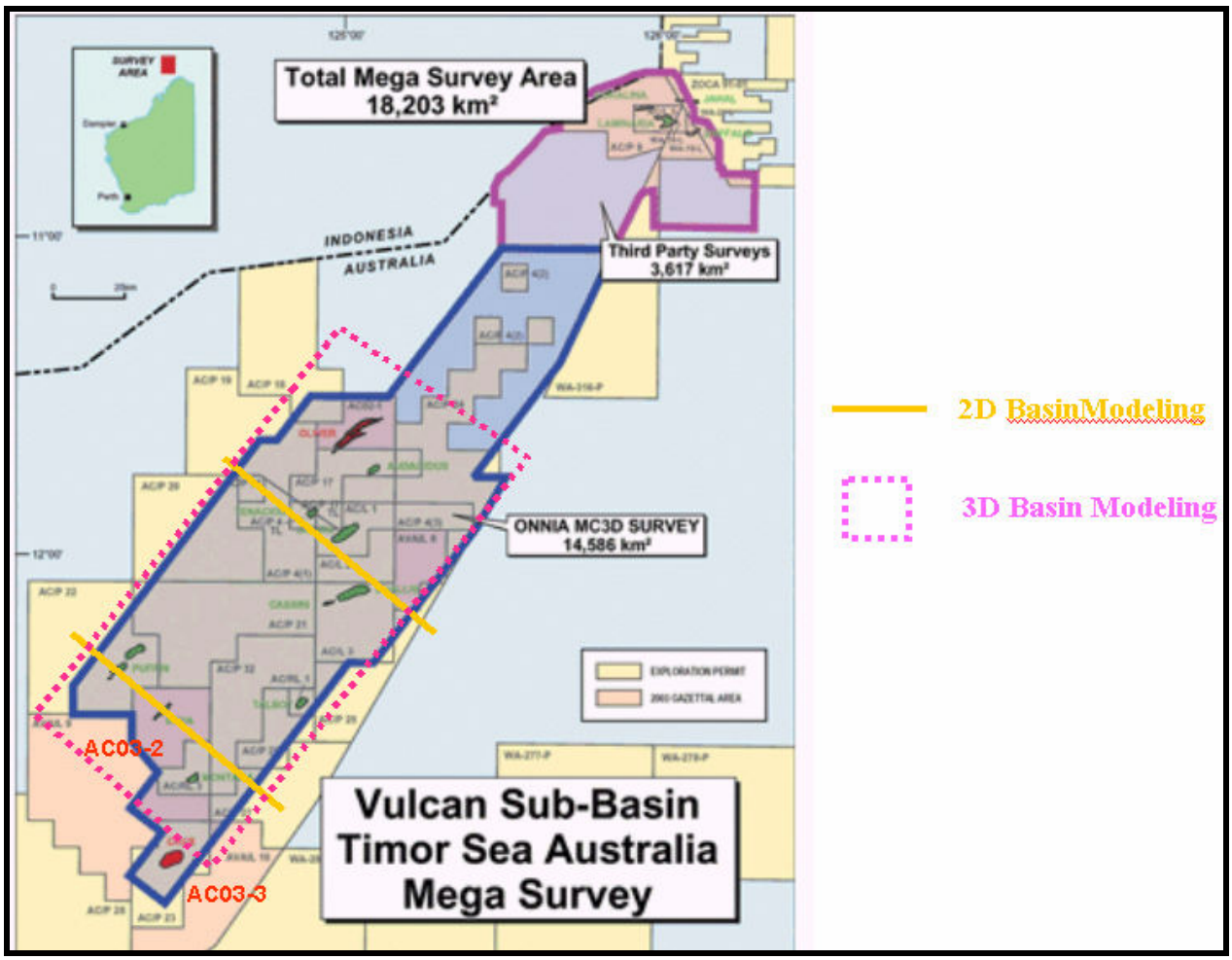

Figure 4-11. Map showing the location of PGS ONNIA 3D seismic survey area (Blue) and the location of 2D and 3D modelling in this study.

In this study, the analysis of the leakage and seepage indicators was carried out using interpreted surface data listed below.

Table 4-4 The list of Interpreted 3D surface data used for this study.

File name	Category	Type (Unit)	Size	Data type
dep.asc	Bathymetry	Depth map (m)	48 MB	ASCII Data (Scatter Set)
WB_150ct.asc		Time map (TWT: ms)	114 MB	
	Seafloor seismic amplitude	Amplitude map (32bit: relative value)		
base_mio.twt	Base Miocene	Time map (TWT: ms)	835 MB	
top_paleo.twt	Top Paleocene	Time map (TWT: ms)	835 MB	

Data location: /usr/users/tfujii/rawdata (dep.asc, WB_150ct.asc)
/disk7/scratch/tfujii (base_mio.twt, top_paleo.twt)

4.2.2 Data loading

Data loading was carried out using the software in GeoFrame 4.0.4 (Schlumberger). The details of files after they were loaded are listed below.

Table 4-5 The list of Interpreted 3D surface data used for this study (after loading).

File name	Category (units)	File size
Depth32813.ads_0	Bathymetry (depth: m)	13 MB
bathymetry32783.ads_str	Bathymetry (twt: ms)	7.5 MB
amplitude.38105.ads_str	Seafloor seismic amplitude (relative value)	20 MB
base_miocene.33035.ads_str	Base Miocene (twt: ms)	207 MB
top_paleocene.37227-59.ads_str	Top Paleocene (twt: ms)	207 MB

Data location: /disk11/ncpgg_data/VULCAN/Default
Control file for the loading: /disk6/ncpgg_home/tfujii/geoframe404_sun/xyznew2.ctl

4.2.3 Gridding

As a next step, gridding of these data was carried out using mapping software (Basemap) in GeoFrame4.0.4. Two kinds of grids were created, grid intervals of 100m by 100m and 50m by 50m respectively. Data files could be displayed smoothly as a result of this work.

4.2.4 Well input

Using the well import function in mapping software, key well data (20 wells; well name, location and depth) were imported in order to analyze the relationship between the locations of identified leakage and seepage features and actual wells.

CHAPTER FIVE

RESULTS AND DISCUSSION

5.1 CALIBRATION OF THERMAL HISTORY AND COMPACTION

5.1.1 Thermal history

In order to optimize the past and present day heat flow input data, a comparison was carried out between simulation results and observed data, including bottom-hole temperature (BHT), T_{max} and vitrinite reflectance (VR). Corrected BHTs, using both the Horner Plot (Horner, 1951) and a correction factor of 1.1, were used for the calibration of the present day temperature. For the calculation of Tmax and V_R, the models of Sweeney (1990) and Sweeney and Burnham (1990) (Easy Ro) were used respectively. The T_{max} value can be used as an indicator of maturity because it increases progressively with increasing thermal maturation; it is, however, influenced by kerogen type, a minimum S_2 value and contamination. In order to eliminate these effects, the criteria of Peter and Nelson (1992) were used (cut off value: S_2<0.5 mgHC/g rock, TOC<0.4%, T_{max}<395 C, HI<150 mg HC/g TOC).

Well data for the model calibration were selected on the conditions that they were:

- located near the major grabens and troughs;
- penetrated the Lower Vulcan Formation, the interpreted principal source rock in the region; and
- there was a sufficient number of analyses available.

Table 5-1 and Figures 5-1 and 5-2 show the summary table of calibrations in 14 selected wells and the heat flow calibration results, respectively.

The calibration results for the 14 wells show moderate to good agreement between the calculated and observed values (Table 5-1). Comparison between calculated and measured BHT values suggests that present day heat flows used in the models are reasonable (Fig. 5-1). Locally, the calculated heat flow underestimates the current day temperatures in the Oliver-1 well. On the other hand, the maturity profiles are affected by high heat flow and variable vitrinite quality (i.e. suppression), so an exact calibration is difficult (Fig. 5-2, and Table 5-1). Two different data sets are used in Vulcan-1B, though the Keiraville Consultants' data are assumed to be more reliable in terms of the consistency with the V_R value of other wells. In general, the calculated

maturity is close to that observed in the vicinity of the source rocks. In some cases, (e.g. in Paqualin-1), the modelled palaeo-heat flow may need to be increased.

Table 5-1. Comparison between observed and simulated thermal maturity indicators in 14 wells in the Vulcan Sub-basin.

Well name	BHT	Ro	Tmax
Allaru-1	Good	High	High
Augustus-1	n.a.	Good	Good
Champagney-1/ST-1	n.a.	Low (slightly)	n.a.
Douglas-1	n.a.	Good	Good
East Swan-2	Good	Good	High
Eclipse-1	n.a.	Good	High
Jabiru-1A	Good	Good	Good
Montara-1	Good	Good	High
Octavius-1	Good	Good	High
Octavius-2	n.a.	High	Good
Oliver-1ST	Low	Good	Good
Paqualin-1	Low	High/Low	Good
Swan-1	Good	Good	High
Vulcan-1B	Good	Low	Good

Good: Modelling results is within 10% of observation in the source rock units.
Low/High: Modelling results is more than 10% lower/higher than observation in the source rock units
n.a.: Data was not available.

5.1.2 Compaction

A comparison was made between the calculated porosity and the observed porosity in several key wells (Fig. 5-3). The calculated porosity (approximately 7%) within thermally mature, Lower Vulcan Formation sediments, at depths of 3500-4000 m, shows a good match with observed well log porosity in Swan-1 and slight under-estimation in Vulcan-1B.

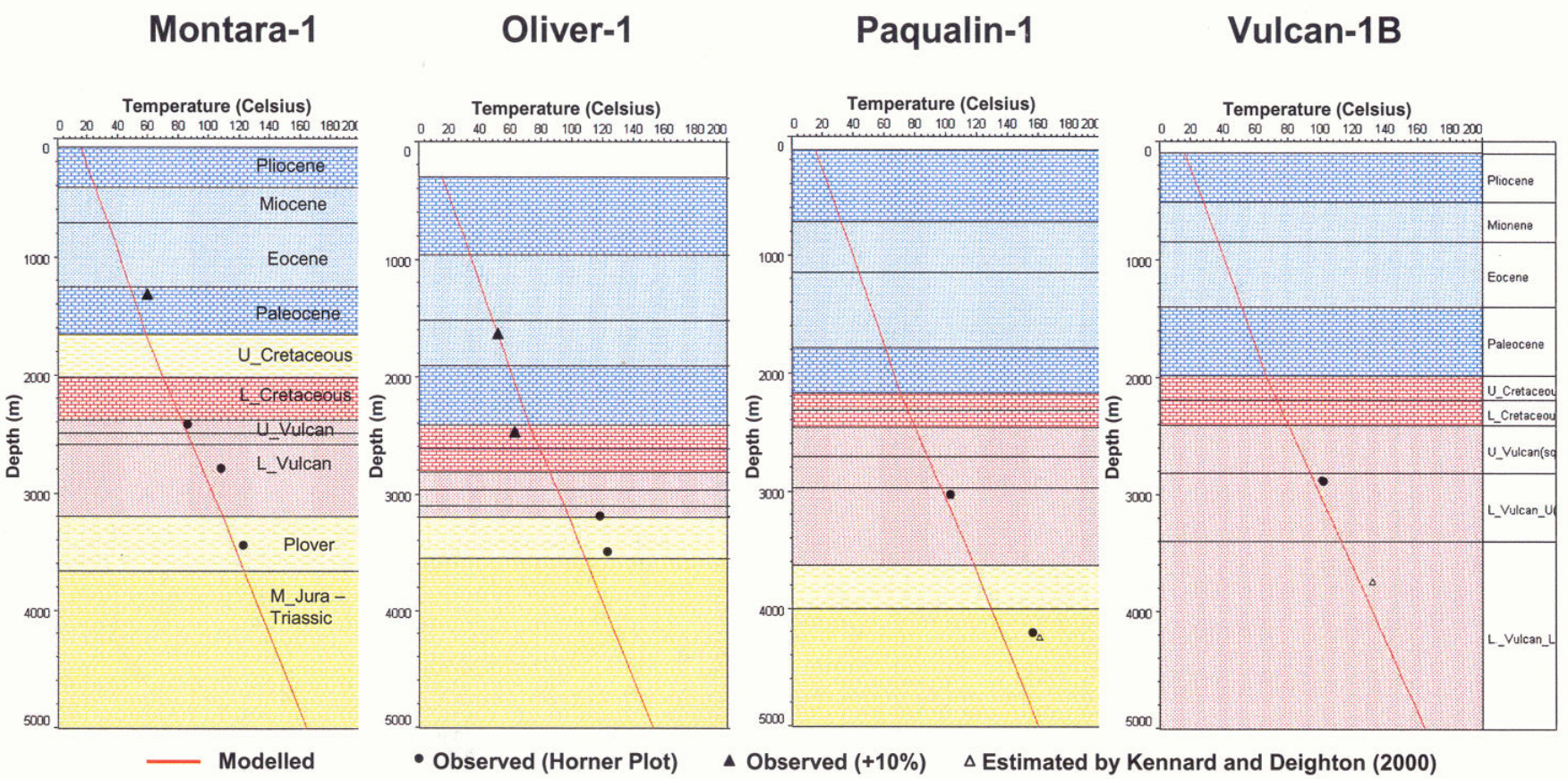

Figure 5-1a. Present day heat flow calibration results (BHT).

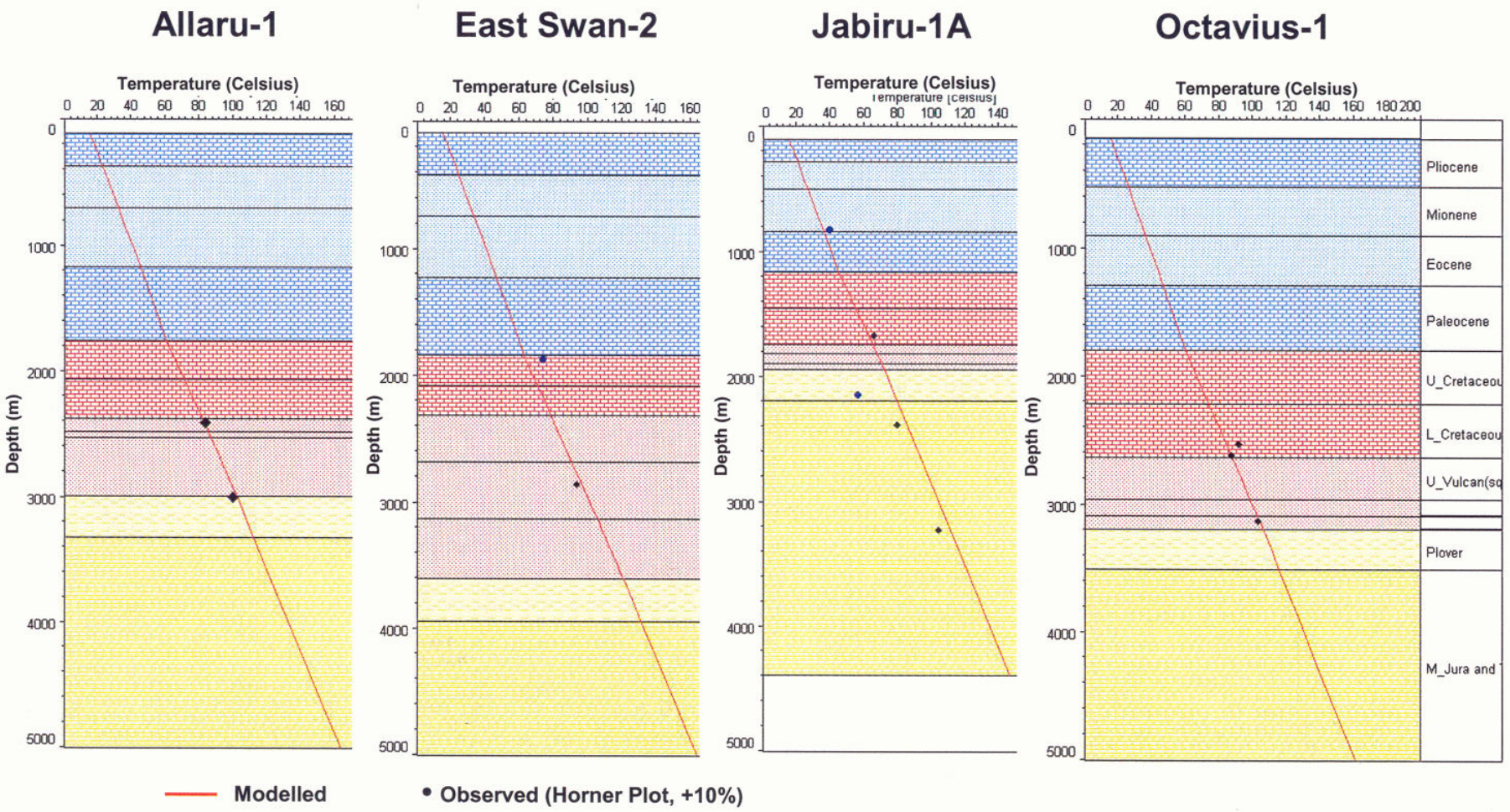

Figure 5-1b. Present day heat flow calibration results (BHT).

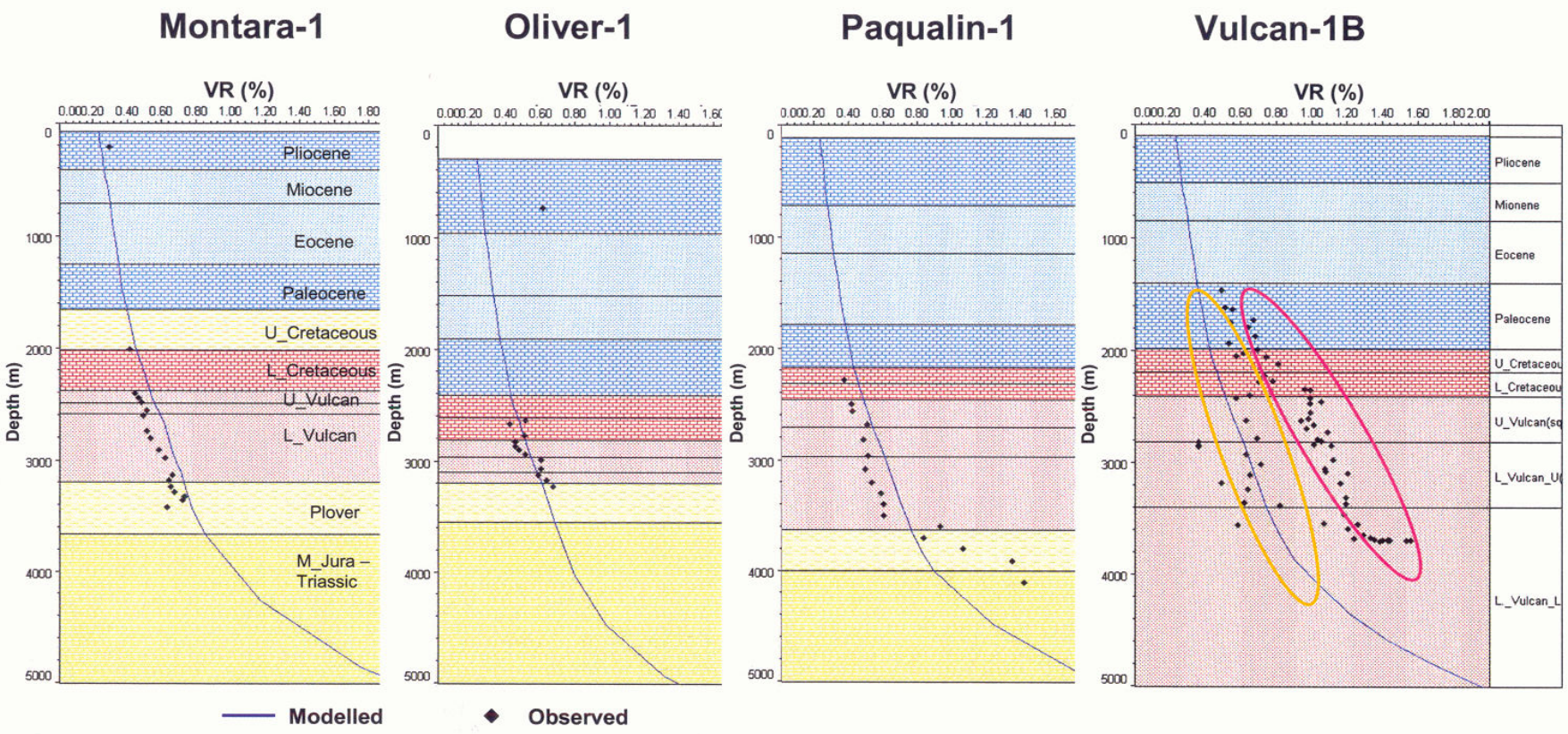

Figure 5-2a. Heat flow calibration results using vitrinite reflectance (VR%).

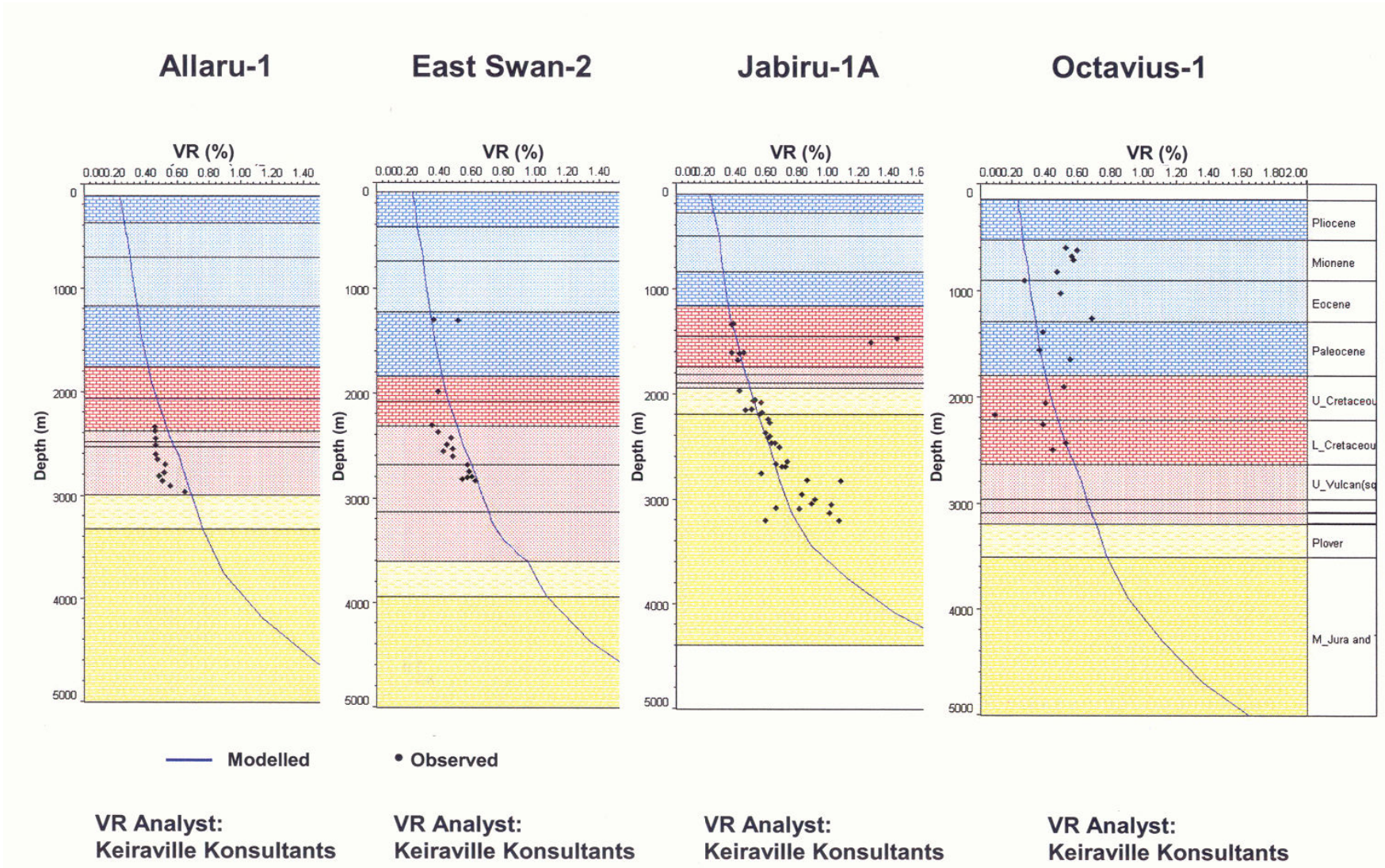

Figure 5-2b. Heat flow calibration results using vitrinite reflectance (VR%).

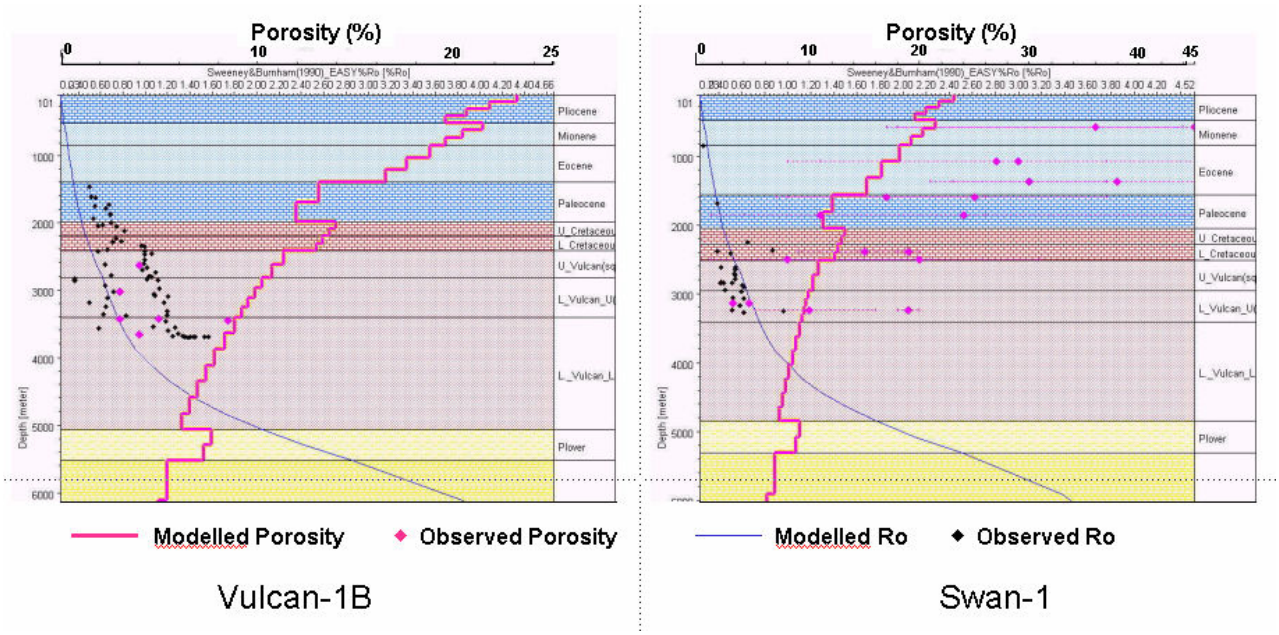

Figure 5-3. Examples of compaction calibration results (Vulcan-1B and Swan-1).

5.2 RESULTS OF 2D MODELLING

The 2D modelling results for VTT-05 and VTT-14 are shown in Figures 5-4 and 5-5, respectively. The simulation calculations were completed in about one hour using a high-end Pentium 4 PC with 2GB of RAM.

5.2.1 VTT-05 (Puffin – Swan Graben – Skua section)

5.2.1.1 Generation and migration in the Swan Graben

Based on the input parameters, the modelling results in Figure 5-4 suggest that oil generation in the Lower Vulcan Formation in the Swan Graben commenced within the lowermost part of the Lower Vulcan Formation in the Late Jurassic (at approximately 144 Ma). These results are consistent with those of Baxter et al (1997) and Kennard et al (1999). The modelling results indicate that at the present day, the upper part of the Lower Vulcan Formation is in the immature part of the oil generation window, while the lower part is within the gas window (Fig. 5-4d).

Horizontal and downward oil/gas expulsion from the Lower Vulcan Formation into the Plover Formation sandstones was active from the Early Cretaceous to the present day. This timing of expulsion onset is significantly earlier than that proposed by Kennard et al (1999), who suggested that oil expulsion began during post-Eocene times. The main reason for this difference is thought to be the difference in the oil saturation thresholds for the expulsion. In our modelling, 10% was used for the threshold, whereas Kennard et al (1999) used 40%. In order to test this hypothesis, a simulation using a 40% threshold was also carried out. As a result, onset of oil expulsion was observed later than in the simulation using a value of 10%, though it was still in the mid-Cretaceous (at approximately 100Ma). As both models used the same burial histories and source rock properties, this difference in timing may reflect the use of a different compaction model. As such, further investigation of the sensitivities in the compaction prediction may be needed.

The model predicts that expelled hydrocarbon from the Lower Vulcan Formation migrated through the Plover Formation carrier bed, both horizontally and vertically, and began to accumulate in the Skua structure during the Early Cretaceous. This result is consistent with the results of a geochemical study by Edwards et al (2004), which indicated that the Skua oil is sourced principally from the Lower Vulcan Formation. The modelling also predicts that the liquid component in the structure increases with time.

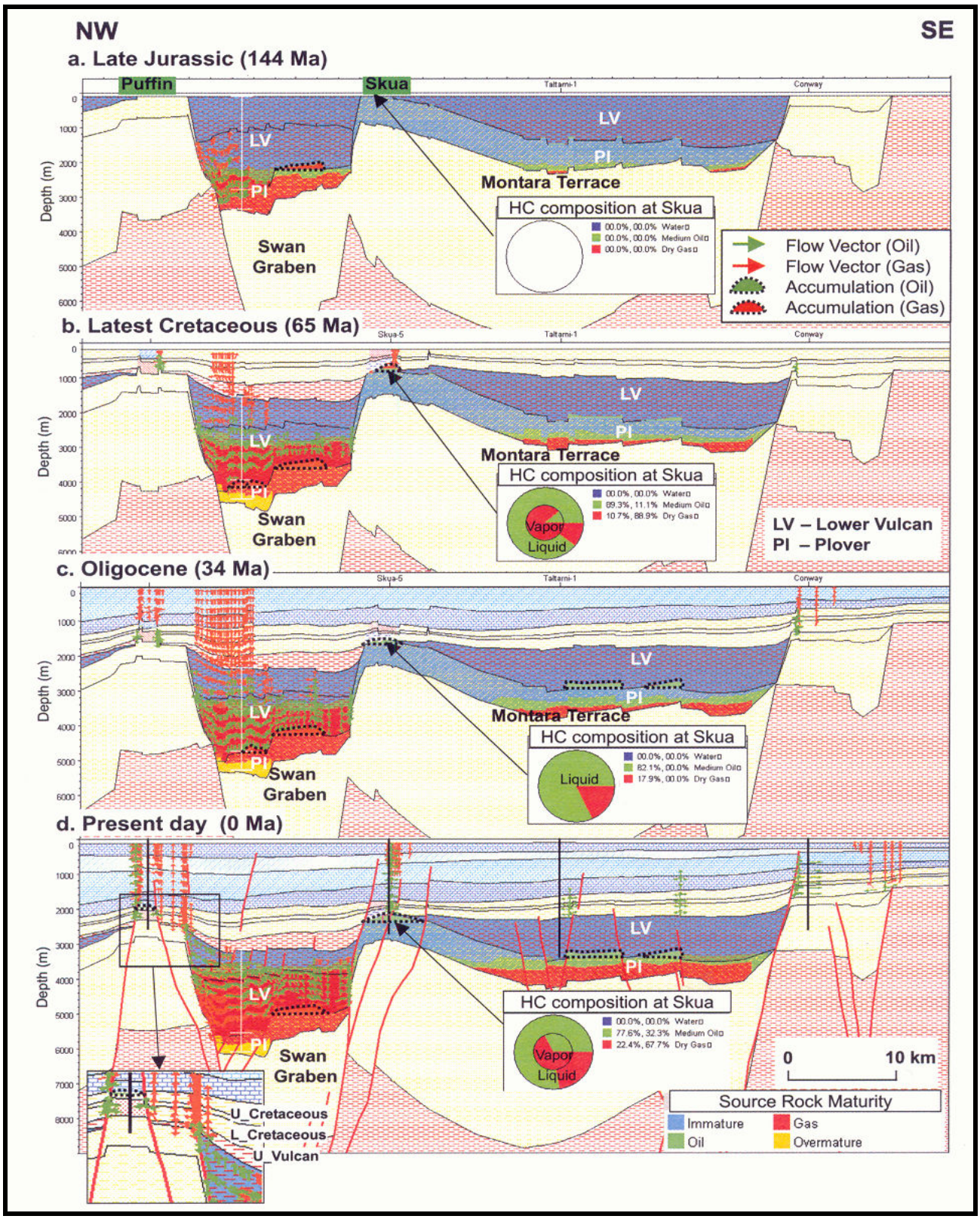

Figure 5-4. 2D modelling results in VTT-05.

In contrast, the modelling suggests that oil migration from the Lower Vulcan Formation into the Late Cretaceous Puffin Formation sandstones in the Puffin Field occurred by lateral migration along the bottom of an Upper Vulcan Formation seal and by vertical

migration above the edge of the seal (Fig. 5-4d). The modelling results indicate that a very thin or absent suite of basal Early Cretaceous sealing units have been critical in allowing the accumulation of hydrocarbons in the Late Cretaceous at the Puffin Field. Such observations probably have wide application to exploration for traps similar to Puffin throughout the region.

Most oil and gas accumulations discovered in the region are trapped within faulted traps and horsts, which formed during Jurassic rifting (Woods, 1992; Ch. 2.2). On the other hand, the principal sealing units in this region are the post-rift, Early Cretaceous marine sediments of the Echuca Shoals Formation (Kivior, 2002; Ch. 2.2). The modelling results in Figure 5-4 suggest that hydrocarbon generation and expulsion in the Lower Vulcan Formation, the principal source unit in the Swan Graben, was active from the Early Cretaceous to the present day. This relationship between hydrocarbon generation/expulsion and structure/seal formation suggests that some amount of hydrocarbons could have been generated before the top seal was deposited or was well-compacted.

Oil/gas generation within the Plover Formation source rocks started in the Late Jurassic and the Plover Formation is presently located within the gas to over mature window at the present day in the Swan Graben (Fig. 5-4d). Additional modelling results, which considered only the source rock potential of the Plover Formation, indicate that oil and gas generated within the Plover Formation could potentially have migrated into the Skua structure. This result is inconsistent with the geochemical results of Edwards et al (2004), which suggested that the oil in Skua was derived principally from the Lower Vulcan Formation. However, carbon isotopic work by Edwards et al. (2000) did suggest that some of the oil in the Skua accumulation could have been sourced from units older than the Lower Vulcan Formation. As such, ambiguities exist in the geochemical data as to the exact source of the oil in Skua.

If the oil in Skua has actually been solely contributed from the Lower Vulcan Formation source rock, then a possible explanation for the inconsistency between the modeling and the geochemistry could be the inability, within PetroMod^{TM}, to account for juxtaposition in a sophisticated manner. Future work, which allows re-gridding for each time step (using the “Palaeo geometry” function in PetroMod^{TM}) should solve this problem.

5.2.1.2 Generation and migration in the Montara Terrace

The modelling results indicate that the Late Jurassic succession (Lower Vulcan Formation) is thermally immature over the Montara Terrace and could thus not have contributed to the hydrocarbon inventory in fields such as Skua, Montara and Padthaway (Fig. 5-4d). The main part of the Plover Formation, however, began to enter the oil window in this region after the Oligocene (Fig. 5-4c) and is in the oil to gas window at the present day (Fig. 5-4d). This result is consistent with the geochemical study results by Edwards et al (2004), which indicated that oil in the Montara and Padthaway accumulations are not sourced from the Late Jurassic Lower Vulcan Formation but from the Early to Middle Jurassic Plover Formation.

5.2.2 VTT-14 (Southern Cartier Trough – Jabiru Trend – Challis)

5.2.2.1 Generation and migration in southern Cartier Trough

The modelling results shown in Figure 5-5 indicate that oil generation within the lowermost parts of the Lower Vulcan Formation in the southern Cartier Trough began in the Early Cretaceous. The lower part of the Lower Vulcan Formation is in the oil and gas window at the present day (Fig. 5-5d), and is typically at a lower thermal maturity than is seen in the Swan Graben.

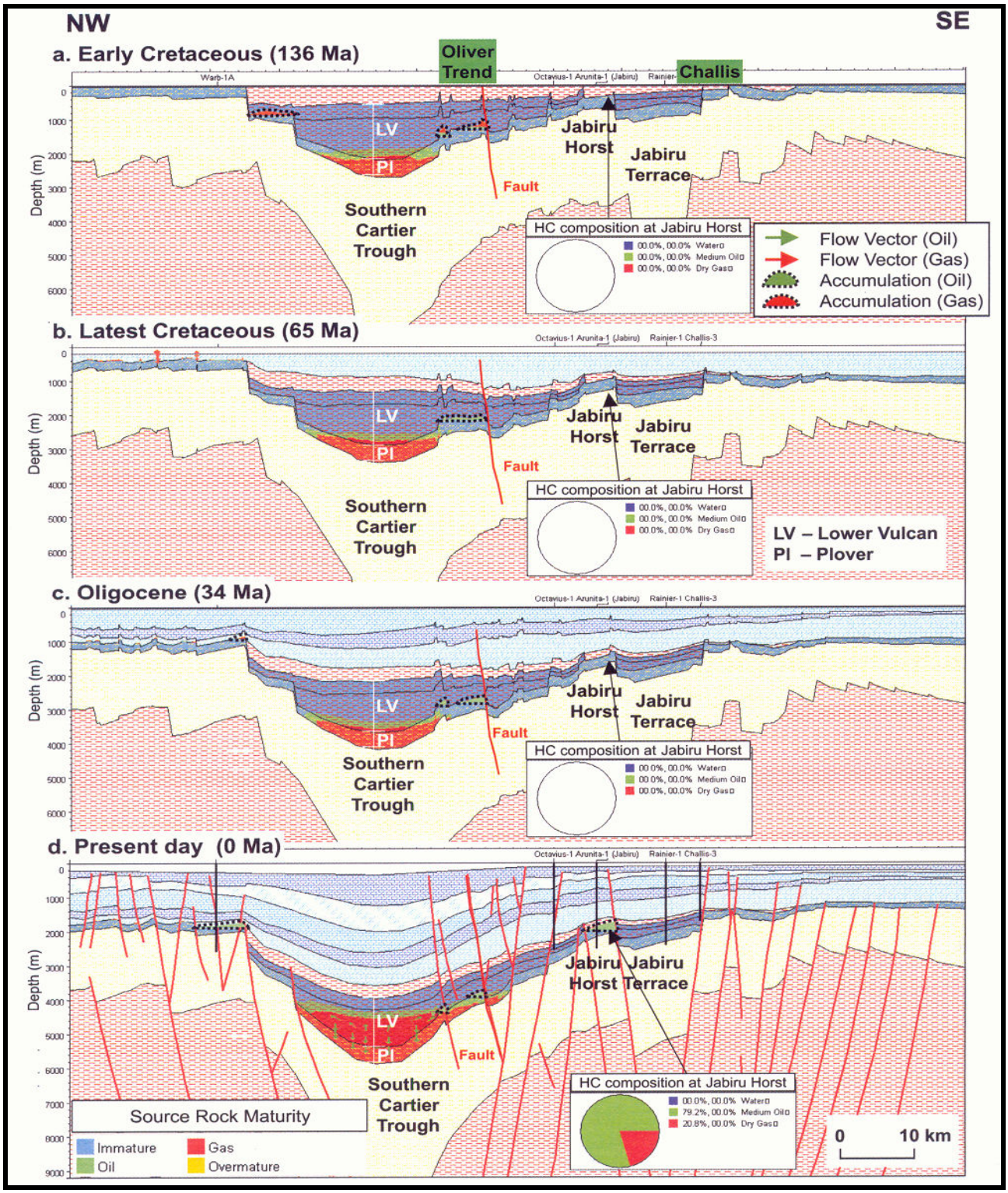

Figure 5-5. 2D modelling results in VTT-14.

Horizontal and downward oil/gas expulsion from the Lower Vulcan Formation into the Plover Formation sandstones was active from the Late Tertiary to the present, which is significantly later than the expulsion modelled in the Swan Graben. This timing for the onset of expulsion is consistent with the study results of Kennard et al (1999), which indicated that oil expulsion was initiated post-Miocene. These results are also

consistent with the past work by Lisk and Eadington (1994), who utilised oil fluid inclusion data in wells located in the southern Cartier Trough. These workers proposed that oil generation in the Cartier Trough took place post-Oligocene (<30 Ma), while expulsion occurred by the Miocene (<20 Ma).

Horizontal oil migration from the Lower Vulcan Formation into, and along, the Oliver structural trend took place via the Plover Formation carrier bed from the Late Tertiary. Oil accumulated in the Oliver trend did not, however, (in this model) migrate further to the south-east (in the up-dip direction) until the present day due to the presence of a relatively large, landward-dipping (down to the south-east) fault (Fig. 5-5d). This fault acted as an effective barrier to migration in the 2D model, and hence oil accumulation into the Jabiru structural trend did not occur until very recently (within the last 5 Ma) in this model.

Oil/gas generation in the Plover Formation within the Cartier Trough started in the Early Cretaceous and the Plover Formation is presently in the gas window (Fig. 5-5d).

5.2.2.2 Generation and migration on the Jabiru Terrace

Oil and gas accumulation within the Challis structure did not occur in the model. This was due to the fact that the Late Jurassic source rocks on the Jabiru Terrace are modeled as thermally immature (Fig. 5-5d), which may suggest that the oil in the Challis structure was not derived from region of the Jabiru Terrace. Geochemical studies by Edwards et al (2004) suggest that oil in Challis is correlated to the Lower Vulcan Formation. Possible source kitchen areas are the mature Cartier Trough or the Swan Graben. My 2D modelling results, however, suggest that oil migration from the Cartier Trough appears to be less likely because of the geology, which would require migration bypassing, or spilling out from, the Jabiru Horst.

5.3 RESULTS OF 3D MODELLING

5.3.1 Generation and migration from the Lower Vulcan Formation

The results of the 3D Hybrid flow simulation are shown in Figure 5-6. The horizontal grid interval used for this simulation was about 2.4 km. The simulation calculations were completed in about 5 hours using a high-end Pentium 4 PC.

5.3.1.1 Swan Graben

The simulation results indicate that oil generation within the Lower Vulcan Formation, the interpreted principal source rock in the region, was first initiated in the deepest parts of the Swan Graben in the Late Jurassic. Oil expulsion within the Swan Graben became active from the Early Cretaceous (Fig. 5-6a). Expelled oil and gas migrated both to the south-east into the Skua structural trend (including the north-east extension of the Skua structure) and to the north-west, into the Puffin structural trend. These results are similar to those obtained from the 2D modelling of VTT-5. Active oil migration from the north-eastern Swan Graben into the Jabiru structure was also simulated in the Early Cretaceous (Fig. 5-6b) and in the latest Oligocene (Fig. 5-6d).

Oil/gas migration along the culmination of the Eclipse-Cassini-Challis structural trends was also active throughout the Tertiary (Figs 5-6d, 5-6f and 5-6h).

5.3.1.2 Paqualin Graben

Gas charge in the Late Cretaceous (Fig. 5-6b) and oil charge during the Tertiary (Figs 5-6d, and 5-6f) were also simulated in the Paqualin Graben. These results are consistent with one of the 3D flow path modelling results of Chen et al (2002), in which the saturation-based and compactional expulsion model by Kennard et al (1999) was used.

5.3.1.3 Cartier Trough

Oil generation in the Lower Vulcan Formation was initiated in the narrow area of the southern Cartier Trough in the Early Cretaceous (Fig. 5-6a). Although subsequent oil expulsion began in this area after the Oligocene, the areal extent of oil generation and expulsion did not extend further to the north-east – that is to the central Cartier Trough - until the latest Miocene (Fig. 5-6e). The geographic extent of generation and expulsion increased throughout the central Cartier Trough suddenly, with rapidly

increasing temperatures experienced from approximately 5 Ma to the present day; this change was due to rapid Pliocene subsidence and burial (Fig. 5-6g). This Pliocene burial resulted in the rapid maturation of the Late Jurassic source system and the expulsion of oil within the last five million years. The modelling results indicate that the central Cartier Trough is probably the main source kitchen for the Oliver accumulation (Fig. 5-6h).

Post-Miocene oil migration from the southern Cartier Trough into both the Octavius structure and the Jabiru structure, via the Plover Formation, was also simulated (Figs 5-6d, 5-6f and 5-6h).

These results are consistent with the results of Lisk and Eadington (1994), who used kinetic simulation and oil fluid inclusion analysis in wells located south of the Cartier Trough. Their study indicated that oil generation in the Cartier Trough took place post-Oligocene (<30 Ma), while expulsion was post-Early Miocene (<20 Ma). The simulation results obtained in the present study are also consistent with the results of Chen et al (2002), who proposed that the Jabiru oil accumulation was sourced from the southern Cartier Trough and that charging occurred in the Miocene. However, the modeling undertaken in this thesis, predicts, not only oil migration into the Jabiru structure from the southern Cartier Trough after the Miocene but also early migration from the north-eastern Swan Graben during the Early Cretaceous (Fig. 5-6b).

5.3.1.4 Comparison of timing

Figs. 5-7 show the temporal variation of the oil generation and expulsion from the Lower Vulcan Formation (Top 4a). Oil expulsion in the central Swan Graben began, although at low rates, in the Early Cretaceous. The modelling suggests that the transformation ratio (that is the extent of transformation of the organic matter) of the Lower Vulcan Formation (Top 4a) in the central Swan Graben at the end of the Early Cretaceous (100Ma) was around 12%, 48% at the end of Early Tertiary (25Ma) and 77% at present day (Fig. 5-7a). Clearly, this indicates that some amount of the earliest-generated hydrocarbons within the Swan Graben could have been lost, as traps such as Skua could have begun receiving charge very soon after deposition of the regional seal.

On the other hand, oil expulsion in the central Cartier Trough intensified in the Late Tertiary, when collision-related sediment loading induced rapid generation and expulsion (Fig 5-7b). Modelling results suggest that the transformation ratio of the Lower Vulcan Formation (Top 4a) in the central Cartier Trough is 45%, even at the

present day.

In the case of both the Swan Graben and the Cartier Trough, it appears that the *principal* phase of expulsion was in the Tertiary.

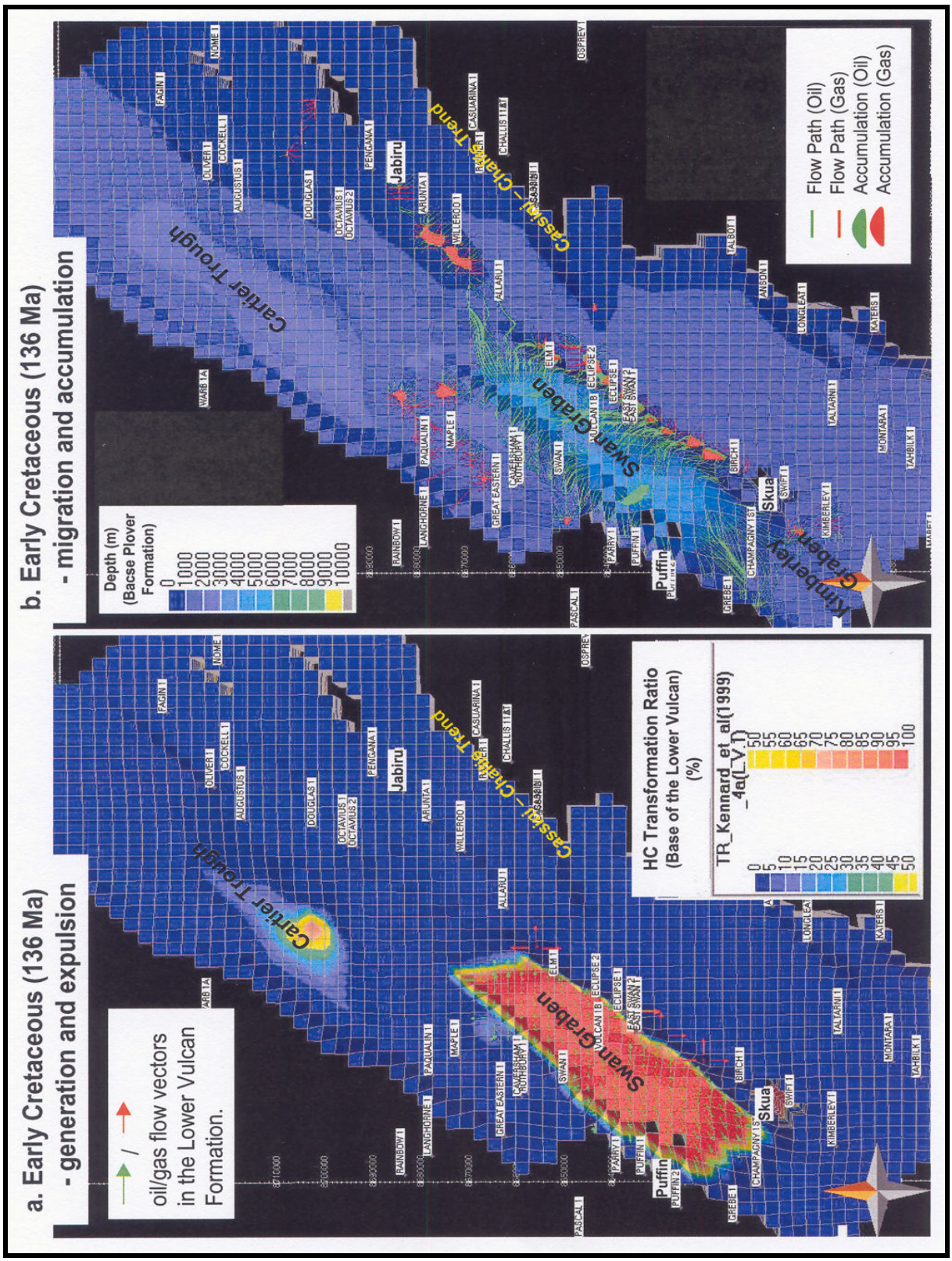

Figure 5-6 a & b. 3D modelling results (source rock potential: only in the Lower Vulcan Formation: 136 Ma).

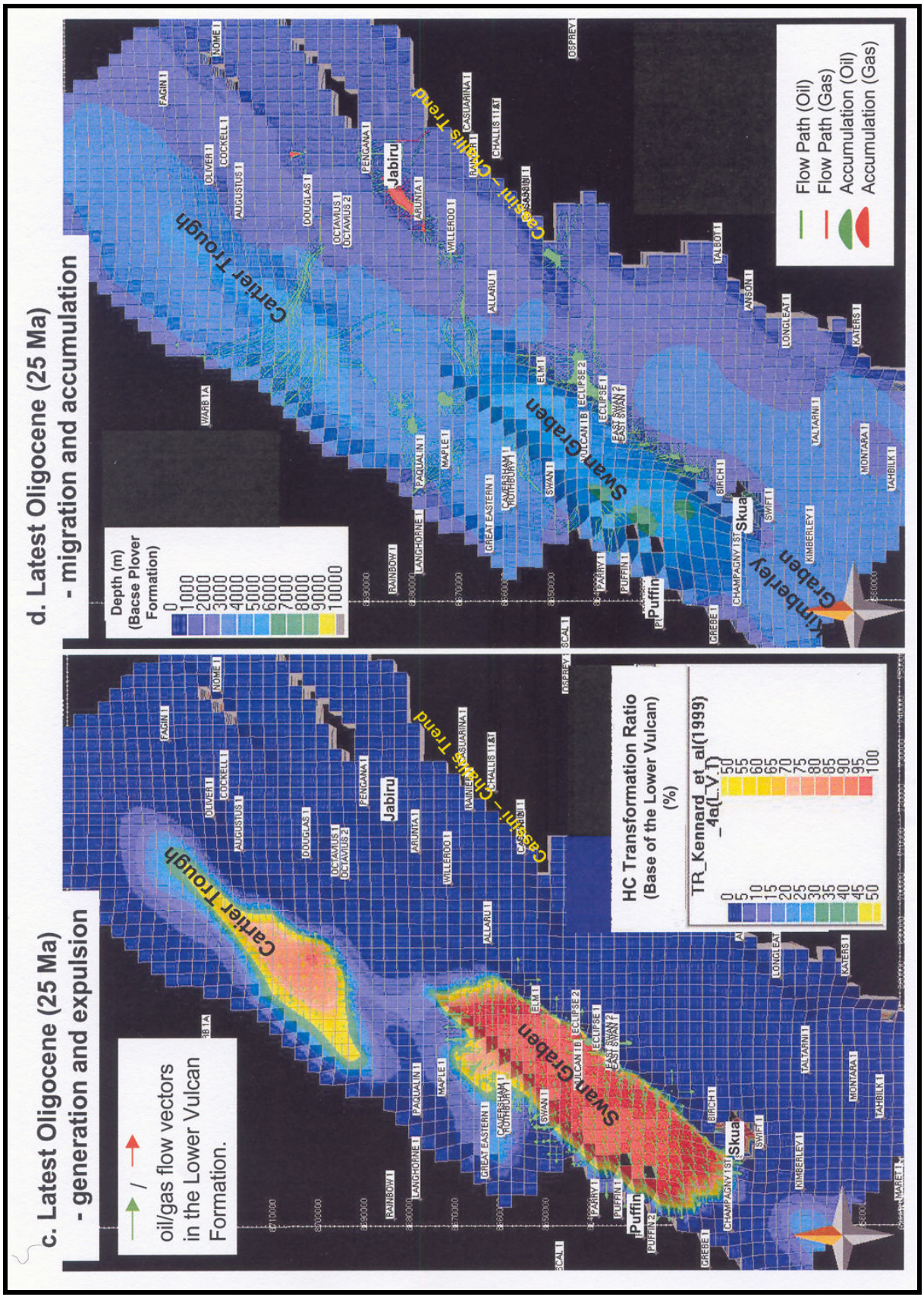

Figure 5-6 c & d. 3D modelling results (source rock potential: only in the Lower Vulcan Formation: 25 Ma)

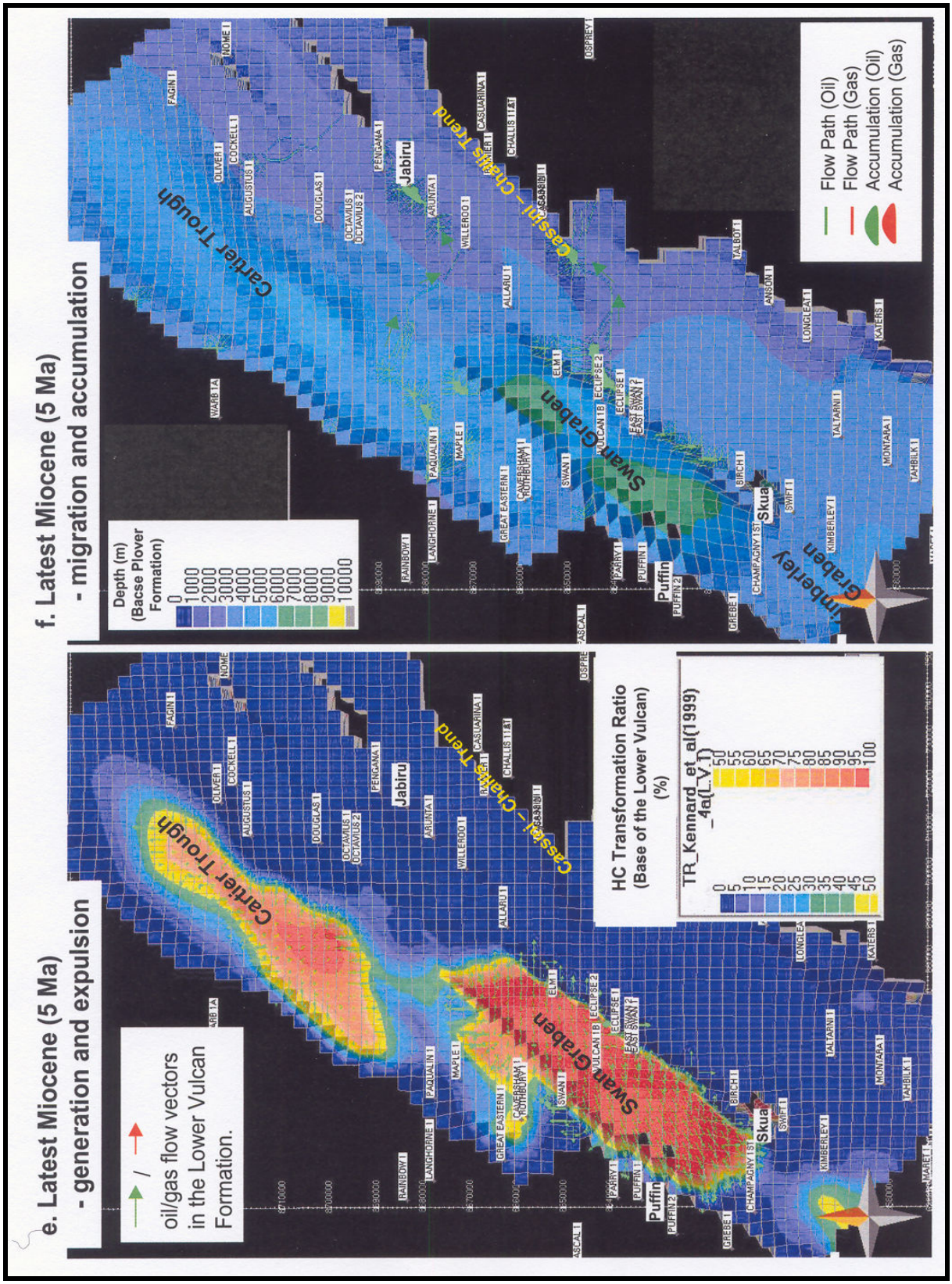

Figure 5-6 e & f. 3D modelling results (source rock potential: only in the Lower Vulcan Formation: 5Ma)

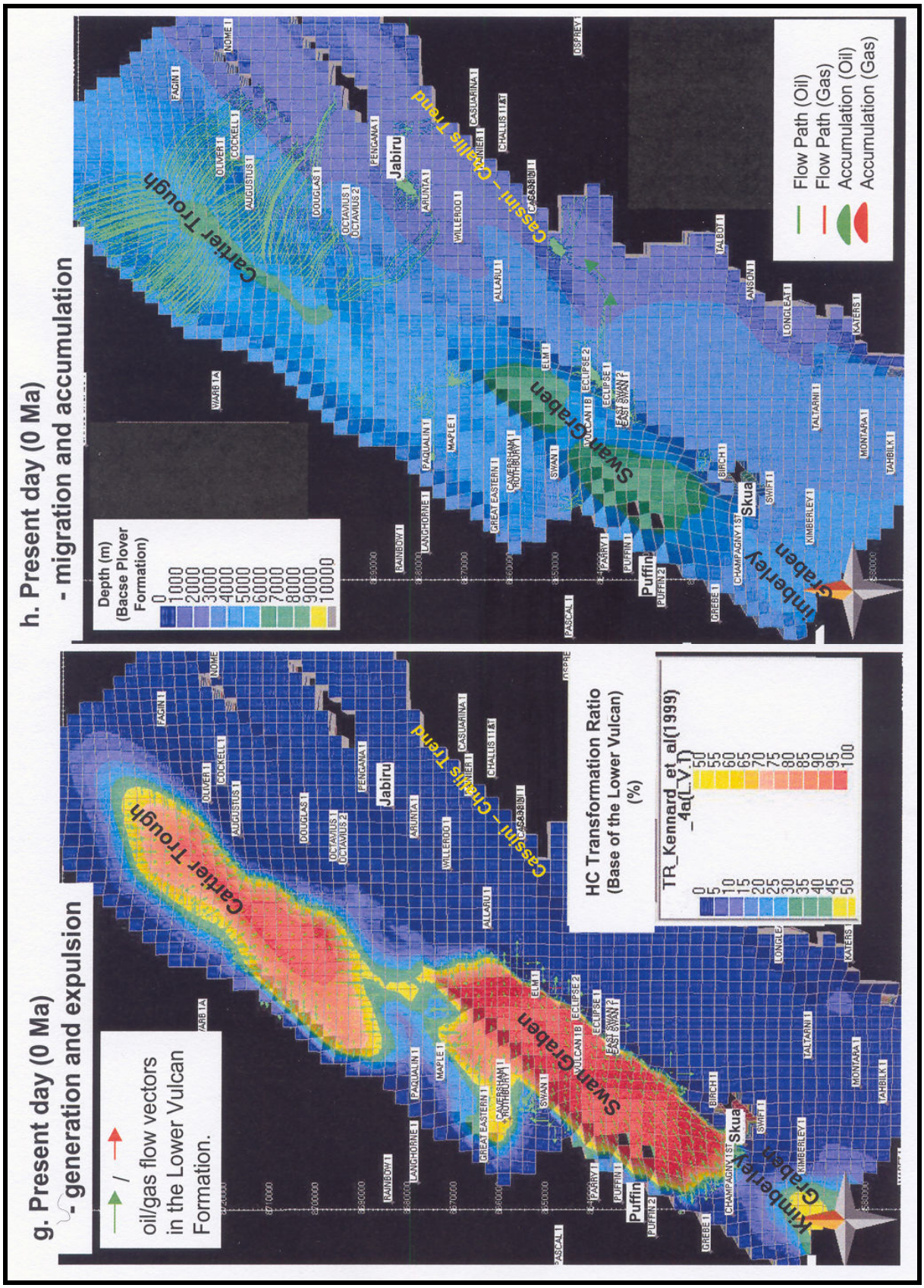

Figure 5-6 g & h. 3D modelling results (source rock potential: only in the Lower Vulcan Formation: 0 Ma)

a. Central Swan Graben

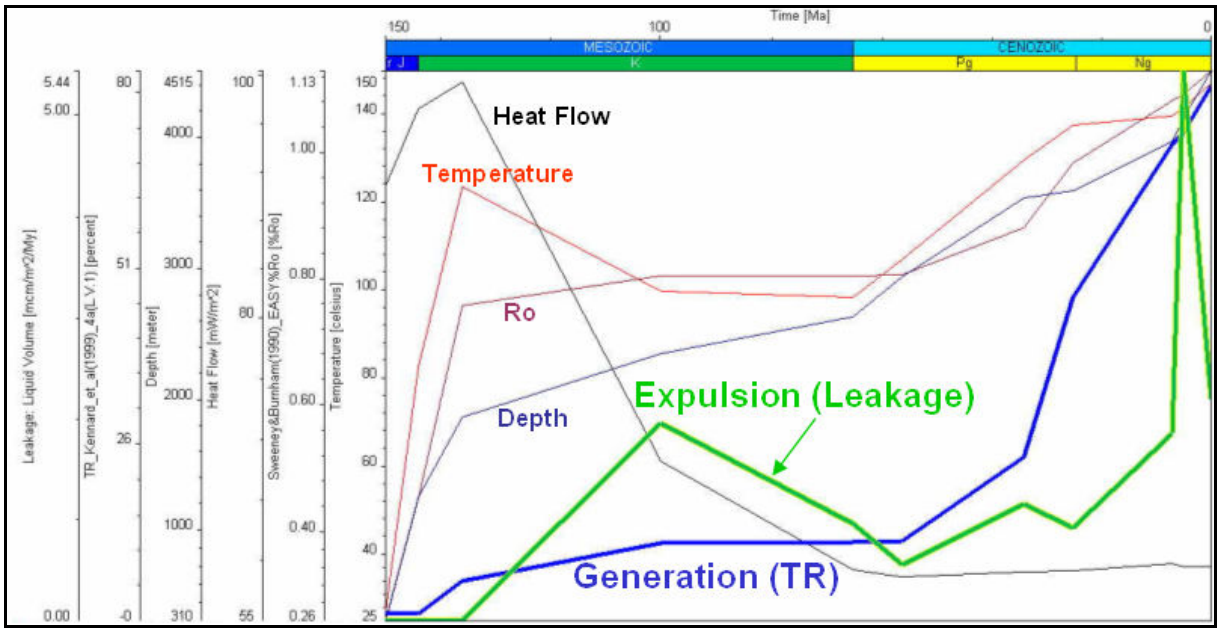

b. Central Cartier Trough

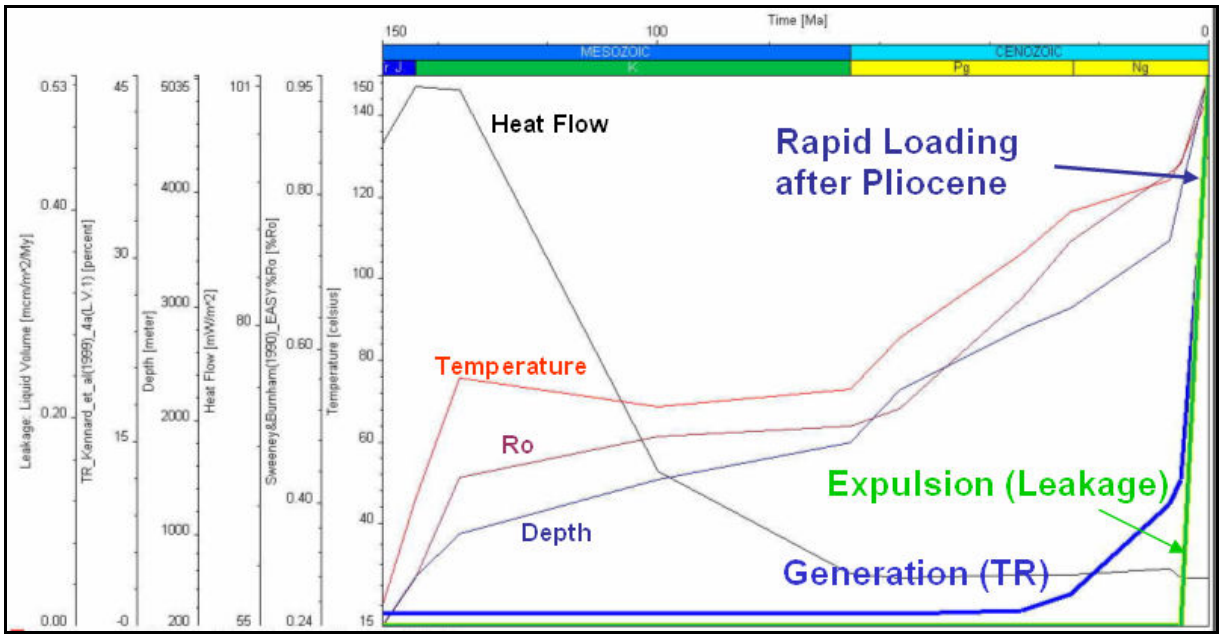

Figure 5-7. Timing of hydrocarbon expulsion from the Lower Vulcan Formation; a). Central Swan Graben: active expulsion from Early Cretaceous to present day. b). Central Cartier Trough: active expulsion from the Pliocene (5 Ma)).

5.3.2 Generation and migration from both the Lower Vulcan and Plover Formations

The 3D hybrid modelling results, considering the source rock potential of both the Lower Vulcan Formation and the Plover Formation, are shown in Figure 5-8. . The horizontal grid interval used for this simulation was also approximately 2.4 km.

5.3.2.1 Swan Graben

In this modelling, oil and gas migration into both the Skua and Puffin structural trends were also reproduced, as shown in Figure 5-8. Significant oil charge around the Eclipse structure was modelled (Figs 5-8b to 5-8f); this result is different to that obtained in the modelling which considered generation from only the Lower Vulcan Formation (Figs 5-6b, and 5-6f). Significant differences in gas migration were also evident in the two models. Migration of gas from the Swan Graben is more active in the model that considered the potential contributions from the Plover Formation, particularly with regard to migration onto the Jabiru Horst (Figs 5-8b to 5-8h).

Minor amounts of oil migration were also modelled from the local kitchen to the south of the Allaru-1 to Cassini-Challis trends (Figs 5-8g, and 5-8h), which was not recognized when only a Lower Vulcan Formation source rock was considered (Figs 5-6f, and 5-6h).

5.3.2.2 Paqualin Graben

Significant oil charge from the Paqualin Graben was modelled (Figs 5-8b, and 5-8f) when a contribution from the Plover Formation was included, again in sharp contrast to the results of the modelling carried out which only considered the source rock potential of the Lower Vulcan Formation (Figs 5-6b, and 5-6d).

5.3.2.3 Cartier Trough

Oil migration from the southern Carter Trough into the Jabiru structure and from the central Cartier Trough into the Oliver structure, was also simulated from the Early Cretaceous (Fig. 5-8b) and the Middle Cretaceous (Fig. 5-8c), respectively. As mentioned previously, the modelling results suggest that oil migration from the Lower Vulcan Formation in the Cartier Trough started from the Oligocene. This means that in the Cartier Trough, the contribution of the Plover Formation source rock is more important than the Lower Vulcan Formation, prior to the Oligocene. In this modelling, however, the source rock parameters of the Plover Formation in Skua-1, which is located adjacent to the Swan Graben, were used. In order to better constrain the contribution from the Plover Formation source rock in the Cartier Trough, further investigation of its source rock potential in this area needs to be undertaken.

5.3.2.4 Kimberley Graben

In the 3D modelling, oil migration from the Plover Formation in the Kimberley Graben, the south-western extension of the Swan Graben, into the Montara and Tahbilk structures occurred from the Late Tertiary (Figs 5-8f to 5-8h). This result is consistent with geochemical results of Edwards et al (2004), which indicated that oil from the Montara and Padthaway accumulations are sourced from the Plover Formation.

5.3.2.5 Montara Terrace

When the source potential of the Plover Formation was considered in the modelling, an active oil charge in the Montara Terrace (Figs 5-8g, and 5-8h) was modelled from approximately 5Ma; this was was not predicted when only the Late Jurassic source system was modelled (Figs5-6f, and 5-6h).

This result highlights the importance of the source rock system within the Plover Formation to the overall hydrocarbon inventory in this area. Oil migration into the Talbot structure is modeled from 5 Ma, when the associated source rock is considered.

5.3.2.6 Modelling Known Accumulations

In terms of hydrocarbon migration processes, most of the oil/gas fields in the region could be simulated successfully at the present day (Fig. 5-9). Specific exceptions were gas migration to Oliver, Montara and Tahbilk. Further studies that could potentially improve the simulation of these fields could include the following:

- Taking into account the effects of the locally high heat flows implied from the heat flow calibration;
- An improvement in the constraints on source rock kinetics and the areal variation of organic richness (TOC), and the organic facies, in the Plover Formation; and
- The possible contribution of deeper source rocks, such as from the Triassic, and even the Permian.

In terms of the hydrocarbon accumulations, the Jabiru accumulation (oil: from both the Lower Vulcan and the Plover Formation) and the Montara accumulation (oil: from the Plover Formation) could be simulated successfully at the present day, as shown in Figure 5-8h. The Jabiru result is interesting, given that the geochemistry data of

Edwards et al. (2004) indicate that the oil in Jabiru is principally sourced from the Late Jurassic source interval.

On the other hand, many of the oil/gas accumulations, such as the Oliver, Challis, Puffin and Skua, could not be simulated successfully by the modeling (note that I am discussing here about accumulation rather than migration). One of the main reasons for the lack of success in modelling the accumulations could be the relatively coarse grid interval that was used in the 3D modelling. The total size of each grid area used in the simulation was about 6 km^2, which is large compared to the size of many of the hydrocarbon accumulations in the Vulcan Sub-basin (which are typically 4 – 10 km^2). The fact that no accumulation was simulated in the Oliver structure in the 3D model may be an example of this.

One conclusion of this study is that a finer grid interval is needed if the hydrocarbon accumulation in each individual structure is to be modeled reliably. A second factor, which contributes to the inability to resolve the known accumulations during the 3D modelling, could be the lack of a top reservoir (Plover Formation) surface in the original horizon data which were modelled. The inability to model the Puffin and Skua fields is an example of this modelling artifact.

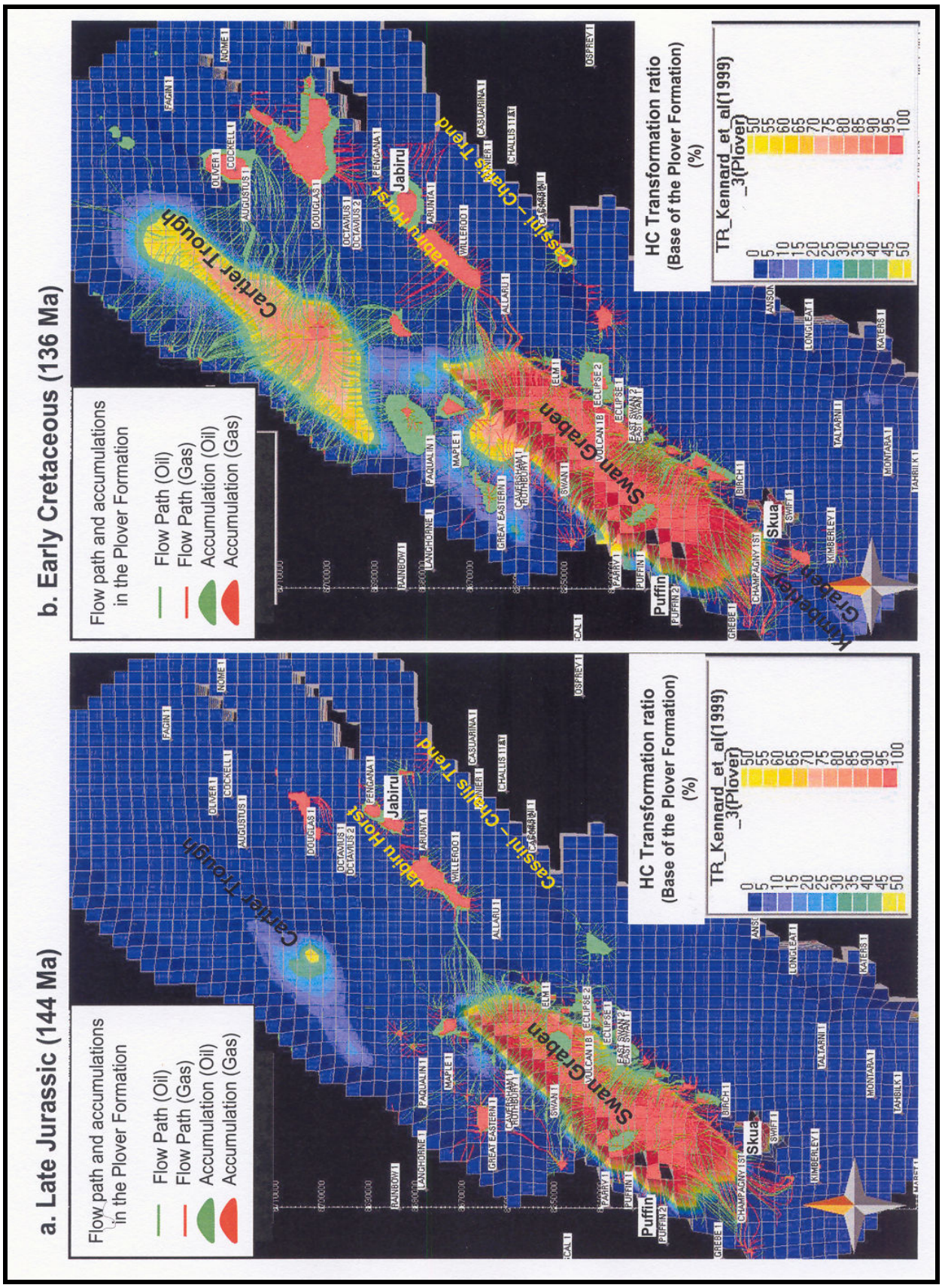

Figure 5-8 a & b. 3D modelling results: source rock potential in both Lower Vulcan Formation and Plover Formation: 144-136 Ma.

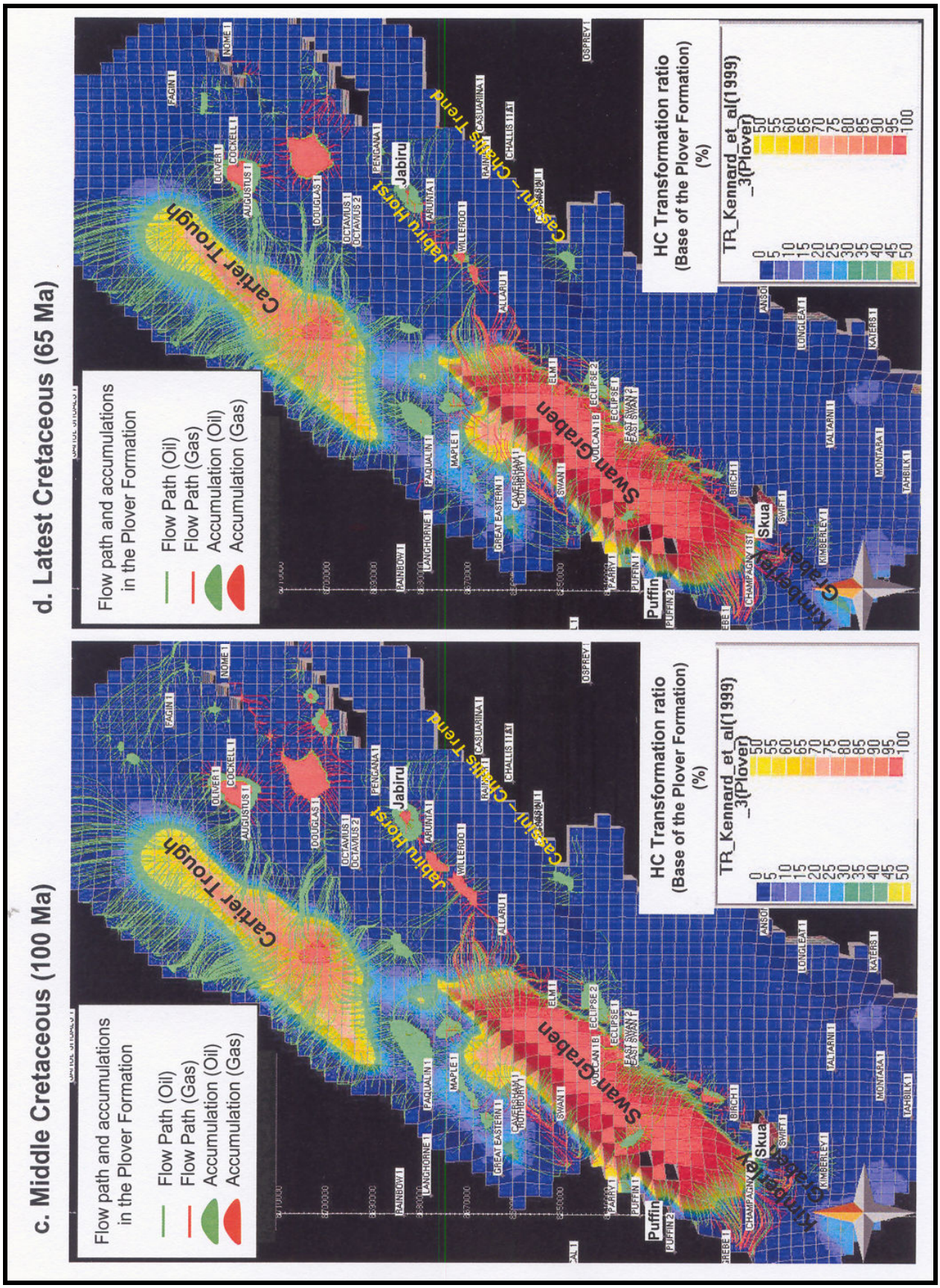

Figure 5-8 c & d. 3D modelling results: source rock potential: in both Lower Vulcan Formation and Plover Formation: 100-65 Ma.

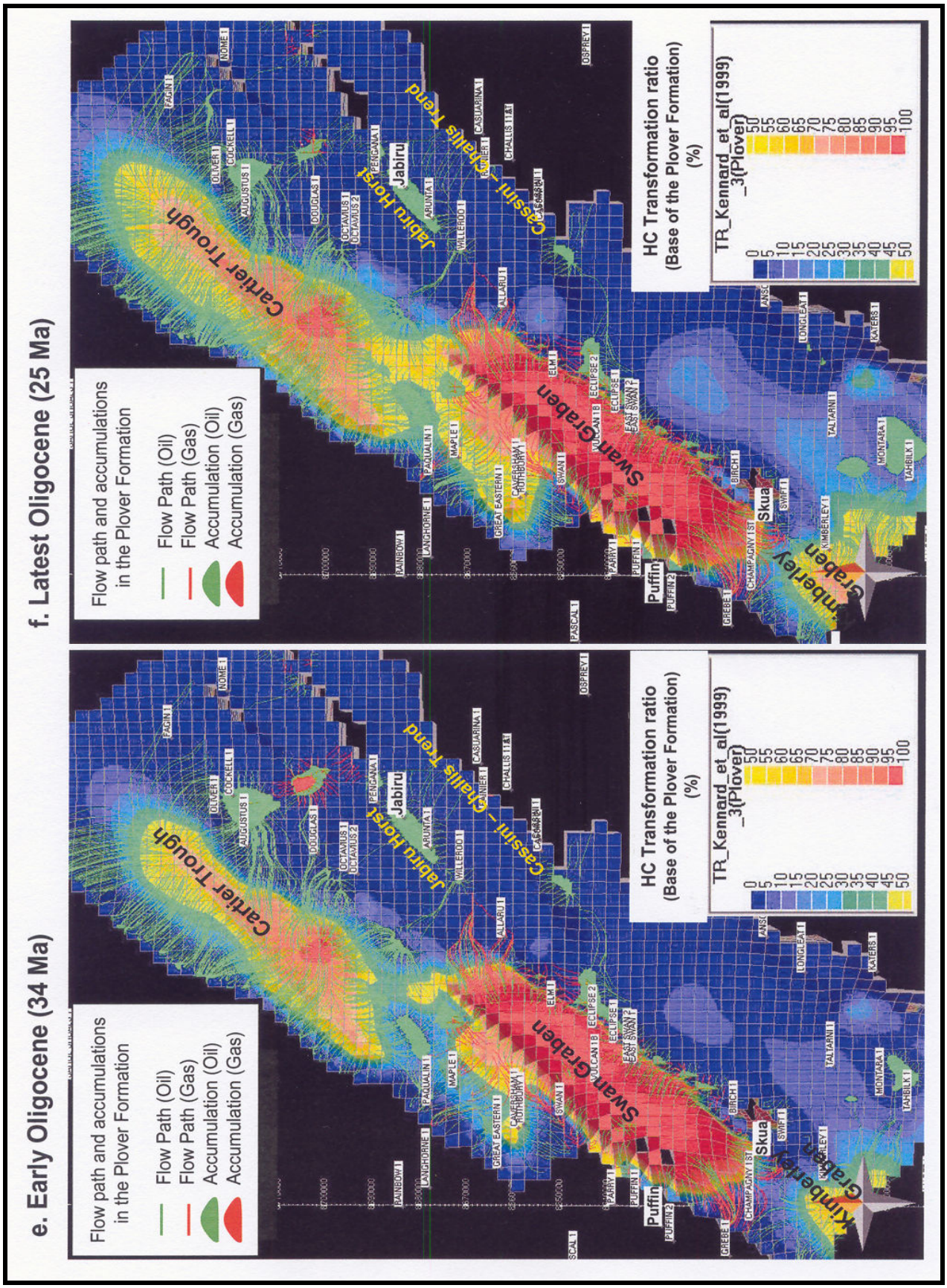

Figure 5-8 e & f. 3D modelling results: source rock potential in both Lower Vulcan Formation and Plover Formation: 34-25 Ma.

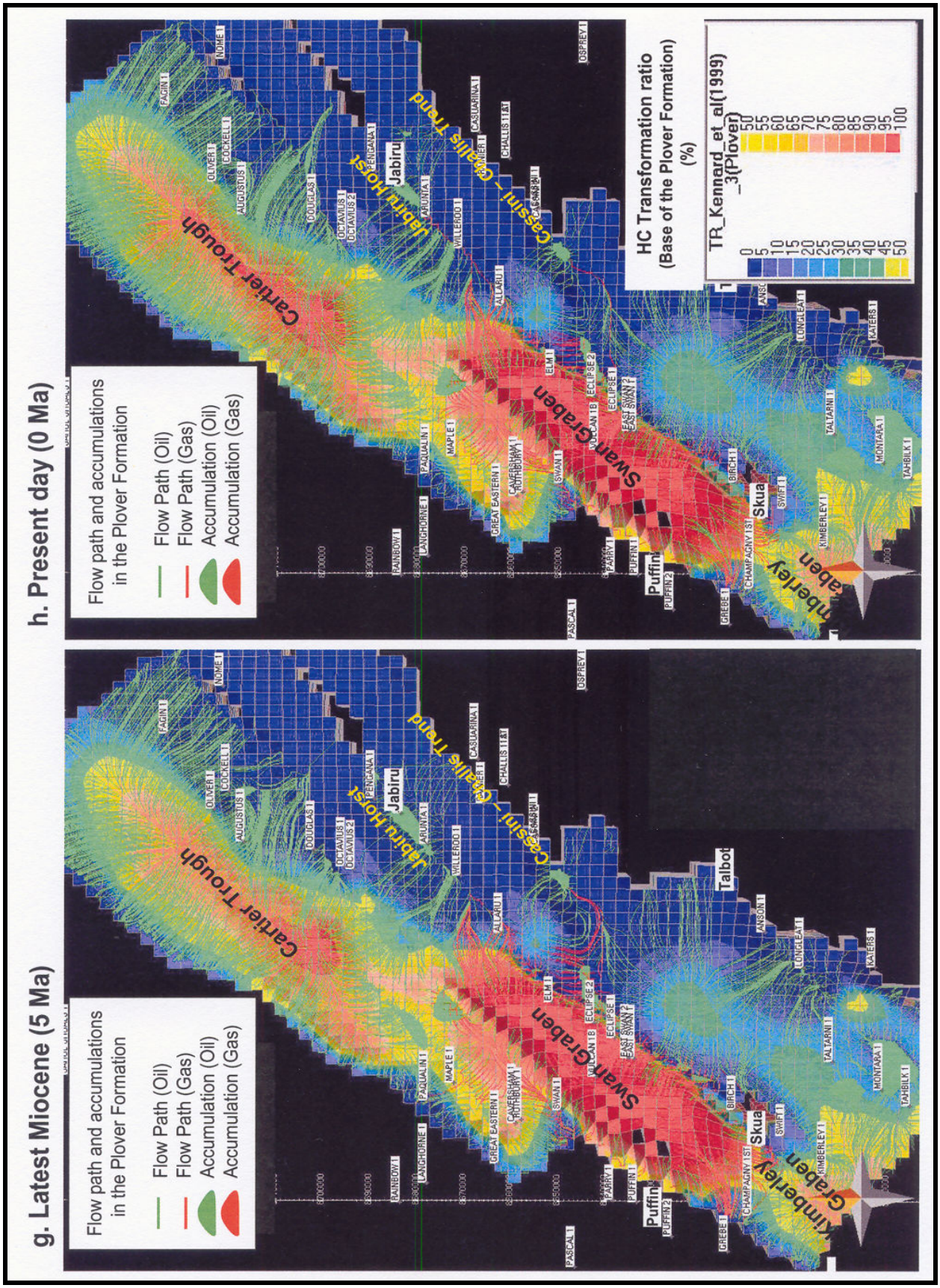

Figure 5-8 g & h. 3D modelling results: source rock potential in both Lower Vulcan Formation and Plover Formation: 5-0 Ma.

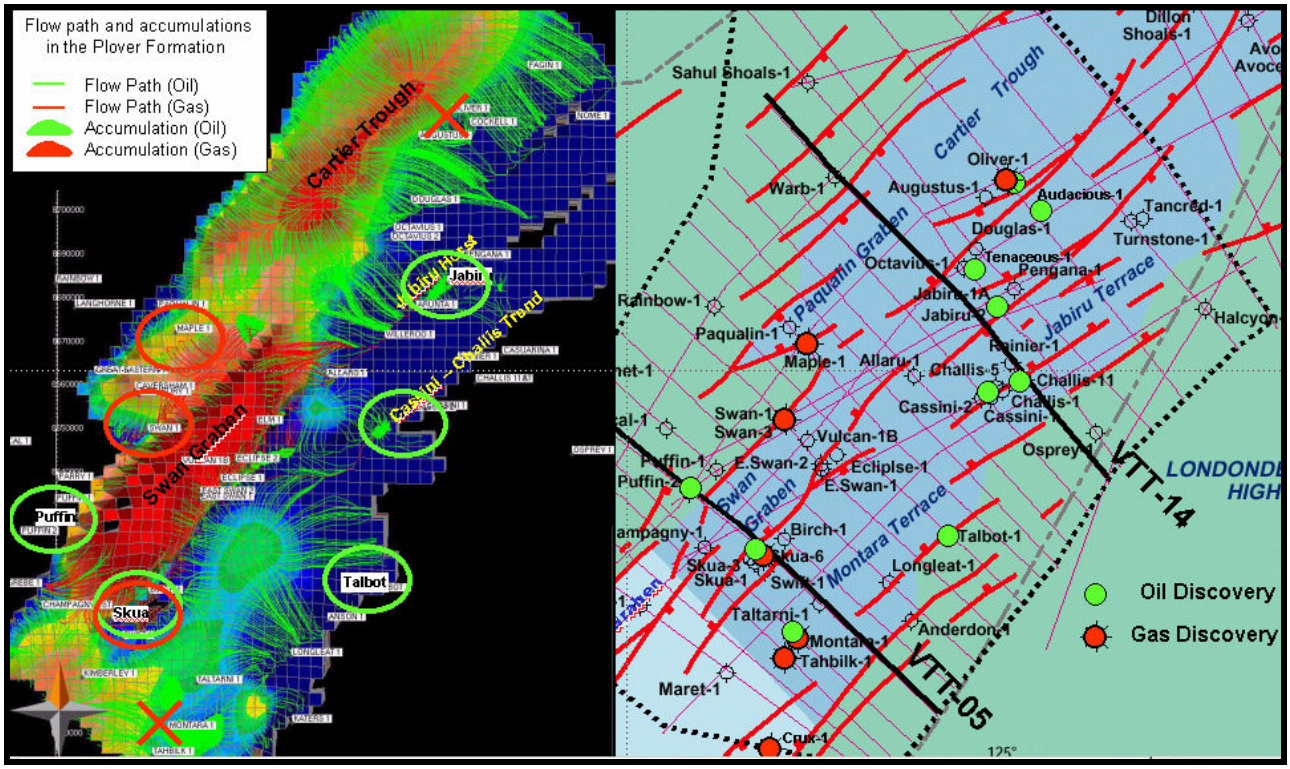

(a) 3D modelling result (b) Actual oil/gas field distribution

Figure 5-9. Comparison between the 3D modelling result (a) and the actual oil/gas field distribution (b). Successfully simulated accumulations are circled, unsuccessful ones are represented by a cross.

5.4 COMPARISON BETWEEN 2D AND 3D MODELLING

5.4.1 Generation and expulsion

In terms of the timing of the generation and expulsion of hydrocarbons, very similar results were obtained from the 2D and the 3D modelling. This indicates that if the simulation were conducted along sections which intersect the source kitchen area, an effective evaluation, in terms of the timing of generation and expulsion, could be carried out effectively using only 2D modelling.

On the other hand, the very significant benefit of the 3D modelling was recognized in understanding the spatial evaluation of the extent of the effective source kitchens. A map of the effective source kitchen area can be created relatively quickly and can provide a precise understanding of the petroleum prospectivity of assorted leads and prospects.

5.4.2 Migration and accumulation

Almost identical simulation results were obtained from the 2D and 3D modelling in relation to the migration of oil and gas from the Swan Graben into the Puffin and Skua structures. This is because both structures face directly into the Swan Graben and the modelled 2D section was oriented along the main migration pathway from the kitchen to these structures. In this case, 2D modelling could be utilised to effectively evaluate petroleum migration.

In contrast, ,different simulation results were obtained for the Jabiru structure from the 2D versus the 3D modelling. The 3D model predicted oil migration not only from the southern Cartier Trough after the Miocene but also early migration from the northern Swan Graben during the Early Cretaceous (Figs 5-6b, and 5-7b). This result indicates that 3D modelling is necessary if hydrocarbon charge from multiple kitchen areas is suspected.

In terms of the simulation of the accumulation of hydrocarbons within individual structures, the 2D modelling can be more useful because it is easier to simulate smaller culminations by utilizing a more appropriate, finer grid. This can be done with the 3D modelling, though computational times are greatly increased.

5.5 CONTROLS ON PETROLEUM MIGRATION AND ACCUMULATION

5.5.1 Control on migration

From the modelling results, horizontal/downward petroleum migration from the Lower Vulcan Formation into the Plover Formation sands is clearly an important migration mechanism and should be considered when assessing plays in the region. In the Swan Graben, in particular, the bounding faults have very large throws and hence hydrocarbon migration across faults is a relatively important process because of the large area of juxtaposition.

The orientation of the large faults, and specifically the trends of the culminations formed by them, is also an important control on petroleum migration. A good example of this is the active oil/gas migration along the culmination of the Eclipse-Cassini-Challis trend, from the eastern Swan Graben to the north-east (Figs 5-6d, f and h).

5.5.2 Control on accumulation and GOR

As has been described previously, not all of the oil/gas accumulations in the Vulcan Sub-basin could be simulated successfully via the 3D modelling, probably due to the relatively coarse grid interval and the lack of a top reservoir (Plover Formation) surface in the original horizon data. In this section, the oil accumulation and controlling factor for GOR will be discussed, especially focused on the Jabiru structure, where oil accumulation was simulated relatively successfully in the 3D modelling without being unduly affected by the above problems.

Figure 5-10 shows the 3D display (bird's-eye view) of a 3D simulation result in which source rock potential was ascribed only to the Lower Vulcan Formation. The left hand side of the figure shows simulated oil/gas accumulations at 136 Ma (in the Early Cretaceous), whereas the right hand depicts the oil/gas accumulations at the present day. Each of the colors visible in each kitchen areas (that is the Swan Graben and the Cartier Trough) represents the transformation ratio of the kerogen (i.e. the ratio of the kerogen that has been converted to hydrocarbon). An increase towards red colors indicates greater source rock maturation and hydrocarbon generation. Green lines extending from kitchen areas indicate oil migration paths and patches located at the end of these lines indicate the extent of hydrocarbon accumulation (red = vapor; green = liquid).

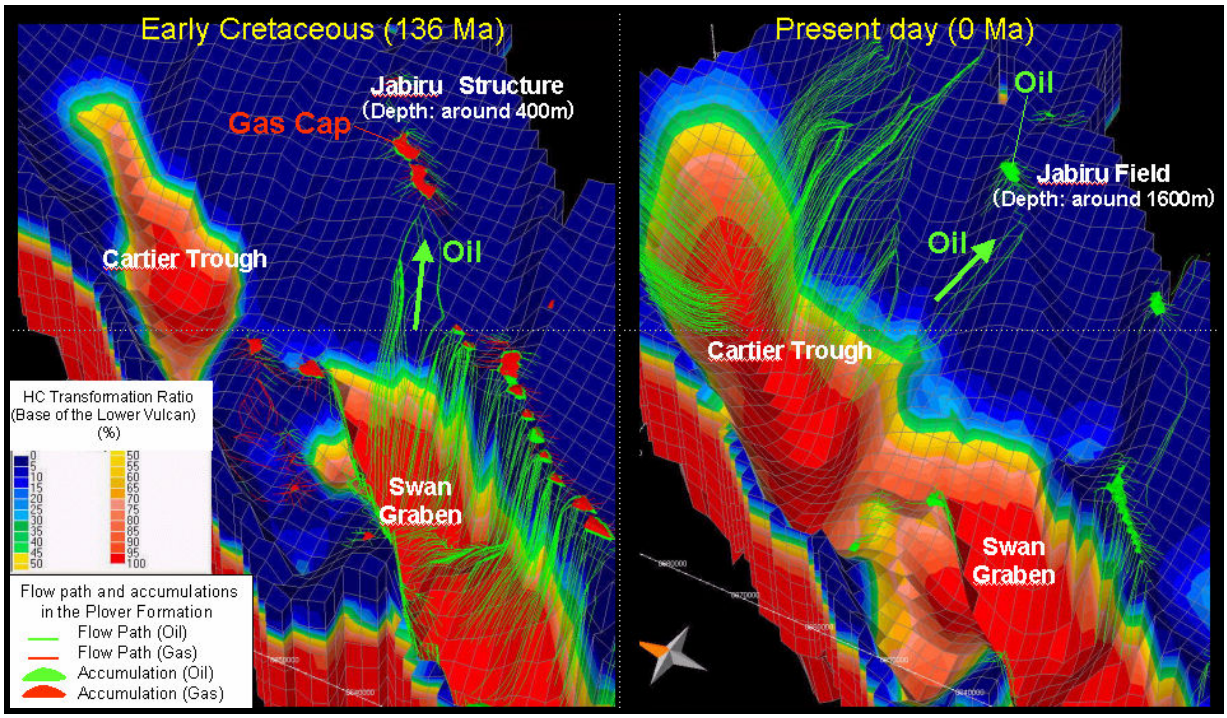

Figure 5-10. 3D display (bird's-eye view) for 3D simulation result (source rock potential: only in the Lower Vulcan Formation).

The simulation suggests that hydrocarbon generation and expulsion from the source rock in the Swan Graben was active at 136 Ma (Figure 5-10, left) and that expelled hydrocarbons migrated into the Jabiru structure along the culmination at the top of the Plover Formation. At this time (~136 Ma), the hydrocarbons that were accumulating in the Jabiru structure were mainly composed of gas. This was because a gas cap had formed in the Jabiru structure due to the low (reservoir) pressure present at this time – the result of the very shallow burial depth (400m) when it was receiving charge. At 136 Ma oil expulsion had not yet begun in the Cartier Trough because the source rock was thermally immature due to the shallow burial depth.

In the model, present day hydrocarbon expulsion is active in the Cartier Trough, whereas hydrocarbon expulsion from the Swan Graben is essentially finished (Figure 5-10, right). Currently, oil expelled from the Cartier Trough migrates into the Jabiru structure along the culmination at the Top Plover Formation. The hydrocarbons that are presently accumulating in the Jabiru structure are composed of liquid hydrocarbon (i.e. oil), which is very different from the situation that existed at 136 Ma. This difference in the model is mainly related to increasing burial and pressure of the Jabiru reservoir which has led to the vapor phase hydrocarbon dissolving into the liquid phase (Figure 5-11).

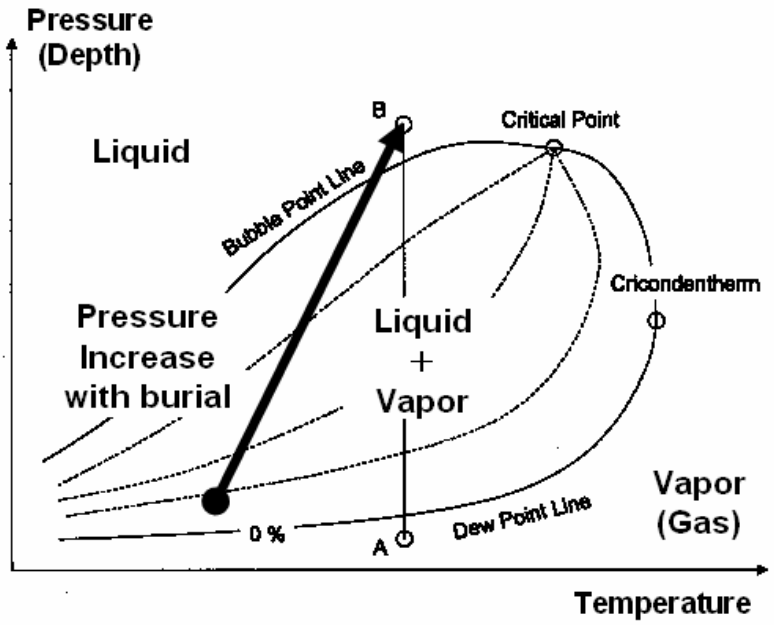

Figure 5-11. Schematic phase diagram of hydrocarbon with pressure path related to burial.

The 3D modelling that was carried out as part of this work suggests the possibility that there could have been a gas cap at the Jabiru structure. Fluid inclusion analysis of the reservoir sands in Jabiru (George et al., 1997) have been interpreted to indicate that the oil water contact (OWC) in the field used to extend deeper than it does at the present day (Figure 5-12; George et al, 1997). This residual zone has traditionally been explained by the fact that the accumulation has leaked as a result of Late Tertiary fault reactivation (George et al, 1997). The results obtained from the present study indicate, however, that it may be that at least some of this residual zone could have formed because the reservoir was charged when at shallow depth and that the volume change was due to an earlier vapor phase dissolving into the liquid phase (Figure 5-13).

Fluid inclusion data such as GOI cannot discriminate between these two possibilities, and this potential ambiguity should be taken into account when interpreting fluid inclusion data in areas where the reservoirs could have been charged “early”, when they were at shallow depths of burial. Failure to recognize this process could lead to an incorrect interpretation of the charge and fill-spill history of a trap. At traps such as Jabiru, other indicators of fault-related leakage are present; these include HRDZs developed over the trap-bounding faults (O’Brien and Woods, 1995). Consequently, at least some of the residual zone is certainly due to fault seal failure. Other traps in the area which have residual zones, such as Challis, do not appear to have HRDZs associated with them and it may be that gas dissolution early in the charge history of such traps may potentially be important.

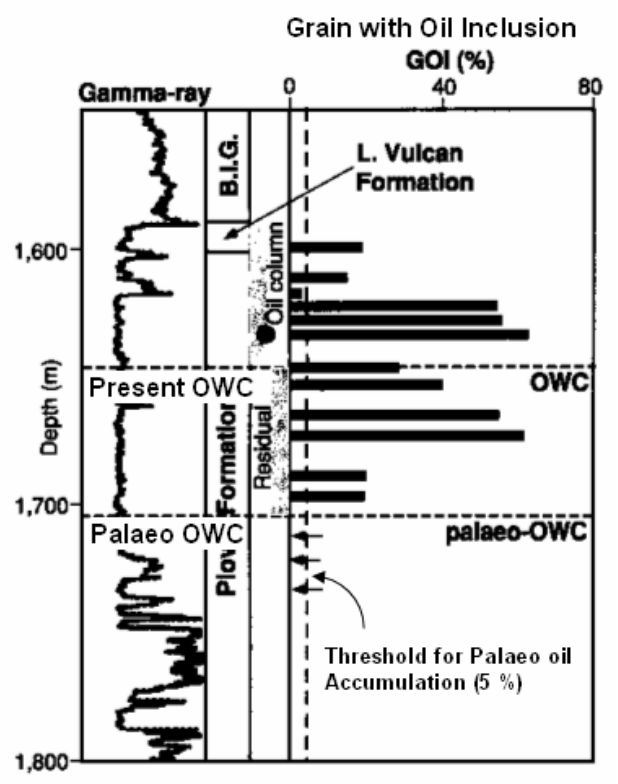

Figure 5-12. Oil inclusion analysis in Jabiru-1A（George et al, 1997).

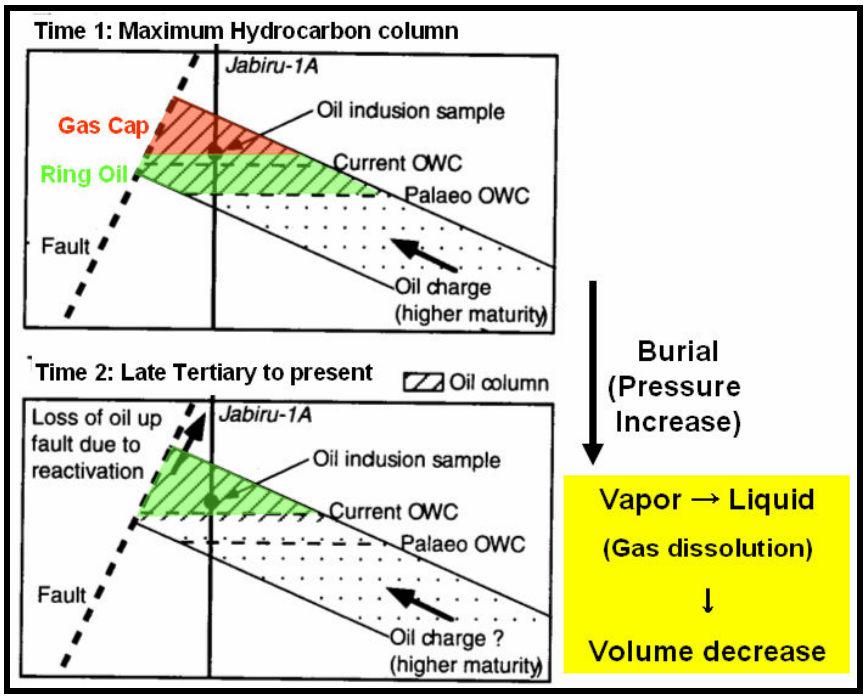

Figure 5-13. Possible oil accumulation model in the Jabiru structure.

5.6 HYDROCARBON IMPLICATIONS FROM MODELLING RESULTS

5.6.1 Possible new (unknown) hydrocarbon fairway suggested from the modelling

Initial models in this study support a contribution of hydrocarbons sourced from the Plover Formation and Vulcan Formation. Exploration plays sourced from the Cartier Trough are expected at the structural trends on the southeastern and the northwestern margins of the Carter Trough. In these plays, a relatively recent (Pliocene) hydrocarbon charge from the Lower Vulcan Formation is evident in the basin modelling. In addition, the modelling results suggest that the contribution of the Plover Formation source rocks is particularly important prior to the Oligocene. From the results of the 3D simulations, a hydrocarbon fairway southeast of the Cartier Trough is expected to extend across a wide region including the Jabiru Horst.

An exploration play sourced from the Swan Graben is also expected at the structural trends along the southeastern and the northwestern margins of the Swan Graben. Hydrocarbon charge sourced from the Paqualin Graben was predicted by the 3D modelling, indicating that this area could be potentially prospective. In addition, the Eclipse-Cassini-Challis structural trend is an important play fairway. If long distance hydrocarbon migration takes place from the Swan Graben to the northeast, beyond the Challis structure, then hydrocarbon charge into a recently gazetted area (AC03-1) could be expected. In this context, the identification of the source rock, which contributed to the gas show in Delamere-1, is important.

It is also recognized that maturation of the Plover Formation within the Kimberley Graben - the southwest extension of the Swan Graben - has occurred within the Neogene. If the Plover Formation source rock in this region is of good quality, then a significant hydrocarbon charge from this area is possible.

5.6.2 Comparison of seep locations with basin modelling predictions

The outputs from PetroMod^{TM} can be used to predict the distribution of hydrocarbon seeps, both at the present day and through time. Present day hydrocarbon seepage has been documented within the Vulcan Sub-basin by a number of studies (O'Brien and Woods, 1995; O'Brien et al., 2002), and so a comparison between the locations and compositions of the predicted and actual seeps may prove informative.

In the 2D modelling for the southern Vulcan Sub-basin (Fig. 5-4d), hydrocarbon flow vectors in the Eocene succession, which is located well above the regional seal, can be used as a proxy for seepage. In this model oil and gas seeps are predicted over the Skua field, associated with the Puffin field, as well as inboard from the Conway-1 well location. In addition, leaky traps are predicted within the central Montara Terrace, though these seeps do not reach the seafloor. These modelled observations appear to agree fairly well with the actual locations of seeps. For example, O'Brien and Woods (1995) documented water column ethane anomalies over and around leaky fault systems on the Skua field as well as seepage inboard from the Conway-1 well location. It appeared that the southern Swan Graben was also an area of generally elevated seepage rates. Moreover, O'Brien and Woods (1995) described HRDZs which occurred over the Tahbilk field on the southern Montara Terrace, though this seepage had no surface expression. Again, the locations of these HRDZs agree well with the results of the modelling.

In a more recent study using much more detailed water column sniffer data, O'Brien et al. (2002) documented oil-prone seepage associated with the Skua field, as well as minor seepage well to the east of Eclipse-1. Low levels of fairly dry gas seepage generally characterized the region around the East Swan. Figure 5-14 shows the simulated oil flow vector distribution in the Eocene unit at the present day: small amounts of oil seepage to the southeast of Montara-1 and the northeast of the Eclipse-1 are predicted in the modelling, which is in partial agreement with the results of the assorted published remote sensing investigation.

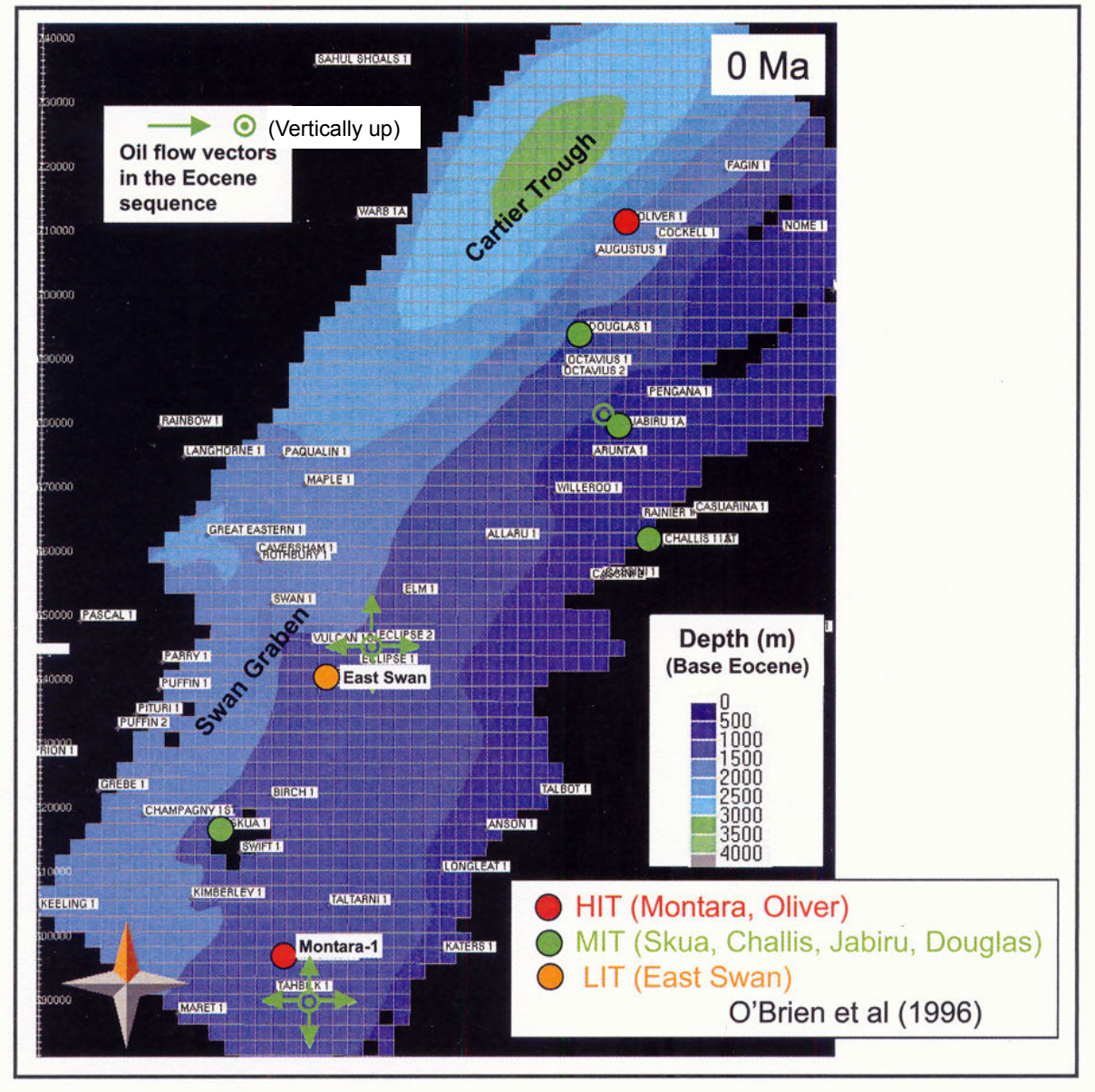

Figure 5-14. Modelled present day hydrocarbon flow vector distribution in the Eocene sequence and trap types (HIT - high integrity trap, MIT - moderate integrity trap, LIT - low integrity Trap (O'Brien et al., 1999a))

5.7 SEISMIC INVESTIGATIONS OF LEAKAGE INDICATORS

A number of seismic attributes were examined to try to better understand and evaluate, at a regional scale, the seismic indicators of leakage and seepage in this region. The approaches that were undertaken included examination of:

- seafloor bathymetry,
- seismic amplitude of the seafloor,
- the Top Paleocene horizon,
- the isochron between the top Paleocene and the base Miocene horizons, and
- time dip of the Top Paleocene horizon.

The overall goal of this preliminary evaluation was to develop an improved way of evaluating leakage indicators.

5.7.1 Bathymetry

An interpretation of key horizons on the Onnia 3D survey data from the Vulcan Sub-basin was provided by PGS. These horizons were loaded and displayed using PetroSeis mapping software. Preliminary analysis of bathymetry horizon data was carried out after quality control checking.

Bathymetry data can be extremely useful in assessing hydrocarbon leakage and seepage, as some workers (Hovland, 1988; Hovland et al., 1994) have proposed that carbonate reef and bank formation, for example, can be strongly controlled by hydrocarbon seepage. As a result the present study includes a brief comparison between the locations of potential seafloor seeps, their expression, and the basin modeling results obtained during this study,

Figure 5-15 shows the present day bathymetry in the northern Vulcan Sub-basin. A row of seafloor knolls in 2-10 km diameter was recognized along the flank of the north-eastern Cartier Trough, whereas a row of much smaller seafloor knolls, in 1-2km diameter, were recognized in the southern part of the eastern Carter Trough. These knolls are distributed along the NE-SW trending faults located in this region (Figure 2-2). Although the existence of these knolls in this area has been pointed out by Hovland et al. (1994), this is the first time that they have been recognized in this area by the use of 3D seismic data.

The seafloor knolls in the north-eastern flank of the Cartier Trough are all clearly larger than those in the south. Exactly why this is the case is somewhat perplexing. It may be that these carbonate knolls have formed as a result of hydrocarbon seepage along these fault systems, as proposed by Hovland et al. (1994) and O'Brien et al.

(2002). Alternatively, their origin may be in no way related to seepage and it might be that less exotic geological processes, such as subsidence rates, may be the controlling factor.

The morphology of the eastern flank of the Cartier Trough has the appearance of a releasing-restraining bend couplet, which, if confirmed, might suggest that the subsidence rates on the north-eastern part of the trough are probably lower than further south, which has facilitated the development of larger bank systems. Shuster et al. (1998) proposed that this region was subjected to left-lateral strike slip stress, which would favour lower subsidence rates in the north-east as compared to further south. If this were confirmed, then the smaller knolls probably occur in an area of relatively higher subsidence and depositional rates – they have been effectively almost "drowned".

If these knolls are in fact hydrocarbon-related, as proposed by Hovland et al. (1994), then the question remains: why are they much larger in the north-east?

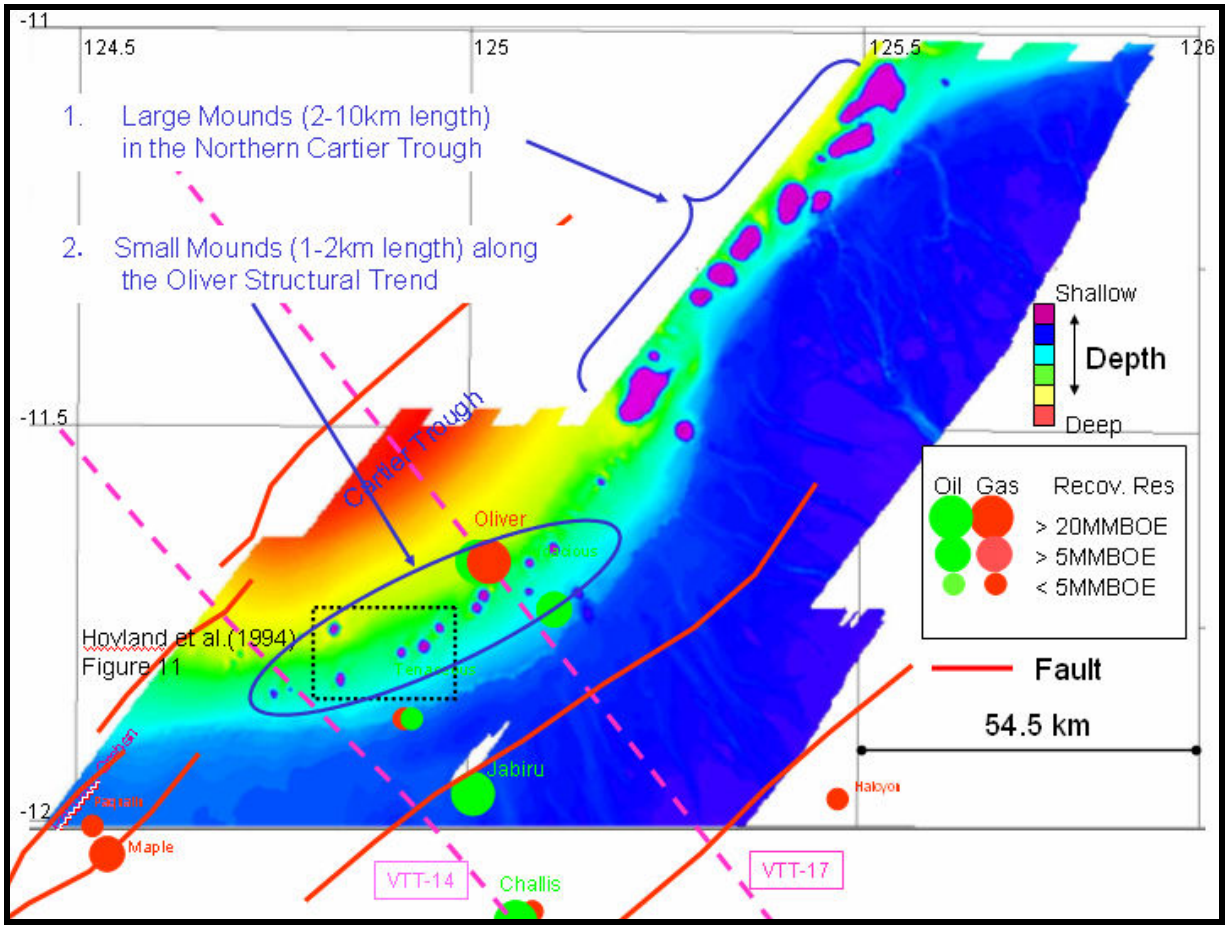

Figure 5-15a Bathymetry map obtained from 3D seismic data (Northern Vulcan sub-basin).

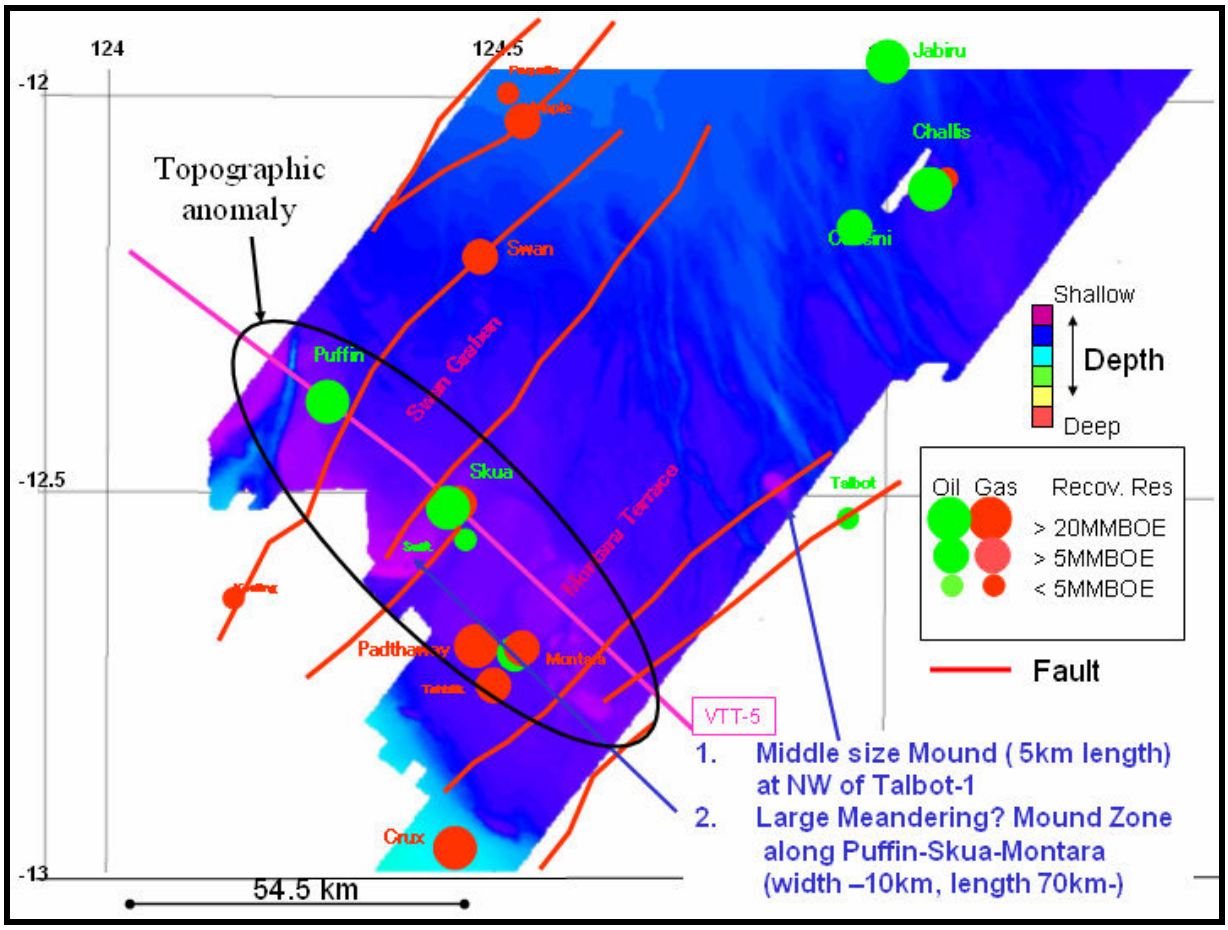

Figure 5-15b Bathymetry map obtained from 3D seismic data (Southern Vulcan sub-basin).

Figure 5-16 shows result of comparison between the distribution of the seafloor knolls in the northern Vulcan Sub-basin and some of the 3D basin modelling results, namely the area of present day hydrocarbon expulsion from the Lower Vulcan Formation. The larger size of the knolls in the north-eastern Cartier Trough is not consistent with basin modelling results in the sense that hydrocarbon expulsion appears to be more active in the southern Cartier Trough than in the north-eastern Cartier Trough. If the locations of the banks are related to seepage, the modelling indicates that the actual relationships are complex – perhaps the amount of hydrocarbon seepage in this area is not controlled only by the total amount of hydrocarbon expulsion from the source rock but also by other factors, such as fault seal integrity. One possibility is that the mounds are larger because, relatively, there is more leakage of hydrocarbons to the northeast, or at least, the “leaky” fault segments extend over longer distances in the northeast compared to the south-western margin of the Cartier Trough. This could be because the underlying rift fault systems have a more north-easterly azimuth, which is parallel to the maximum horizontal stress direction (Mildren and Hillis, 2000) and hence tend to leak more than the west-southwest trending flanking faults along the south-western part of the Cartier Trough. If there is more leakage in the north-east, it

could be due to a complex interplay between the amount of hydrocarbons expelled and migrating in the region and the relatively low fault seal integrity.

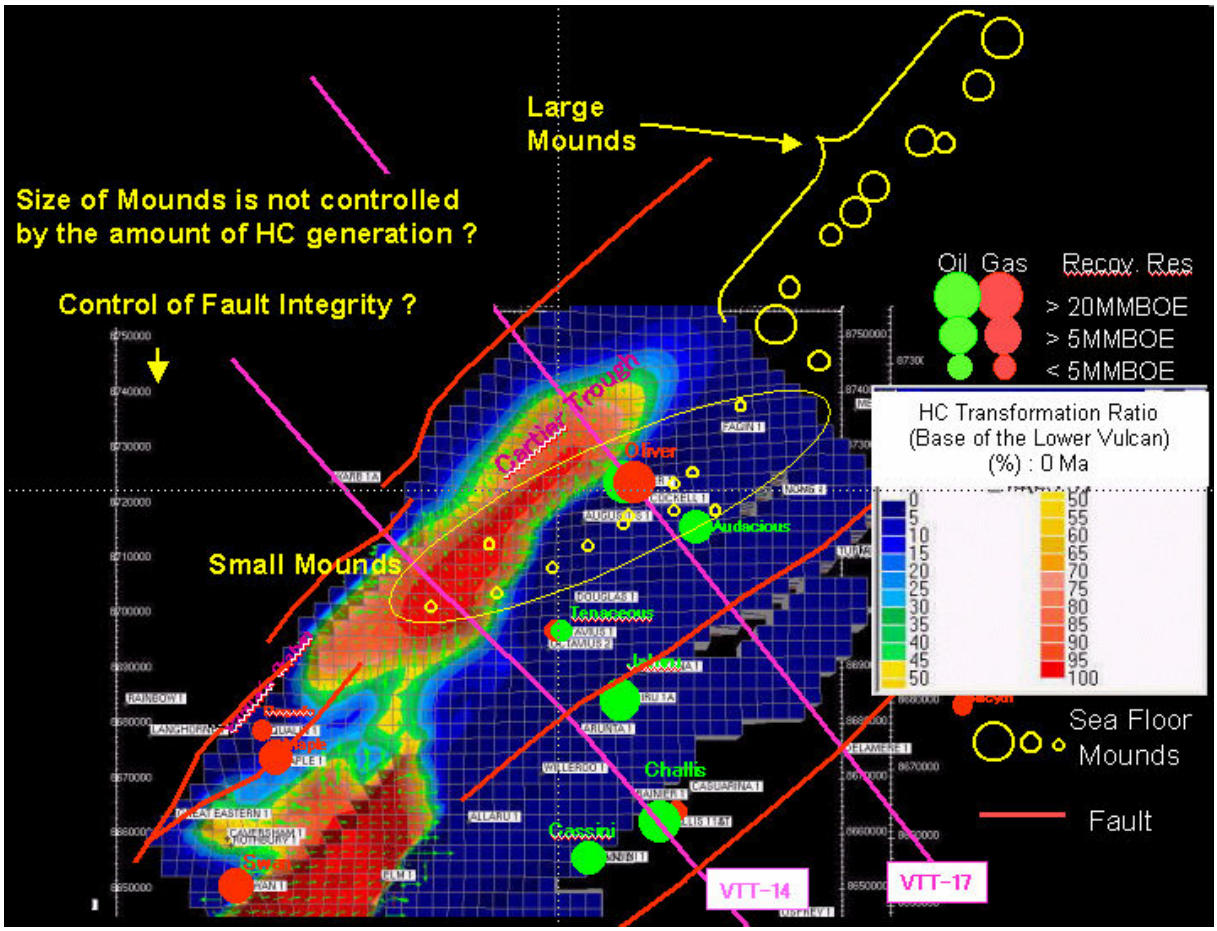

Figure 5-16 Comparison between modelled hydrocarbon expulsion area in the Lower Vulcan Formation and actual distribution of seafloor mounds in the northern Vulcan Sub-basin.

5.7.2 Seafloor amplitude

The seafloor and near-seafloor seismic amplitude was displayed using the mapping software in GeoFrame.

In the northern Vulcan Sub-basin, seafloor seismic amplitude values show positive (plus) anomalies at the location of each seafloor knoll (Figure 5-17a). This can be caused by the higher seismic velocities at the location of these carbonate mounds that were related to carbonate cementation processes. The amplitude analysis also defined NE-SW trending linear areas where the seismic amplitude is relatively lower than within other parts. These areas are probably the boundaries between different seismic surveys that have varying seismic phase.

In the southern Vulcan Sub-basin, a belt of positive amplitude anomalies were recognized which trended from Puffin to Skua through to Montara (Figure 5-17b). This represents almost the same area in which a northwest-southeast trending, topographically positive area is present on the seafloor. A positive amplitude anomaly was also recognized to the northwest of Talbot-1, where a small seafloor knoll is visible in Figure 5-15b. These observations suggest that the relatively low relief culmination shown in Figure 5-15b could also be carbonate knoll or a zone of enhanced carbonate cementation. This region is a major fault relay zone that essentially marks the boundary between the Browse and Bonaparte Basins (O'Brien et al, 1996, 1999). This has been proposed to be a zone of enhanced hydrocarbon focus (O'Brien et al., 1996, 1999) and could provide one mechanism for the observed cementation.

Amplitude anomalies were also recognized to the west of Challis-1 and to the southwest of Cassini-1.

(a) Northern Vulcan sub-basin

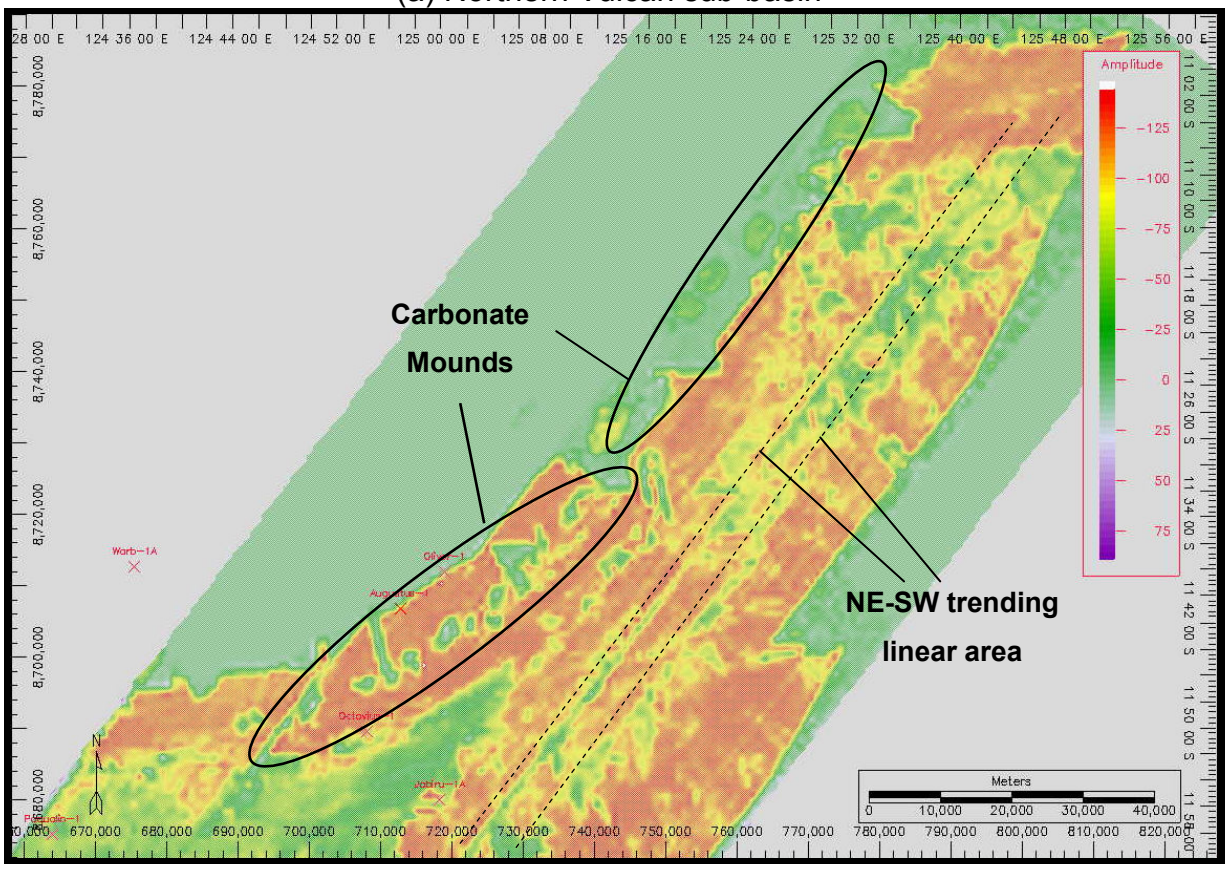

(b) Southern Vulcan Sub-basin

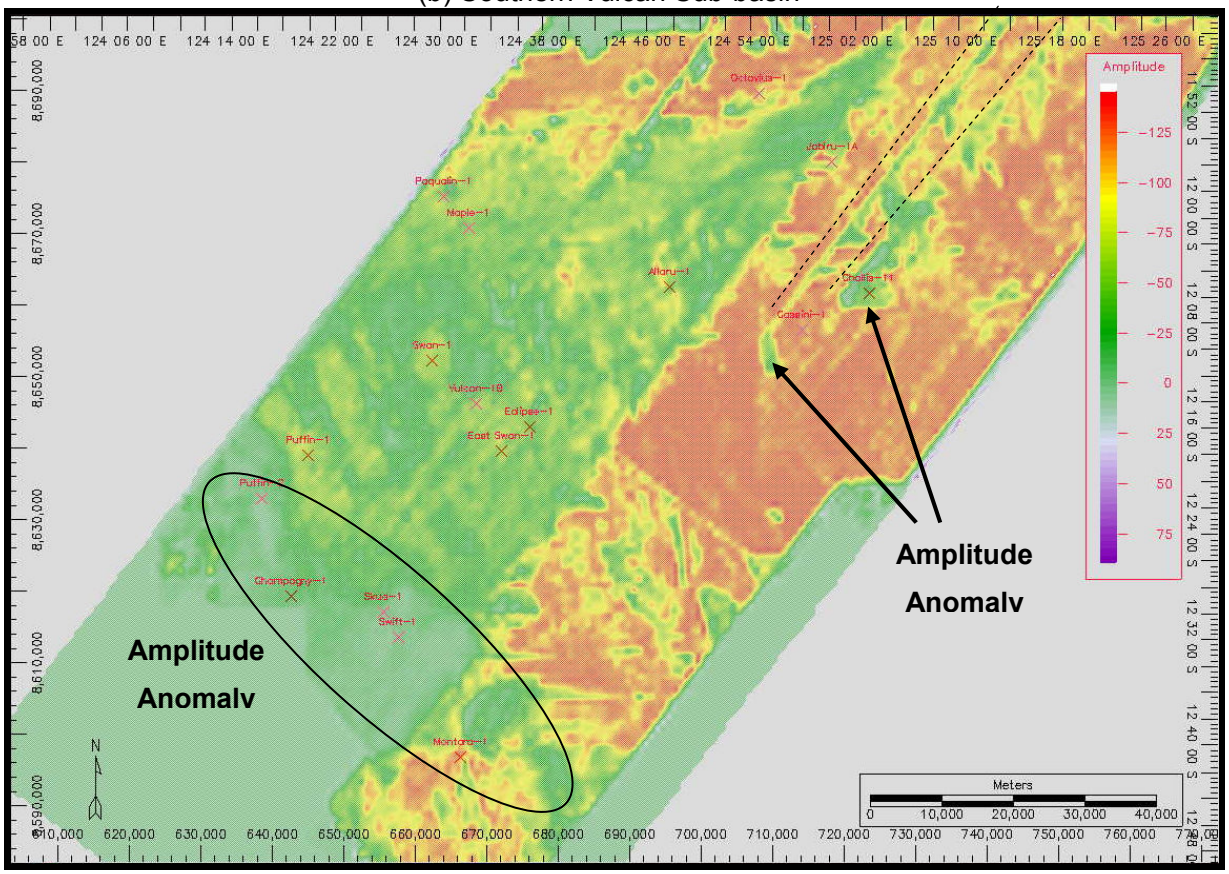

Figure 5-17 Seafloor amplitude map in the Vulcan Sub-basin (extracted 16 or 32 msecs window at seafloor). Note that the amplitudes are reverse mapped from 8 bit to 32 bit.

5.7.3 Top Paleocene Horizon

Linear seismic travel time (TWT) anomalies were recognized in an *en echelon*, ENE-WSW direction, in the southeastern Cartier Trough (Figure 5-18a). The south-eastern margin of the trough has a structural trend in an NW-SE direction (Figure 2-1). The TWT linear anomalies (Figure 5-18a) can be divided into two types, symmetric ridges (around Oliver-1 and Augustus-1) and step shapes (around Octavious-1 and Jabiru-1). A localized TWT anomaly was also recognized to the northwest of the Paqualin-1 well location.

In the southern Vulcan Sub-basin, on the other hand, localized TWT anomalies were present between Swan-1 and Vulcan-1B (Figure 5-18b), as were NE-SW trending line features around Allaru-1.

5.7.4 Isochron between the Top Paleocene and the Base Miocene

An isochron between the Top Paleocene and the Base Miocene was constructed in order to analyze seismic velocity anomalies within the Eocene sandstone. These anomalies would most likely be due to the presence of hydrocarbon-related diagenetic zones or HRDZs (O'Brien & Woods, 1995). A new grid was constructed using the gridding operation function in the mapping software IESX.

New grid (ms) = Top Paleocene grid (ms) – Base Miocene grid (ms)

Figure 5-19 shows the constructed isochron. In the northern Vulcan Sub-basin, linear, ENE-WSW trending anomalies were present in the area from the southeast Cartier Trough to the Jabiru Terrace; these anomalies had TWTs (of about 50-100ms) which were relatively less than those in the surrounding areas (about 200ms). Linear, ENE-WSW trending anomalies were also recognized in the area from Vulcan-1B to Allaru-1; the TWT (about 200-230ms) around these anomalies is significantly less than that of their surroundings (about 300ms). On the other hand, local patchy anomalies of "pulled up" TWT were recognized to the north of Paqualin-1, area between Swan-1 and Vulcan-1B, and around East Swan-1. These linear anomalies are distributed along major faults (Figure 5-19).

These linear anomalies could not be recognized clearly using only the Top Paleocene time structure map. This emphasizes the importance of using isochrons in mapping zones of potential fault failure and leakage in this region.

(a) Northern Vulcan sub-basin

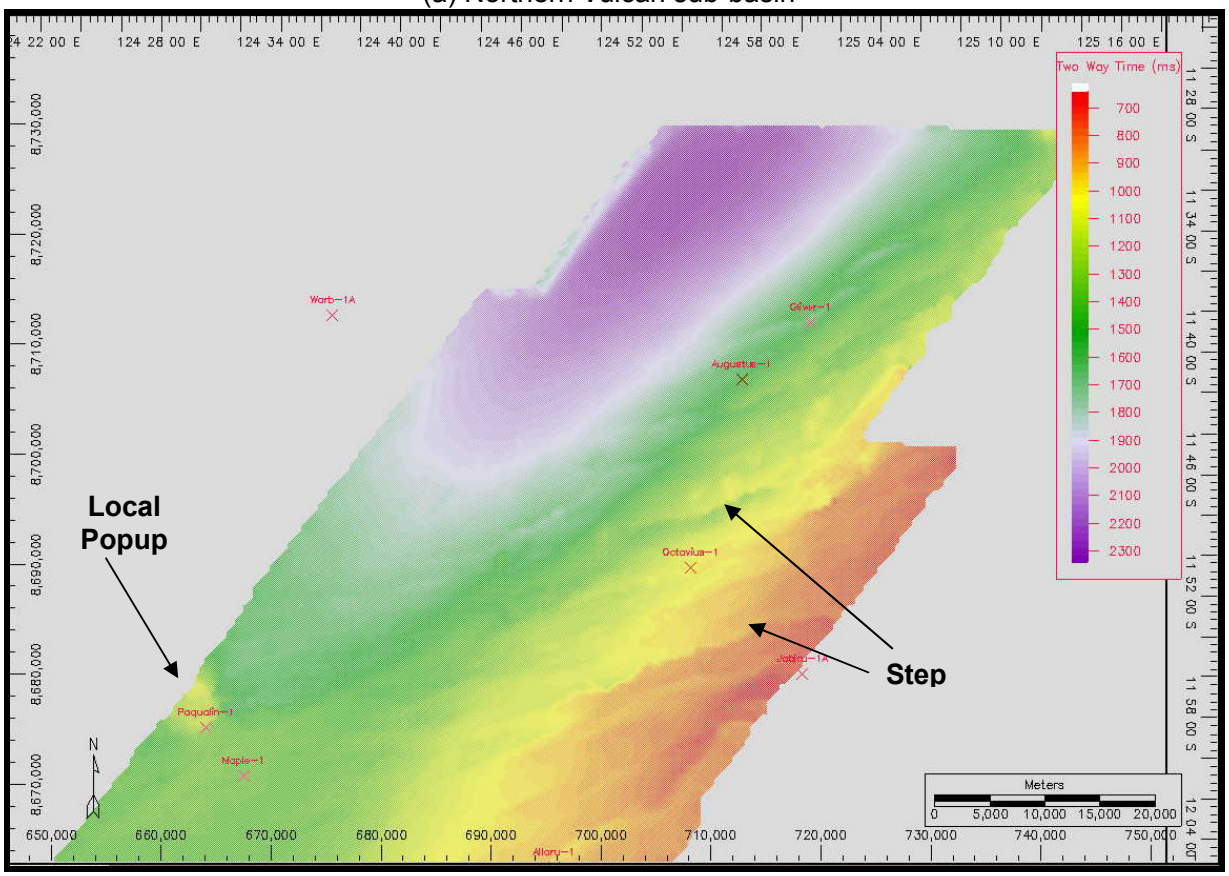

(b) Southern Vulcan sub-basin

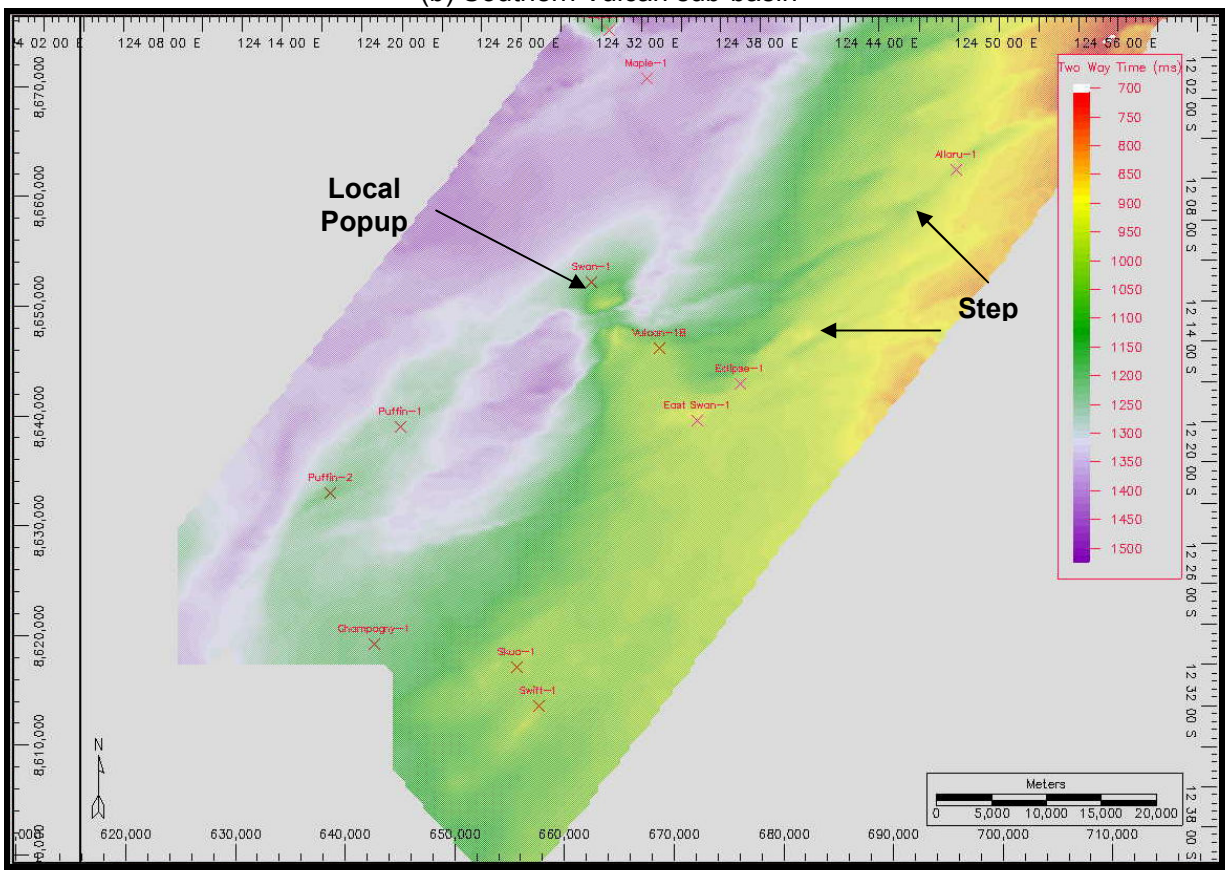

Figure 5-18. Top Paleocene Two-Way-Time map in the Vulcan Sub-basin.

(a) Northern Vulcan sub-basin

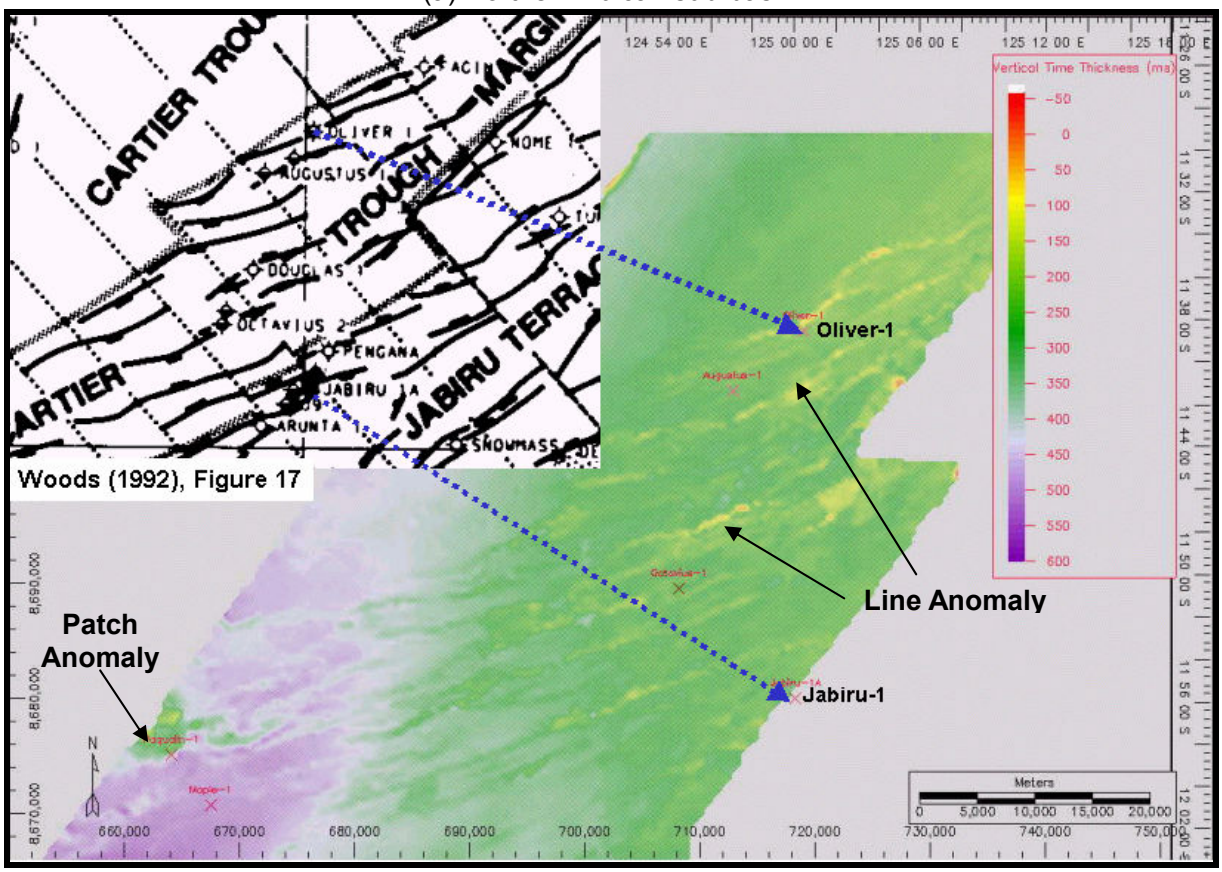

(b) Southern Vulcan sub-basin

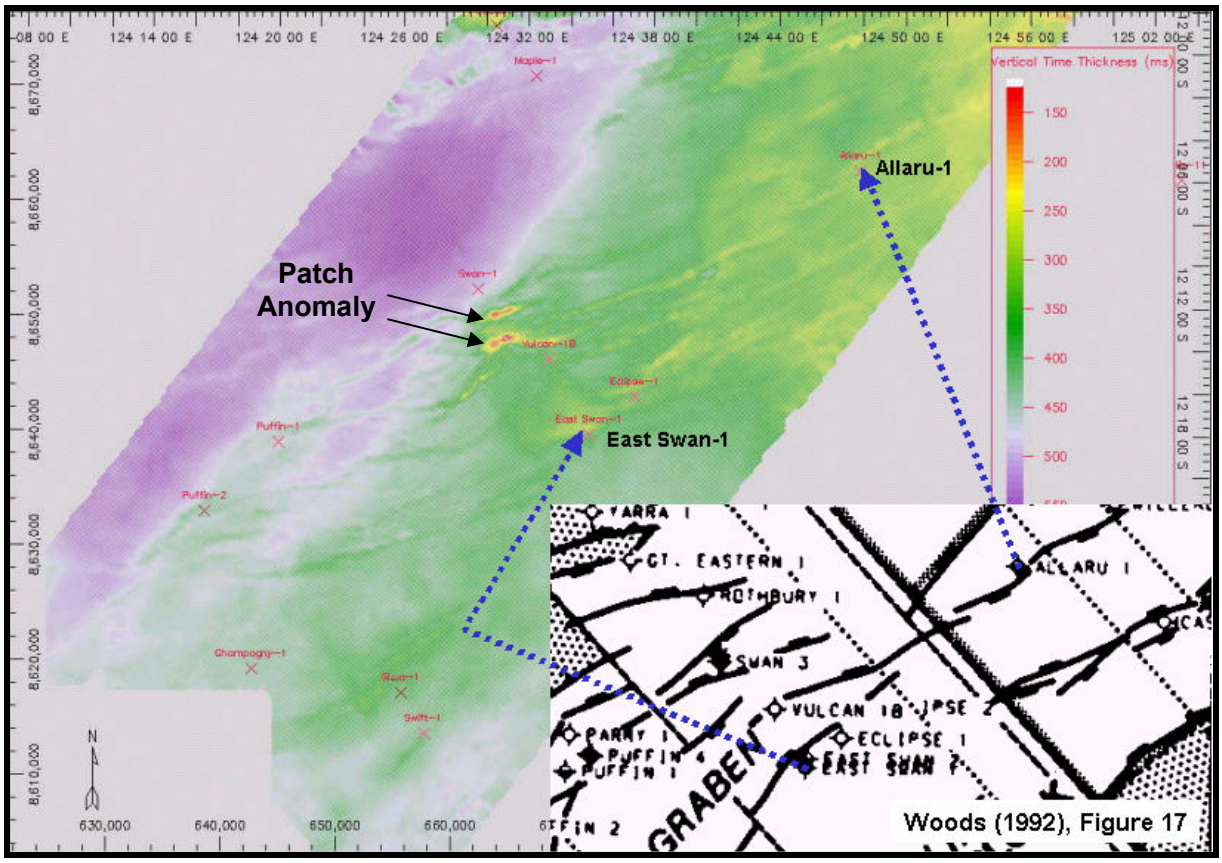

Figure 5-19 Top Paleocene to Base Miocene isochron and fault distribution.

5.7.5. Time dip of the Top Paleocene

In order to extract the relative change of the gradient of the Top Paleocene surface, mapping of time-dip of the Top Paleocene was undertaken (Fig. 5-20). The definition of the time dip used for this analysis is:

Time dip of the Top Paleocene (sec/m) = Time difference (sec) / Horizontal distance (m)

5.7.6. Extraction of HRDZs from 3D seismic data

5.7.6.1. Methodology

It is assumed that the localized TWT isochron anomalies shown in Chapter 5.7.4 reflect either the fault itself or HRDZs formed by hydrocarbon leakage and oxidation along the fault zone. In order to detect the HRDZs *per se*, it is necessary to distinguish the HRDZs from the fault itself. The following examination was carried out.

Figure 5-21 shows the expected response of the Base Miocene and Top Paleocene to the typical geological structures and phenomena such as anticlines, HRDZs and normal faults. Firstly, the isochron between the Base Miocene and the Top Paleocene indicates that both HRDZs and normal faults show a negative response and hence they can be distinguished from a simple anticline.

Secondly, two different methods can be used to distinguish between HRDZs and normal faults; one is the method of focusing on the Top Paleocene geometry itself and the other is focusing on the time dip of the Top Paleocene. The former method relies on distinguishing whether the Top Paleocene geometry is that of a local pop-up or that of a step shape that is most likely relatable to a fault. One of the shortcomings of this method is that it can be difficult to distinguish when the Top Paleocene surface is declining to the footwall side. The other shortcoming is that it is difficult to recognize a small topographic change without considering the time range and color for the display. The second method makes use of the isochron anomaly area to see if it is composed of a double line or single line. The advantage of this method is that it is easy to recognize small topographic changes because the method is focused on the inclination or slope rather than absolute value. It would be effective to utilise both approaches by combining the methods. Figure 5-22 shows the procedure of HRDZ extraction which was designed based on the above concepts.

(a) Northern Vulcan sub-basin

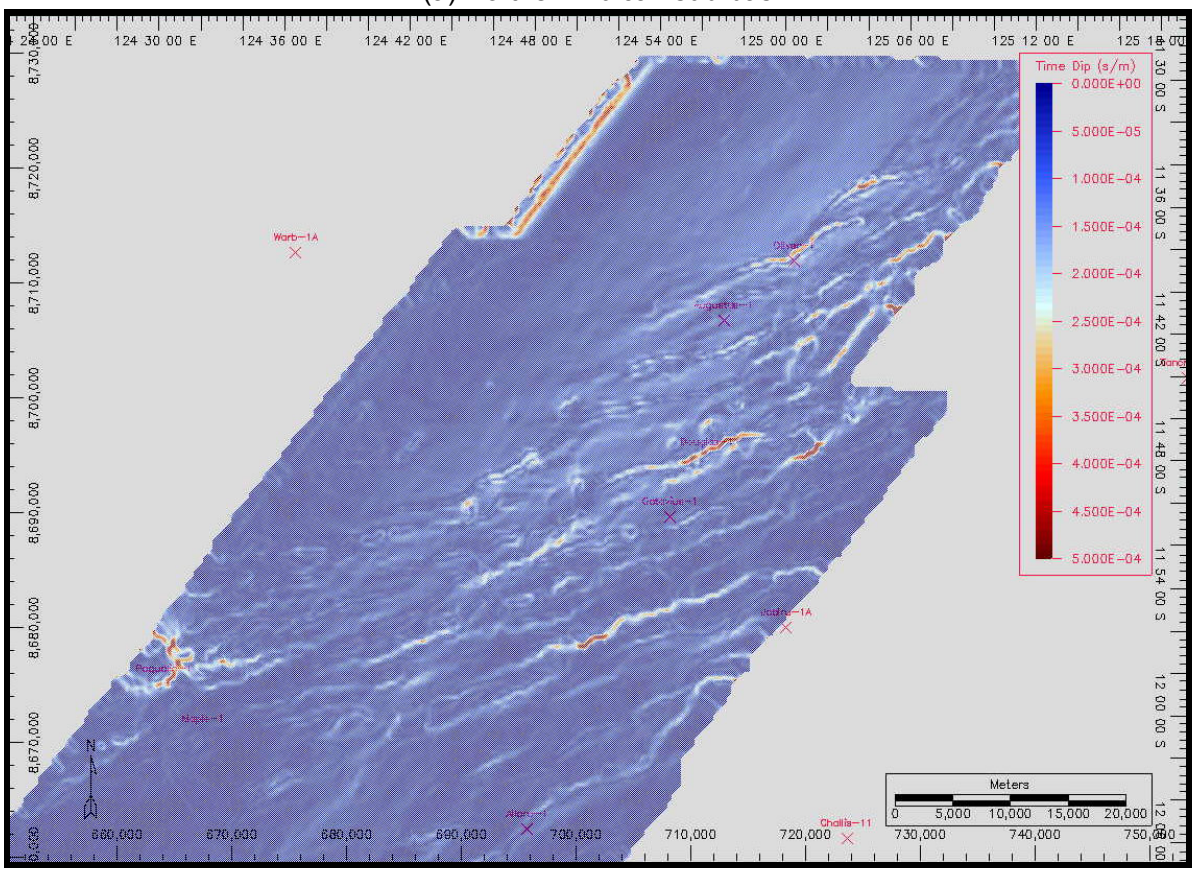

(b) Southern Vulcan sub-basin

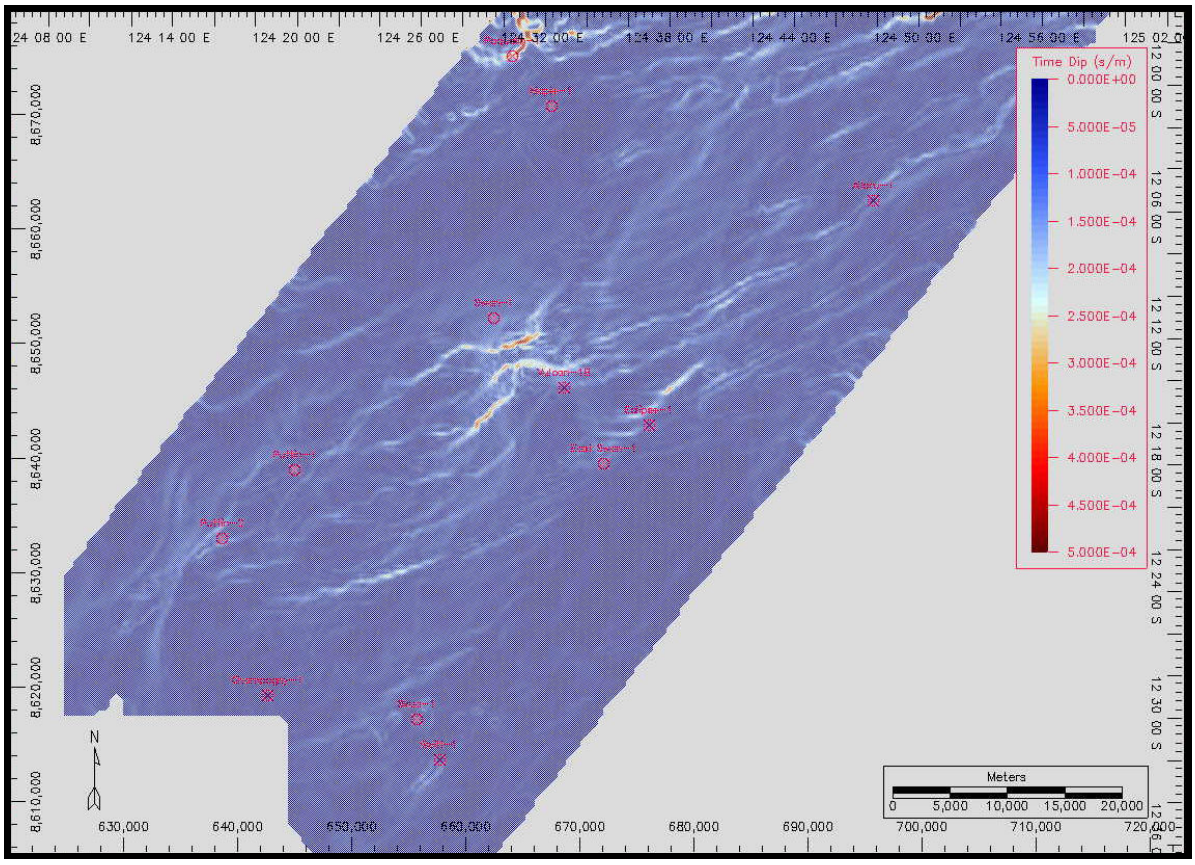

Figure 5-20. Results of the Top Paleocene time dip analysis from the southern (a) and northern (b) Vulcan Sub-basin.

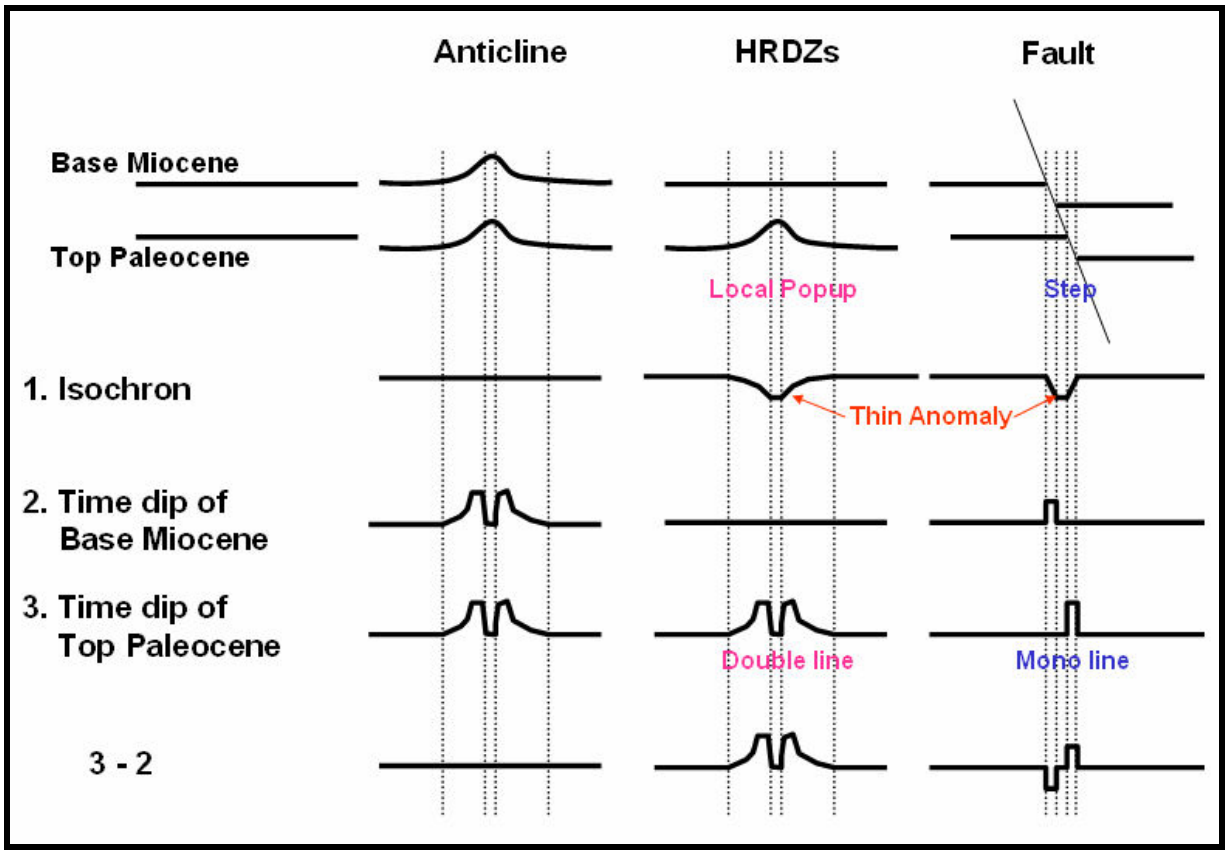

Figure 5-21 Expected response of the Base Miocene and Top Paleocene corresponding to the typical geological structures and phenomena (Anticline, HRDZs and normal fault).

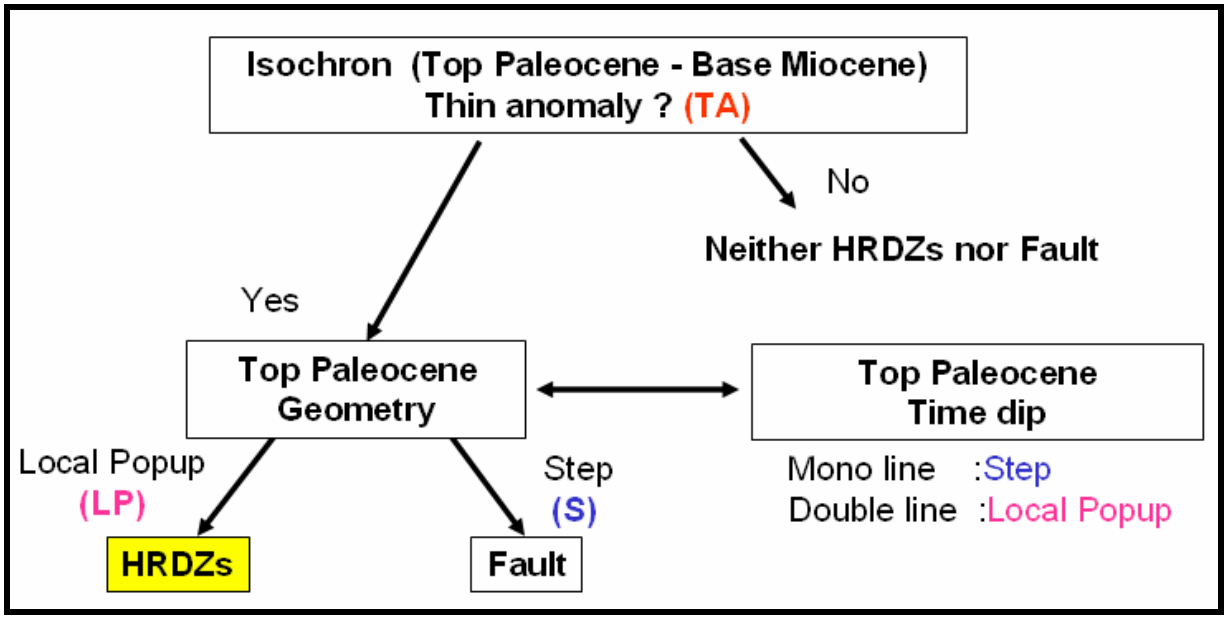

Figure 5-22. A possible procedure to extract HRDZs from 3D seismic data.

5.7.6.2 Results

Figure 5-23 shows the actual example of extraction of HRDZs in the southern Vulcan Sub-basin, based on the procedure shown in Figure 5-17. Several thin anomalies were recognized through the isochron in the area from Swan-1 to East Swan-1 (upper left of Figure 5-23). As a next step, some of these thin isochron anomalies, that were assumed to be related to the fault itself, were eliminated based on characteristics of the Top Paleocene geometry and Top Paleocene time-dip. Finally, isochron anomalies that are assumed to be HRDZs were extracted at two locations between Swan-1 and Vulcan-1B, and the east of East Swan-1 (lower right of Figure 5-23).

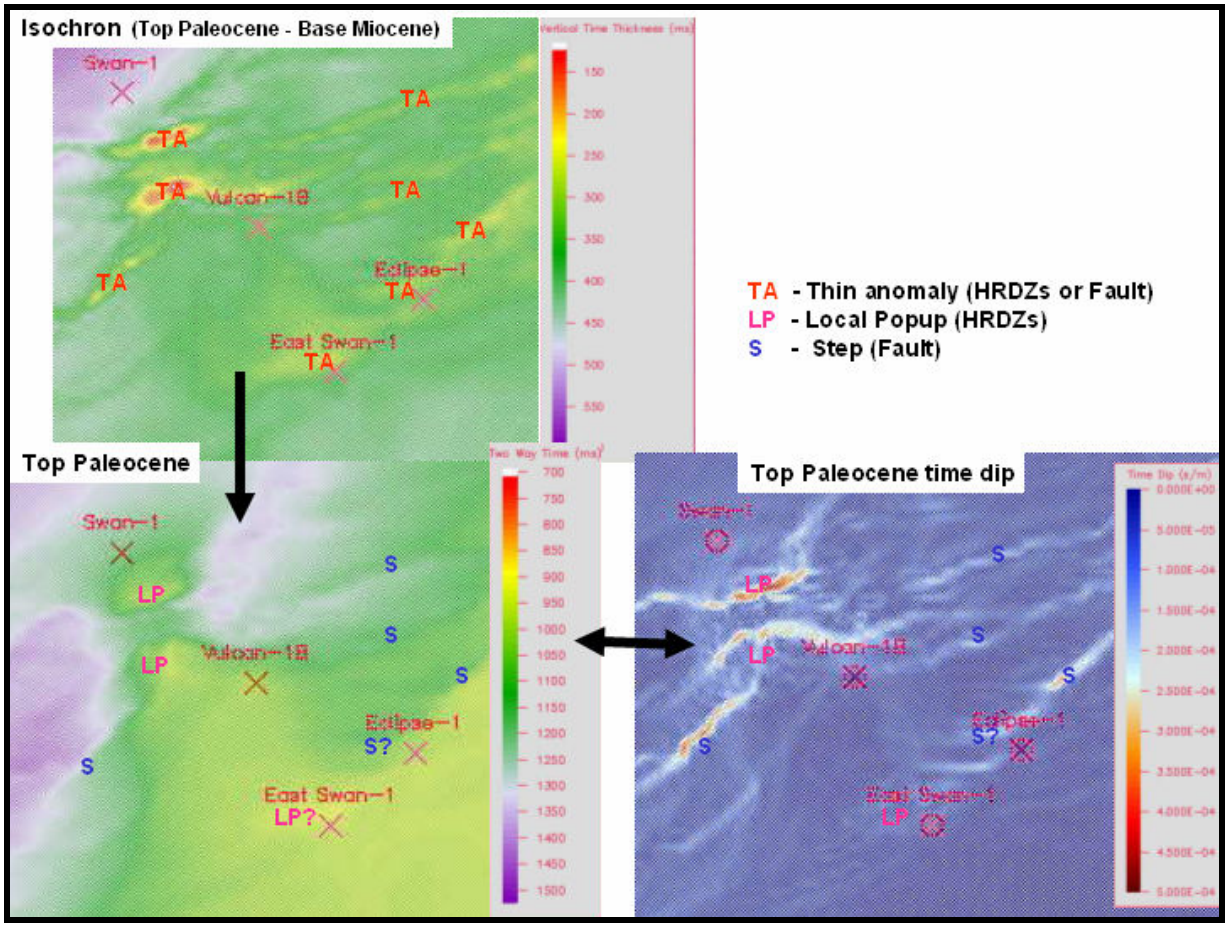

Figure 5-23. Examples of extraction of HRDZs in the southern Vulcan Sub-basin.

Based on above procedure, HRDZ identification was carried out using the Top Paleocene and Base Miocene surface data in the northern and southern Vulcan Sub-basin (Figure 5-24 and 5-25), with possible HRDZs described below.

Northern Vulcan Sub-basin (Figure 5-24b)

1. 14 km east from Augustus-1 (1-2 km length, small size)
2. 13 km southeast from Augustus-1 (5 km length, large size)
3. 12 km northwest from Octavius-1 (5 km length, large size)
4. 7 km southwest to west-southwest from Jabiru-1A (1-2 km length, small size)
5. Adjacent north of Paqualin-1 (5-7 km length, large size)

Southern Vulcan Sub-basin (Figure 5-25b)

6. 3 km southeast from Swan-1 (5 km length, large size)
7. 2 km northeast from Vulcan-1B (8 km length, large size)
8. Adjacent north of East Swan-1 (5 km length, large size)
9. Adjacent north of Skua-1 (10 km length, large size)
10. Adjacent southeast of Swift-1 (5 km length, large size)

Most of extracted HRDZs (No. 4, 6, 7, 8, 9, and 10) have already been identified by O'Brien et al (1995 and 1999a), while some of them (No. 1, 2, 3, and 5) have not been reported before.

In this study, an extraction method for HRDZs was developed and a preliminary test carried out. However, this extraction test was conducted on large scale coarse map data. Further detailed investigations considering the following issue is necessary.

- Definition of "thin anomaly" of isochron (threshold, pattern recognition)
- Color scaling of the Top Paleocene two way time map (application of dynamic scaling display)
- Discrimination between HRDZ anomalies and those caused by horst blocks and salt domes
- Comparison of the extracted HRDZ distribution with fault seal integrity and basin modelling results

(a) Isochron between the Top Paleocene and Base Miocene

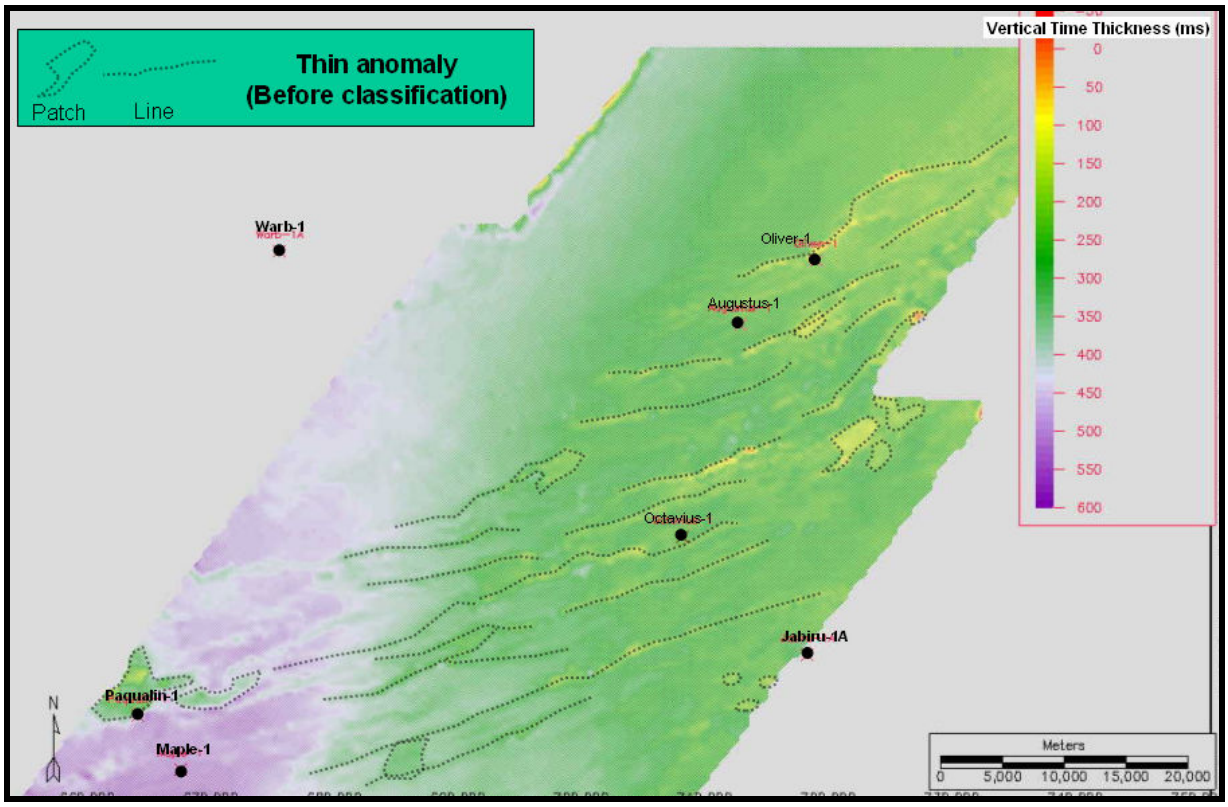

(b) Top Paleocene Two-Way-Time map

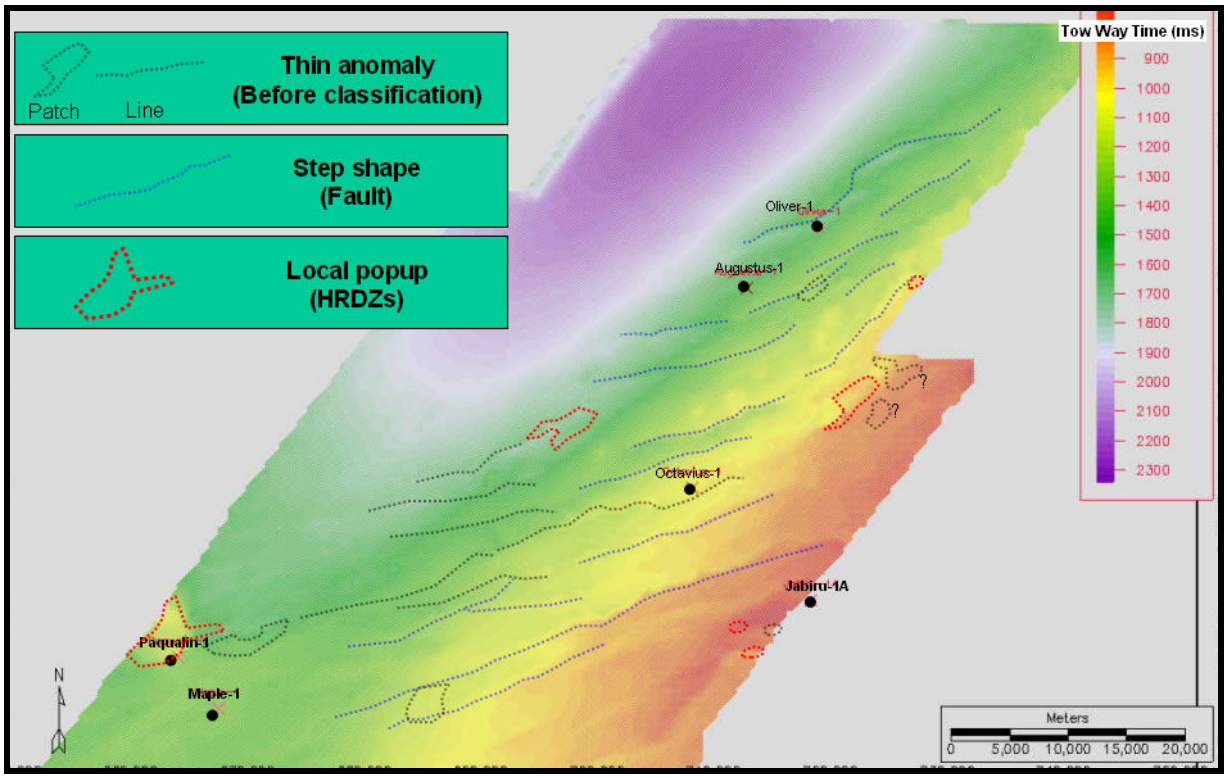

Figure 5-24. Results of extraction of HRDZs in the northern Vulcan Sub-basin ((a) Isochron between the Top Paleocene and Base Miocene, (b) Top Paleocene Two-Way-Time map).

(a) Isochron between the Top Paleocene and Base Miocene

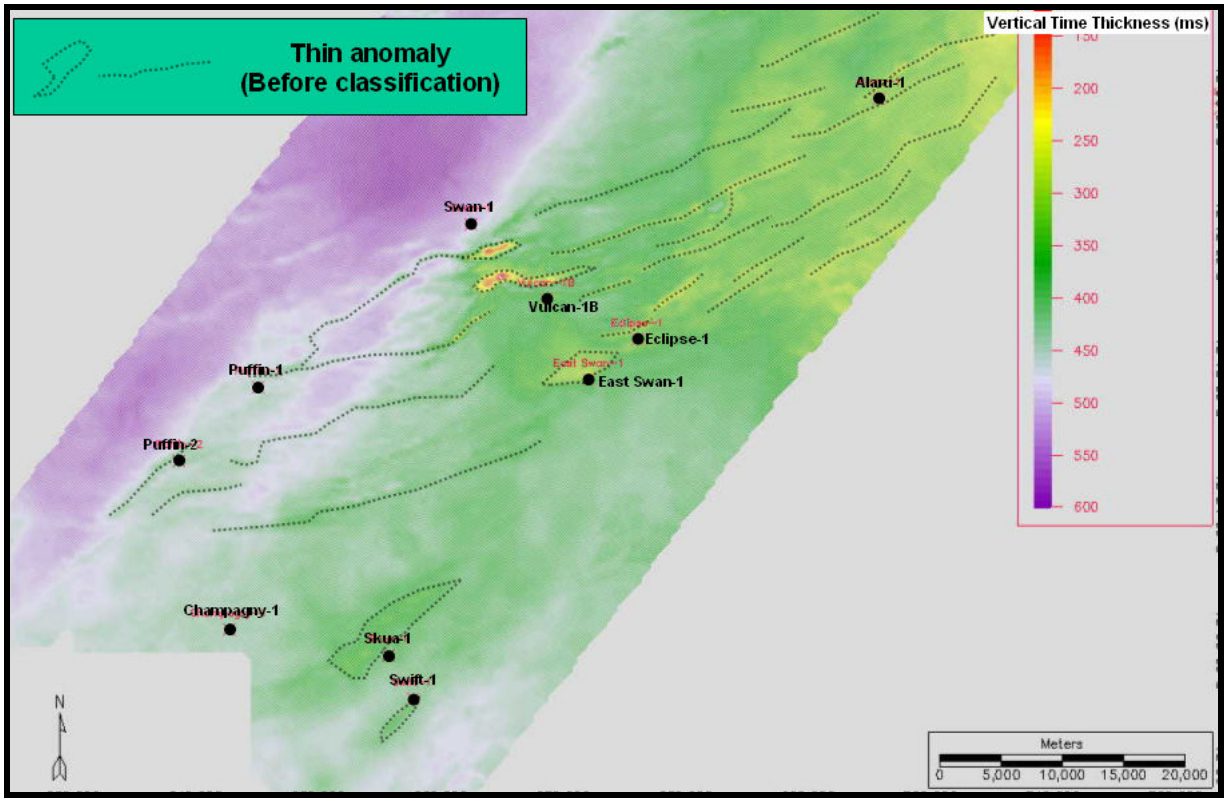

(b) Top Paleocene Two-Way-Time map

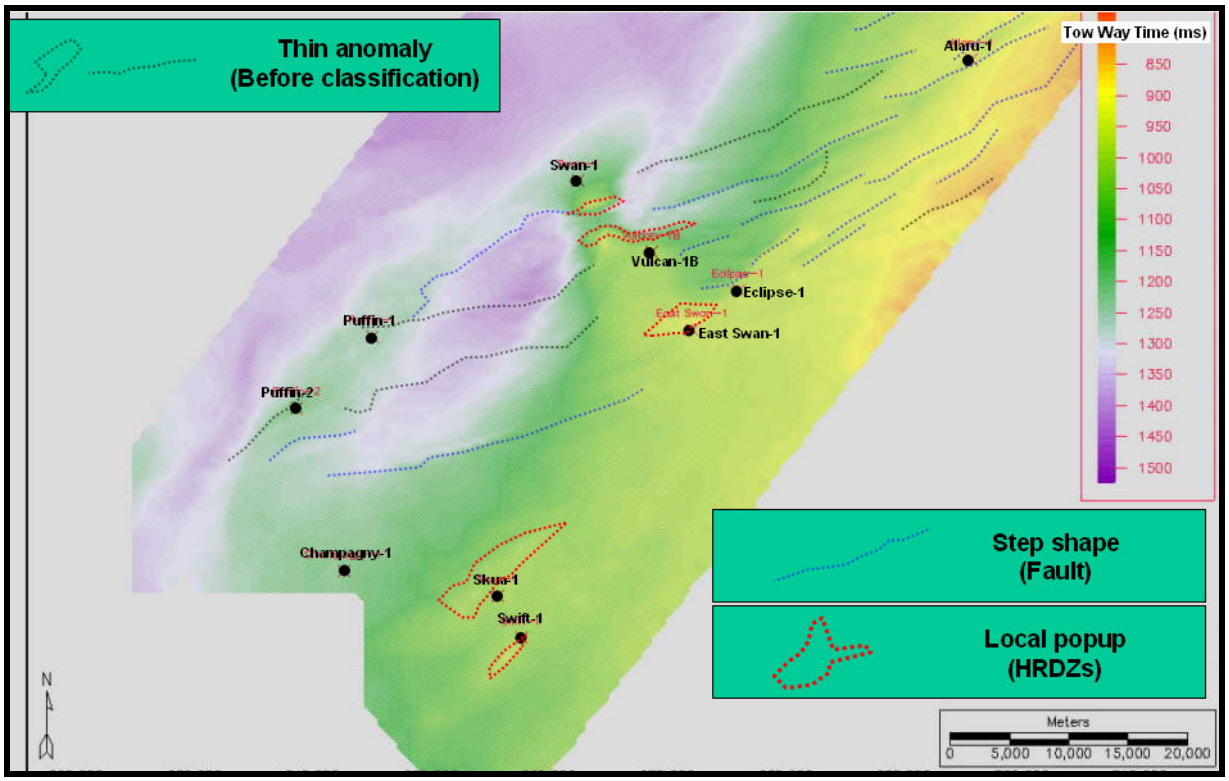

Figure 5-25. Extraction of HRDZs in the southern Vulcan Sub-basin ((a) Isochron between the Top Paleocene and Base Miocene, (b) Top Paleocene Two-Way-Time map).

CHAPTER SIX

HYDROCARBON IMPLICATIONS

The modelling results indicate that exploration plays sourced from the Cartier Trough can be expected at the structural trends on the southeastern and the northwestern margins of the Cartier Trough. The basin modelling suggests that Pliocene hydrocarbon charge from the Lower Vulcan Formation is a key part of these plays. The results also suggest that the contribution from source rocks in the Early to Middle Jurassic Plover Formation was important prior to the Oligocene. The 3D simulations indicate the presence of a hydrocarbon fairway southeast of the Cartier Trough that extends across a wide region, including the Jabiru Horst.

The modelling also predicts the presence of an exploration play sourced from the Swan Graben; this play is associated with the southeastern and the northwestern margins of the graben. A hydrocarbon charge originating from the Paqualin Graben was also predicted, and indicate that this region could be prospective. The Eclipse-Cassini-Challis structural trend is an important play fairway in the simulations. If long distance hydrocarbon migration takes place from the Swan Graben to the northeast, beyond the Challis structure, then hydrocarbon charge can occur into the region encompassing the gazetted area AC03-1. Identification of the source rock which contributed to the gas show in Delamere-1 would help to define this potential play

Maturation of the Plover Formation within the Kimberley Graben - the southwest extension of the Swan Graben - was simulated during the Neogene. If the Plover Formation source rock in this region is of good quality, then a significant hydrocarbon charge from that area is also possible.

Traditionally, most of the residual zones within the Timor Sea have been attributed to fault seal reactivation and failure. However, the modelled early gas cap which developed in the Jabiru structure appears to have formed as a result of gas exsolution, as the migrating hydrocarbons entered the Jabiru trap, and its shallow flanks, which was then only located a few hundred metres below the surface. In the model, the rapidly decreasing pressure allowed the gas to form a separate phase, with the result that, in the Early Cretaceous, the Jabiru trap was composed of a relatively large gas cap with a thinner (“black oil”) oil leg. Progressive burial through the Tertiary, and the attendant increase in pressure, resulted in the gas going back into solution. The associated decrease in the bulk volume of the hydrocarbon accumulation produced

an apparent “residual” oil zone at the base of the column, purely through a change in phase, rather than through loss of hydrocarbons from fault seal failure, for example.

The processes outlined in this scenario would be essentially indistinguishable from those produced by fault seal failure when assessing traps using fluid history tools such as GOI. Such a process could be critically important in the case of shallow, low-relief traps (with small vertical closures), where only the exsolved gas could be trapped, with the “black oil” component lost below the spill of the trap. Small, sub-commercial gas fields would thus be located around the periphery of the source depocentres - though they would be the result of an early rather than late gas charge. Minor gas discovery in Pengana-1(NE of Jabiru field) and Delamere-1 (NE of Challis field) could be the example for this model. Small black oil accumulations could be developed inboard from such gas fields.

A new 3D seismic-based technique has been used to predict HRDZ occurrence in the study area. Application of this technique in the Vulcan Sub-basin has predicted previously reported and some new potential HRDZs. Although preliminary, the technique shows distinct promise in identifying zones of hydrocarbon migration/trap leakage in the subsurface which can be used to constrain fault seal analysis and basin modeling studies.

CHAPTER SEVEN

CONCLUSIONS AND FUTURE DIRECTIONS FOR RESEARCH

New insights regarding the petroleum systems in the Timor Sea have been obtained via the application of 2D and 3D basin modelling.

The 2D and 3D modelling results in the Swan Graben indicate that oil/gas expulsion from the Lower Vulcan Formation into the Plover Formation sandstone was active from the Early Cretaceous to the present day. The timing of onset of expulsion appears to be earlier than suggested by Kennard et al (1999).

The 2D and 3D modelling results in the Swan Graben, the Paqualin Graben and the Cartier Trough indicate that downward and horizontal oil/gas expulsion from the Lower Vulcan Formation into the Plover Formation carrier bed is an important mechanism for oil/gas accumulation in the Skua, Puffin, and Jabiru structures. The 3D modelling results from the central Cartier Trough indicate rapid maturation and oil expulsion of the Late Jurassic source system in very recent (<5Ma) times, mainly driven by rapid, collision-related, Pliocene subsidence and attendant sediment loading.

Petroleum migration from the Plover Formation in the Kimberley Graben to the Montara and Tahbilk accumulations was also simulated, a result consistent with the geochemical results of Edwards et al (2004). Oil and gas migration from the Swan Graben along the culmination of the Eclipse-Cassini-Challis trend was also active after the Cretaceous. This result shows that the direction of the large faults, which define the trends of the culminations, is one of the most important controls on petroleum migration.

2D modelling of the southern Swan Graben shows that a very thin or absent suite of basal Early Cretaceous sealing units is critical in modelling the accumulation of hydrocarbons in the Late Cretaceous sands at the Puffin Field. Such a combination of facies may be important in controlling the prospectivity of other, as-yet undrilled traps, which are similar plays to Puffin.

Different simulation results were obtained from the 2D and 3D modelling, in relation to oil migration into the Jabiru structure. The 3D modelling predicted oil migration not only from the southern Cartier Trough after the Miocene, but also early migration from the northern Swan Graben in the Early Cretaceous. This result indicates that 3D modelling is particularly useful if the hydrocarbon charges from multiple kitchen areas

are present.

Most gas accumulations in the region, such as the Oliver, Montara and Tahbilk accumulations, could not be simulated. Further studies, which take into account the locally high heat flow, implied from the heat flow calibrations (Oliver-1 in Fig. 5-1a), improved source rock kinetics, areal variation of organic richness (TOC) and the organic facies in the Plover Formation are necessary. The possible contribution of deeper source rocks such those in the Triassic or even Permian, should also be considered.

The modelling highlights the fact that the Early to Middle Jurassic Plover Formation appears to make a key contribution to the hydrocarbon inventory of the Vulcan Sub-basin. If this is correct, then the development of a better understanding of both its distribution, and more particularly, the distribution of the most organic-rich facies within the Plover Formation, is crucial if exploration is to be successful well away from the areas where charging from the traditional, Late Jurassic source system can be relied upon.

Based on the 3D modelling result for oil accumulation into the Jabiru structure, the interpreted residual zones in this and perhaps other fields could at least partially be explained by early charging, and large initial gas cap formation, followed by burial and hydrocarbon volume reduction due to gas solution into the liquid phase. Whilst fault seal failure is an important mechanism for the formation of residual zones, the new, phase-related mechanism of formation of the residual zones may be important and needs to be considered.

This initial modelling work has provided a useful first step in examining the first-order processes controlling petroleum accumulations within the Vulcan Sub-basin. Future work, involving a rigorous examination of the sensitivity of the models to compactional and thermal parameters, and a greater emphasis on the processes of fluid flow in and around fault systems, will be critical to their further refinement and usefulness.

A new method to extract HRDZs from 3D seismic data has been developed. This method utilizes the Top Paleocene surface, the isochron between the Base Miocene and Top Paleocene and the time dip data of Top Paleocene. As a result of the preliminary application to the Vulcan Sub-basin, unreported HRDZs have been identified in the northern Vulcan Sub-basin. Further investigation to confirm the validity of this method will be necessary, including definition of “thin anomalies” on isochron data, the color scaling of the Top Paleocene two way time map, the discrimination

from anomalies by horst blocks and salt domes and comparison of extracted distribution of the HRDZs with fault seal integrity data and basin modelling results.

Future key research, which draws together many elements which have just been touched upon in this thesis, such as HRDZ/leakage mapping and seismic attribute work, should allow a more reliable estimation of gas-oil-ratio (GOR) pre-drill.

A workflow has been developed (Figure 7-1) which includes inputs from basin modelling, leakage and seepage mapping, and fault seal and fault reactivation studies. Predictive models derived from these workflows should be calibrated or optimized iteratively using actual well data, which is the most important component in the basin modeling study. Implementation of this work should ultimately allow a more reliable estimation of GOR prior to drilling.

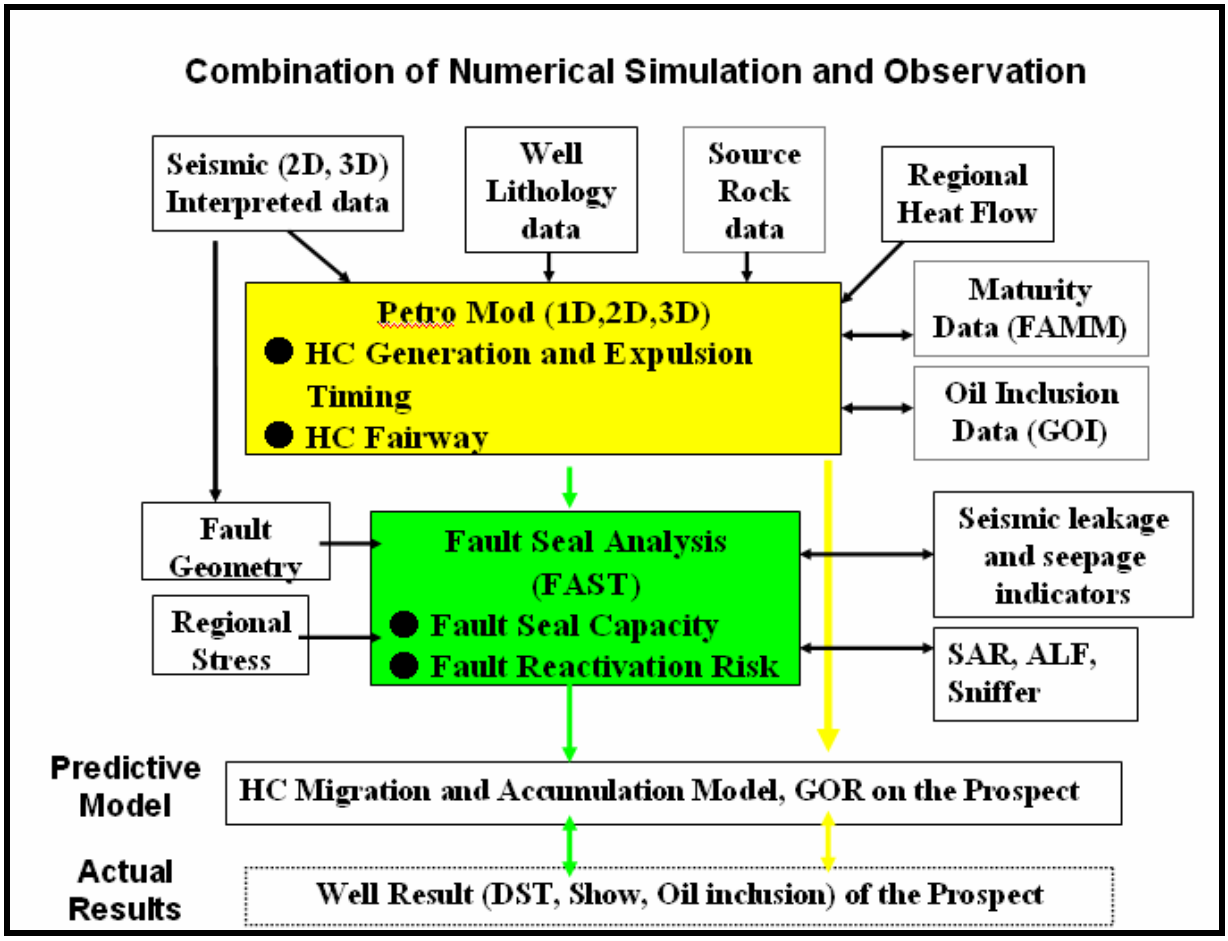

Figure 7-1 A schematic diagram showing the proposed work-flow for future work aimed at predicting GOR prior to drilling.

APPENDIX 4-1

HORIZON AND FAULT IMPORT FOR BASIN MODELLING

1. 2D line data

1-1. Data format

In PetroMod^{TM}, the following ASCII format files are used for both horizon and fault line input.

Nodal line 1
Number of data
X: horizontal distance from left end (m) Y: Depth from the surface (m)
……
Nodal line 2
Number of data
X: horizontal distance from left end (m) Y: Depth from the surface (m)
……

The following is an example of horizon input ASCII file used in the 2D tutorial (PetroMod^{TM} users manual: Tutorial /Tutorial_2D /Data).

```
3
 0.00000e+00    1.92802e+02
 2.99592e+04    1.79949e+02
 5.00000e+04    1.79949e+02
5
 0.00000e+00    4.48586e+03
 9.51087e+03    4.47301e+03
 2.01087e+04    4.55013e+03
 3.55978e+04    4.55013e+03
 4.43745e+04    4.52571e+03
3
 4.43745e+04    4.52571e+03
 4.48370e+04    4.52442e+03
 5.00000e+04    4.49871e+03
```

For this study, the following 2D depth converted line file in GeoSec format was obtained from Chen (2002).

VTT-05			VTT-14		
File name	Age (Level)	Size (KB)	File name	Level	Size (KB)
line05present.ihf	**Present day**	**38**	**line14present.ihf**	**Present day**	**72**
line05miocene.ihf	Top Miocene	38	line14miocene.ihf	Top Miocene	68
line05eocene.ihf	Top Eocene	37	line14eocene.ihf	Top Eocene	63
line05palaeocene.ihf	Top Paleocene	35	line14palaeocene.ihf	Top Paleocene	46
line05cretaceous.ihf	Top Cretaceous	34	line14cretaceous.ihf	Top Cretaceous	40
line05topvalancinian.ihf	Top Valanginian	28	line14topvalancinian.ihf	Top Valanginian	33
line05toptithonian.ihf	Top Tithonian	23	line14toptithonian.ihf	Top Tithonian	30
line05topkimmeridgian.ihf	Top Kimmerdgian	19	line14topkimmeridgian.ihf	Top Kimmerdgian	33
line05topcallovian.ihf	Top Callovian	21	line14topcallovian.ihf	Top Callovian	24
line05toppermian.ihf	Top Permian	8	line14toppermian.ihf	Top Permian	11

From the above 20 files, only the two present day files were used in this study.
Further study using the other 18 horizon files (restored model) through the Paleo Geometry function in PetroMod^{TM} 2D would allow the development of a much more detailed migration history possible.

1-2. Loading procedures

The data loading procedures applied in this study are listed below.

A. Firstly, the GeoSec format files obtained from Chen (2002) were converted to PetroMod^{TM} ASCII format (shown in 1-1-1) using Excel, and were imported in PetroMod^{TM}. This work was not completed due to the problem of data recognition in PetroMod^{TM} (not all data could be read).
B. Secondly, the GeoSec format files were successfully imported into PetroMod^{TM} (GeoSec format files can be seen by changing "*.DAT" to "*").
C. These data were saved in the following folder in the PC.
   C: /PetroMod71/data/Vulcan_study2D
D. In these files, Starting points for the southeast (x, y) and sea level (z) are as below:

Line Name	x (East-West)	y (North-South)	z (depth)
VTT-05	701731	8576734	31100
VTT-14	745172	8635336	0

1-3. Horizon/fault data assignment

In Horizon/fault data assignment in SeisStrat2D, the following things are very important, although they were not mentioned in 2D Tutorial.

A. Each horizon or fault should be stretched to both sides completely using “Extrapolate Both Ends” in pop-up menu by clicking right mouse button on the line (this is important for the recognition of the horizon interval).
B. Hanging up problem occurred when I tried to close “Assign Interval Icon” after assigning the interval. This problem was solved by creating new folder (Vulcan_study2D) and creating a new input file again (Vulcan_study is an old folder which has this problem).

2. 3D surface data

2-1. Data format

In PetroMod^{TM} -3D, the following formats data can be imported.

a. IES... (Maps/Horizons in IES format)
b. ZMAP (Maps and fault lines in ZMAP format)
c. IRAP (Maps and fault lines in both ASCII and binary IRAP format)
d. CPS3 (Seismic horizons and fault lines from Geoframe projects)
e. Seisworks3D (Seismic horizons and fault lines from Landmark projects - the function is only sensitive when connected to a Landmark data source)
f. Input 3D Geometry... (Maps/horizons from an IES Input 3D model)

It is very important to know that fault data should be imported as “Fault line data”.
In PetroMod^{TM}-3D, fault data should be imported as 2D line data (intersection between each horizon surface and fault surface: Allan line), rather than as surface data.

For this study, the following 3D depth converted surface files in 3DMove format (VBL) were obtained from Chen (2002).

File name	Age (Level)	Size (MB)	Comments
0-Present_3D.vbl	**Present day**	**11.8**	Present depth surface
1-Miocene.vbl	Top Miocene	6.63	Restored model by Chen (2002)
2-Eocene.vbl	Top Eocene	8.34	
3-Palaeocene.vbl	Top Paleocene	7.81	
4-Cretaceous.vbl	Top Cretaceous	7.41	
5-Valanginian.vbl	Top Valanginian	3.3	
5-Valanginian-flat.vbl	Top Valanginian	3.29	
6-Tithonian.vbl	Top Tithonian	2.58	
6-Tithonian-flat.vbl	Top Tithonian	2.54	
7-Kimmeridgian.vbl	Top Kimmerdgian	2.45	
7-Kimmeridgian-flat.vbl	Top Kimmerdgian	2.31	
8-Callovian.vbl	Top Callovian	1.38	
8-Callovian-flat.vbl	Top Callovian	1.1	

From above 13 files, only the present day file was used in this study.

Again, further study using another 8 files (restored model) through “Paleo geometry function” in PetroMod™ 3D would make more detailed migration history analysis possible. It is recommended to use “–flat” file by Chen.

2-2. Loading procedures

Data loading procedures applied in this study are as below.

A. First, 3DMove format horizon surface files obtained from Chen (2002) were loaded into 3DMove and exported as **Z Map format** (We first tried to read ASCII format file, but could not be read in PetroMod™). Grid interval was set as X*Y = 184*200.
B. Fault line file (Allan line) was also created on 3D Move using ”Allan Mapper” menu, and exported as ASCII file.
C. These files were saved in following folder in PC for PetroMod™.
   C: /PetroMod71/data/3D Modeling
D. Secondly, these Z Map (horizon surface) / ASCII (fault line) format files

were imported in PetroMod^{TM}.

E. ASCII format fault line files were narrowly imported in PetroMod^{TM}-3Dbut they were displayed as discontinuous lines (Fig. 1). The data appear to have been saved as mesh data, not continuous line data, in 3Dmove. Merging each dot in PetroMod^{TM} looked like time-consuming work, so new fault lines were created in PetroMod^{TM} by tracing these imported fault data.

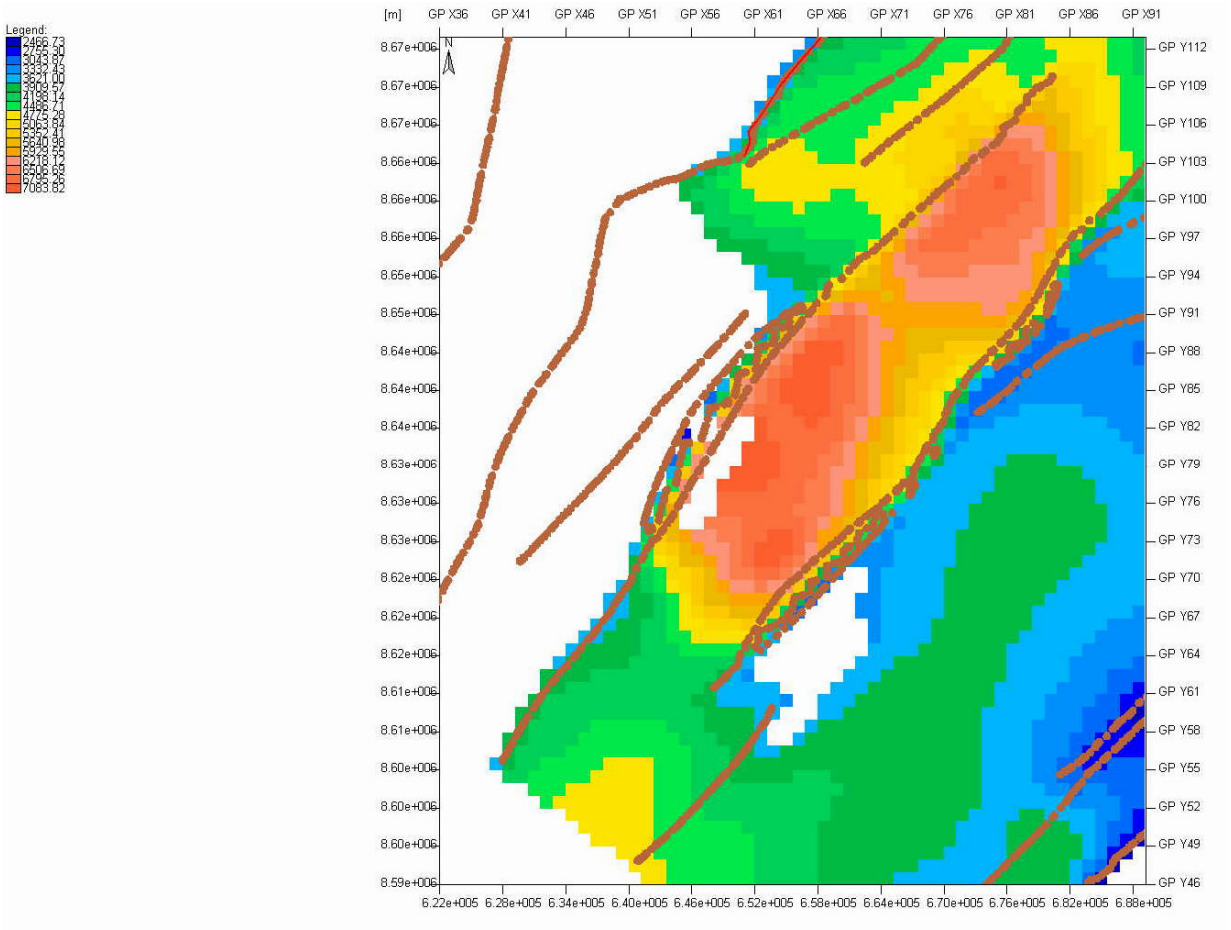

Figure 1. Example of imported fault line data (ASCII format).

F. These data were saved in the following folder in the PC.

C: /PetroMod80/data/Vulcan_study3D

G. In these files, the coordinate limits are as follows:

	x (East-West)	y (North-South)	z (EDT)
Min	580,000	8540,000	-18,000
Max	800,000	8780,000	2,000
range	220,000	240,000	20,000

Appendix 4-1-2.
WELL CORRELATION RESULTS TO DETERMINE FACIES INPUT.

Source data: AGSO, 1999—Vulcan Sub-basin Composite Well Log CD-ROM, Commonwealth of Australia, 1999.

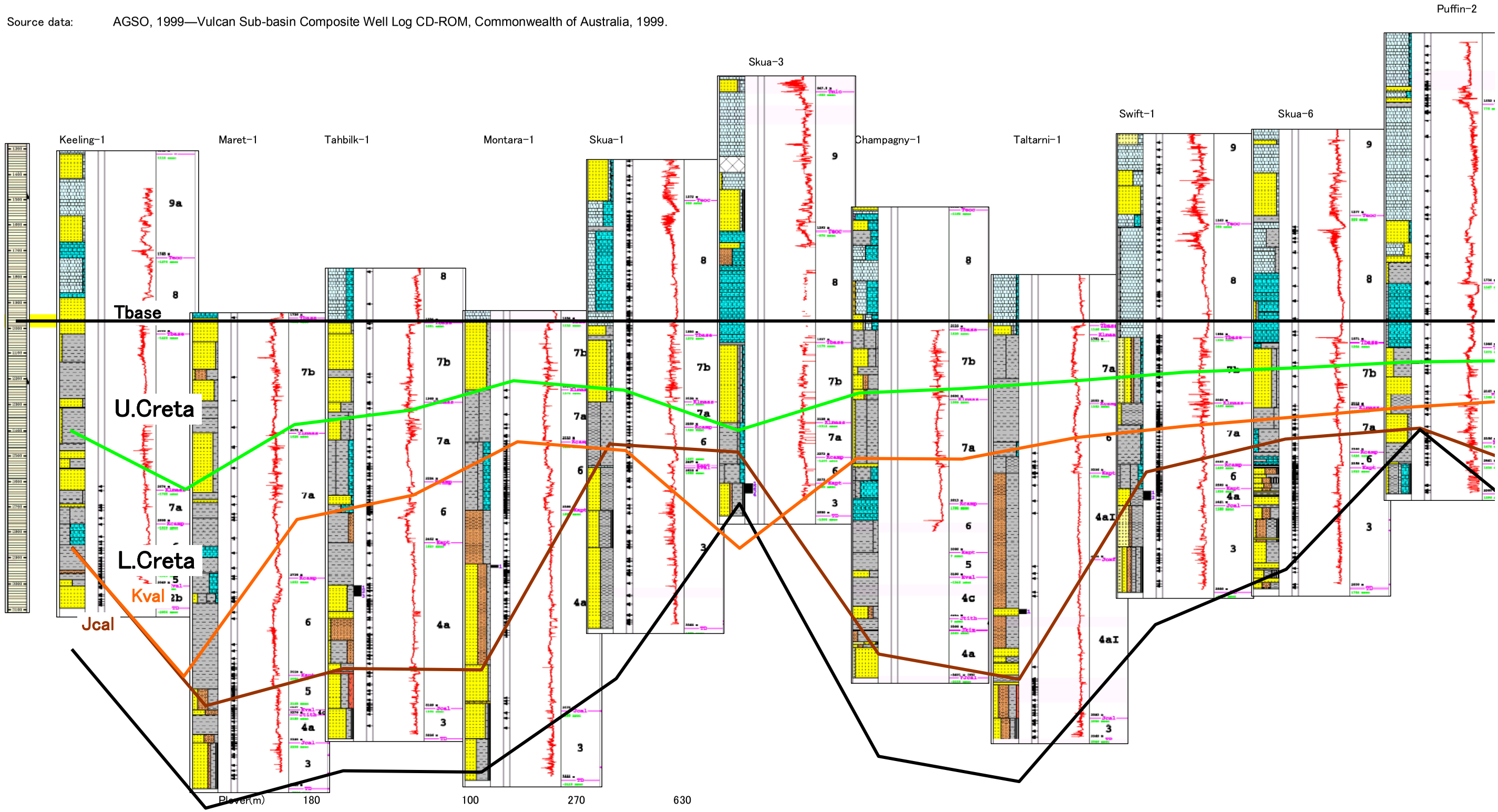

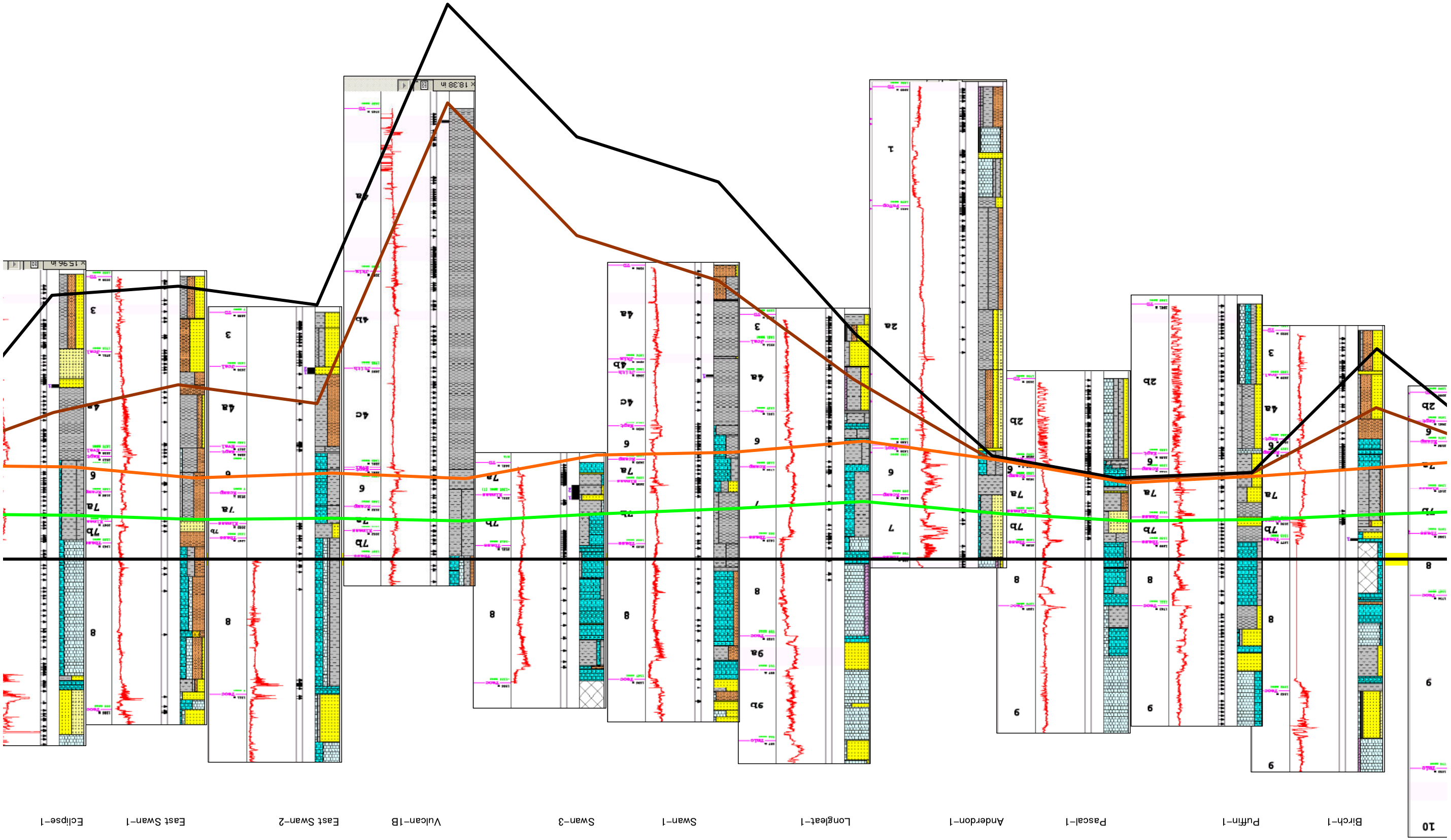
Eclipse–1
East Swan–1
East Swan–2
Vulcan–1B
Swan–3
Swan–1
Longleat–1
Anderdon–1
Pascal–1
Puffin–1
Birch–1

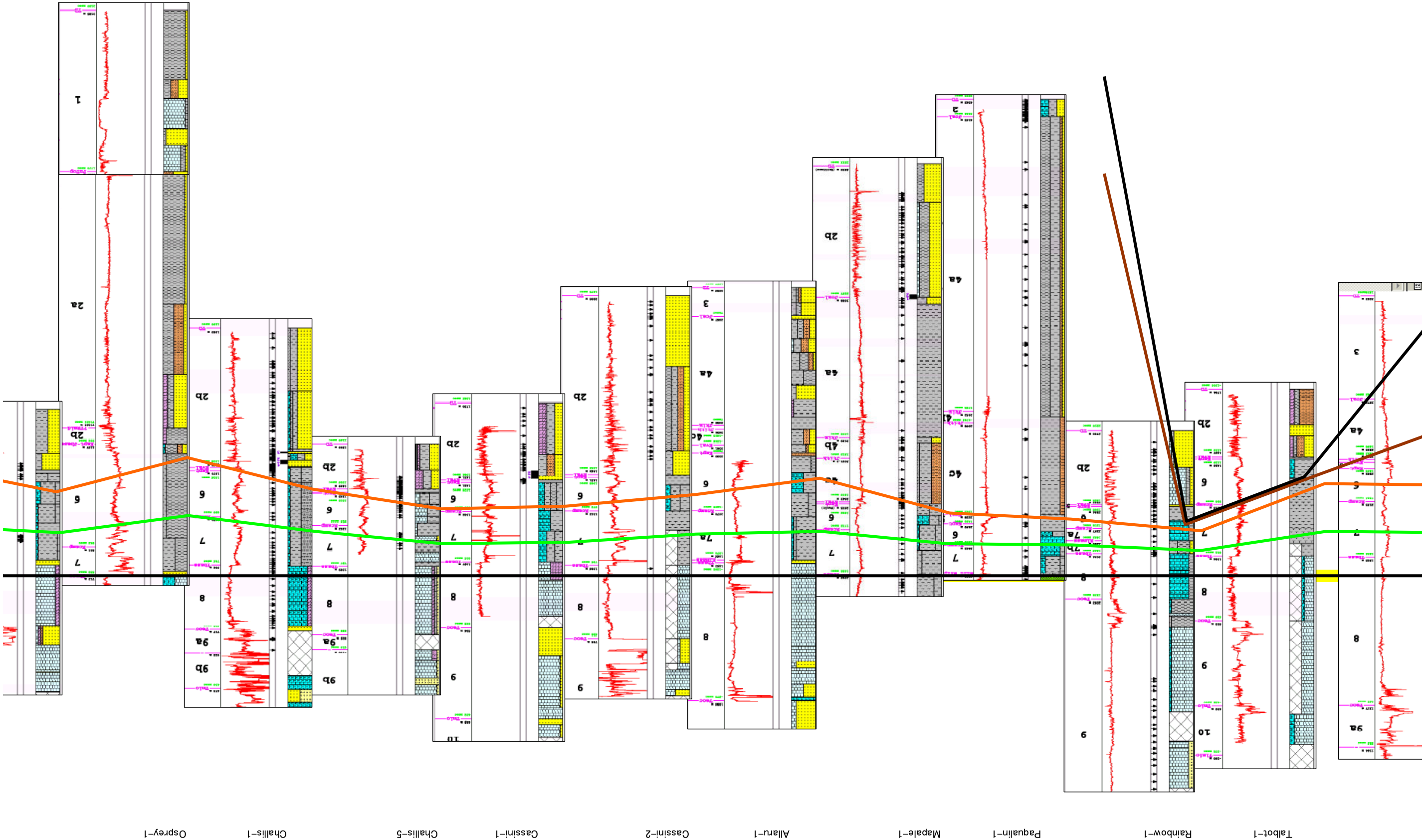
Talbot–1
Rainbow–1
Paqualin–1
Mapale–1
Allaru–1
Cassini–2
Cassini–1
Challis–5
Challis–1
Osprey–1

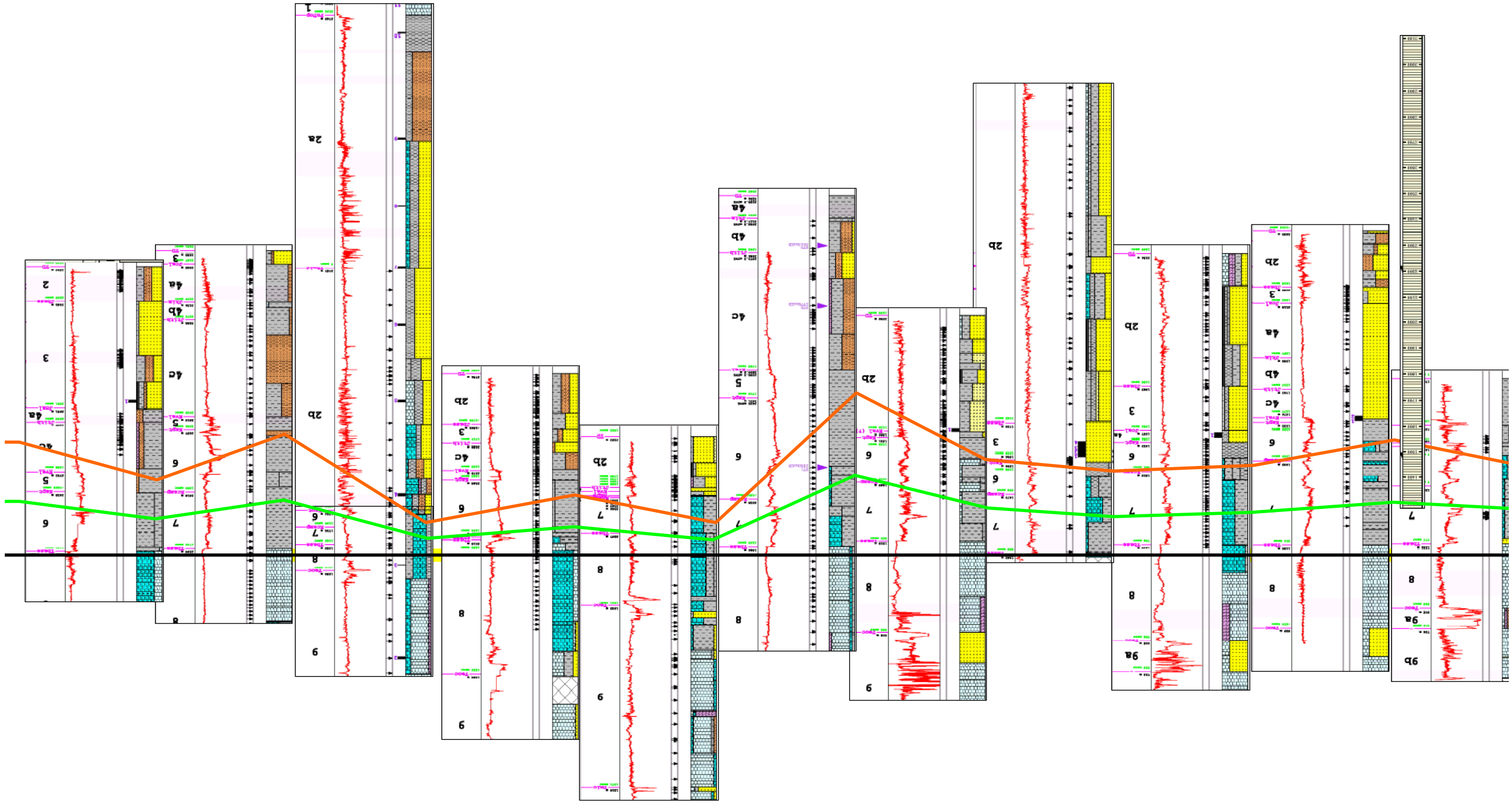
Chalis–11
Rainer–1
Jabiru–2
Jabiru–1a
Penegana–1
Octavius–1
Warb–1
Douglas–1
Sahul Shoals–1
Augustus–1
Oliver–1

Turnstone-1 Tancred-1 Halcyon-1

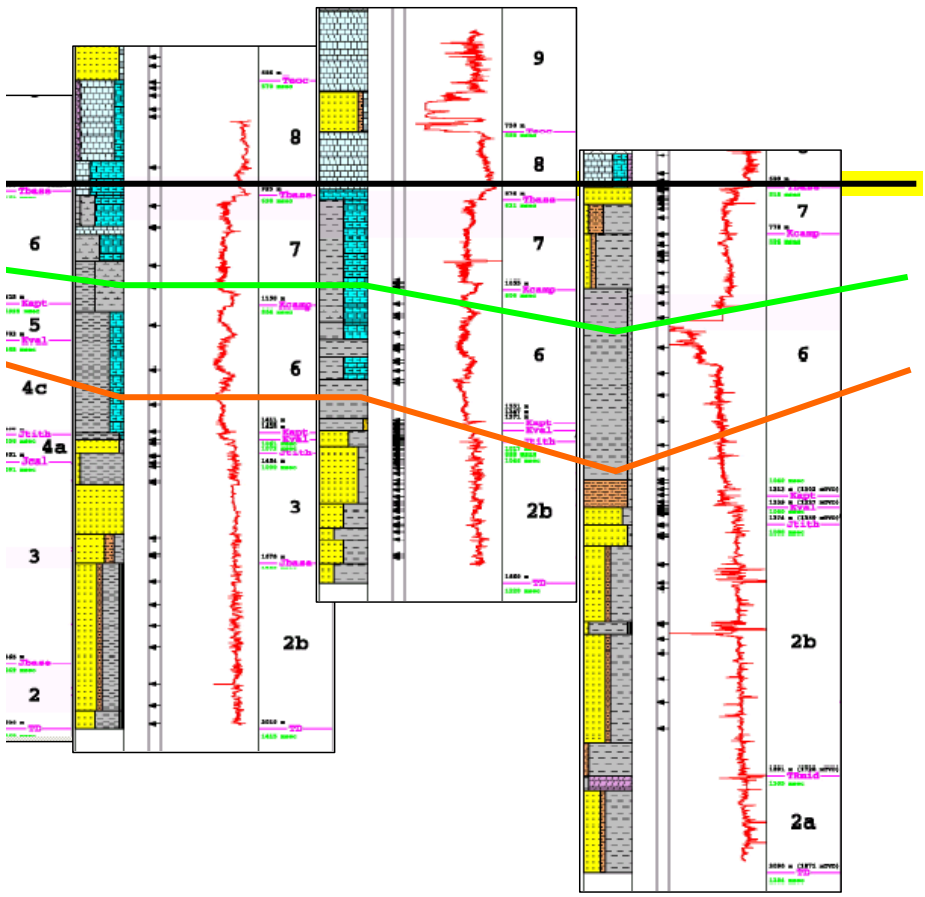

APPENDIX 4-1-3

KEROGEN KINETIC PARAMETERS USED FOR MODELLING

Kerogen Primary Reaction (Kerogen to Oil)

L. Vulcan_L (sq 4a) – East Swan-2 (sq 4a) Bulk kinetic data

Kinetic Analysis

Basin Name	Vulcan Sub-basin
Well Name	East Swan-2
Data Source	AGSO #9803 Kennard et al.(1999)

IH =	269	mg/g
A =	1.22E+14	1/sec
	3.86E+27	1/Ma

Ea (kca/mol)	Reaction Potential (%)	GOR Gas/Oil Ratio (frac.)	Gas Potential (%)	Oil Potential (%)
40				
41				
42				
43				
44				
45				
46				
47				
48				
49				
50				
51				
52				
53				
54	65.28	0.69	26.65	38.63
55	13.83	0.33	3.43	10.40
56	19.77	0.33	4.91	14.86
57				
58				
59				
60				
61	0.19	6	0.16	0.03
62				
63				
64				
65				
66				
67				
Sum	99.07		35.15	63.92

HI oil	172
HI gas	95

L. Vulcan_U (sq 4b) – Vulcan-1B (sq 4b) Bulk kinetic data

Kinetic Analysis

Basin Name	Vulcan Sub-basin
Well Name	Vulcan-1B
Data Source	AGSO #3851 Kennard et al.(1999)

HI =	503	mg/g
A =	3.02E+15	1/sec
	9.54E+28	1/Ma

Ea (kca/mol)	Reaction Potential (%)	GOR Gas/Oil Ratio (frac.)	Gas Potential (%)	Oil Potential (%)
40				
41				
42				
43				
44				
45				
46				
47				
48				
49				
50				
51				
52				
53				
54				
55				
56				
57				
58				
59	99.85	0.56	35.84	64.01
60				
61	0.15	0.56	0.05	0.10
62				
63				
64				
65				
66				
67				
Sum	100		35.90	64.10

HI oil	322
HI gas	181

U. Vulcan (sq 4c) – Paqualine-1 (sq c) Bulk kinetic data

Kinetic Analysis

Basin Name	Vulcan Sub-basin
Well Name	Paqualin-1
Data Source	AGSO #9813 Kennard et al.(1999)

HI =	337	mg/g
A =	4.81E+13	1/sec
	1.52E+27	1/Ma

Ea (kca/mol)	Reaction Potential (%)	GOR Gas/Oil Ratio (frac.)	Gas Potential (%)	Oil Potential (%)
40				
41				
42				
43				
44				
45				
46				
47				
48				
49				
50				
51				
52	39.58	0.43	11.90	27.68
53	44.57	0.56	16.00	28.57
54	13	0.56	4.67	8.33
55				
56				
57				
58				
59				
60				
61				
62				
63				
64				
65				
66				
67				
Sum	97.15		32.57	64.58

HI oil	218
HI gas	110

Plover (sq 3) – Skua-1 (sq 3) Bulk kinetic data

Kinetic Analysis

Basin Name	Vulcan Sub-basin
Well Name	Skua-1
Data Source	AGSO #9824 Kennard et al.(1999)

HI =	336	mg/g
A =	1.20E+14	1/sec
	3.78E+27	1/Ma

Ea (kca/mol)	Reaction Potential (%)	GOR Gas/Oil Ratio (frac.)	Gas Potential (%)	Oil Potential (%)
40				
41				
42				
43				
44				
45				
46				
47				
48				
49				
50				
51				
52				
53	46.58	0.42	13.78	32.80
54	5.27	0.42	1.56	3.71
55	26.94	0.14	3.31	23.63
56	0.33	0.14	0.04	0.29
57	12.86	0.14	1.58	11.28
58	1.69	0.42	0.50	1.19
59	2.56	1.27	1.43	1.13
60				
61	3.04	10	2.76	0.28
62				
63				
64				
65				
66				
67				
Sum	99.27		24.96	74.31

HI oil	250
HI gas	84

Kerogen Secondary Cracking (Oil to Gas)

L. Vulcan_L (sq 4a),

L. Vulcan_U(sq 4b),

Plover (sq 3)

–Kinetic Parameters for the Cracking of Light Oil from Kennard et al (1999)

Kinetic Analysis

Basin Name	Vulcan Sub-basin
Well Name	
Data Source	Kennard et al.(1999)

HI =		mg/g
A =	1.11E+16	1/sec
	3.50E+29	1/Ma

Ea (kca/mol)	Reaction Potential (%)	GOR (Gas/Oil Ratio)	Gas Potential (%)	Oil Potential (%)
58	0.79			
59				
60				
61				
62				
63	0.61			
64				
65				
66	34.69			
67	28.77			
68	15.04			
69	11.2			
70	6.04			
71				
72	0.97			
73	1.89			
74				
75				
Sum	100		0.00	0.00

HI oil	0
HI gas	0

REFERENCES

AGSO, 1996—Vulcan Tertiary Tie (VTT) Basin Study, Vulcan Sub-basin, Timor Sea, Northwestern Australia.

AGSO, 1999—Vulcan Sub-basin Composite Well Log CD-ROM, Commonwealth of Australia, 1999.

AZIZ, K. and SETTARI, A., 1979, Petroleum Reservoir Simulation, Elsevier Applied Science Publishers, London, 476 p.

BAILEY, W., SHANNON, P. M., WALSH, J.J. and UNNITHAN, V., 2003—The spatial distributions of faults and deep sea carbonate mounds in the Porcupine Basin, offshore Ireland. Marine and Petroleum Geology (2003), in press

BAXTER, K., COOPER, G.T., O'BRIEN, G.W., HILL, K.C. AND STURROCK, S., 1997—Flexural Isostatic modelling as a constraint on basin evolution, the development of sediment systems and palaeo-heat flow: Application to the Vulcan Sub-basin, Timor Sea. APPEA Journal 37 (1), 136-53.

BAXTER, K., HILL, K.C. AND COOPER, G.T., 1999—Quantitative modelling of the Jurassic -Holocene subsidence history of the Vulcan Sub-basin, North West Shelf: constraints on lithosphere evolution during continental breakup. Australian Journal of Earth Science, 45, 143-54.

BEARDSMORE, G.R. AND O'SULLIVAN, P.B., 1995—Uplift and erosion on the Ashmore Platform, North West Shelf: conflicting evidence from maturation indicators. APEA Journal 35 (1), 333-43.

BETHKE, C.M., 1985—A Numerical Model of Compaction-Driven Groundwater Flow and Heat Transfer and its Application to the Paleohydrology of Intracratonic Sedimentary Basins, Journal of Geophysical Research, vol. 90, no. B8, pp. 6817-6828.

BLEVIN, J.E., BOREHAM, J.C., SUMMONS, R.E., STRUCKMEYER, H.I.M. AND LOUTIT, T.S., 1998—An effective Lower Cretaceous petroleum system on the North West Shelf: evidence from the Browse Basin. In: Purcell, P.G. and Purcell, R.R. (Eds), The Sedimentary Basins of Western Australia 2. Proceedings of the PESA Symposium, Perth, WA, 1998, 397-420.

CALHOUN, J.C. 1976—Fundamentals of Reservoir Engineering. The noted series from The Oil and Gas Journal, fifth printing, University of Oklahoma Press.p51.

CHEN, G., HILL, K.C., HOFFMAN, N. AND O'BRIEN, G.W., 2001—3D Palaeo-Migration Pathway Analysis: An Example from Timor Sea. In: HILL, K.C. & BERNECKER, T., (Eds), *A Refocussed Energy Perspective for the Future:* Proceedings of Eastern Australasian Basins Symposium, Petroleum Exploration Society of Australia, Special Publication, 629-36.

CHEN, G., HILL, K.C. AND HOFFMAN, N., 2002—3D structural analysis of hydrocarbon migration in the Vulcan Sub-basin, Timor Sea. In: Keep, M. and Moss, S.J. (Eds), The Sedimentary Basins of Western Australia 3. Proceedings of the PESA Symposium, Perth, WA, 2002, 377-88.

CLARKE, R.H. AND CLEVERLY, R. W., 1990—Leakage and post accumulation migration. In Caprocks and Seals, Gel. Soc. Lond. Conference 1990.

DE BOER, R.A., 2004—The Puffin Sandstone, Timor Sea, Australia: Anatomy of a submarine fan. In Ellis, G.K., Baillie, P.W. & Munson, T.J. (Eds), Timor Sea Petroleum Geoscience: Proceedings of the Timor Sea Symposium, Darwin. Northern Territory Geological Survey, Special Publication 1, 373-390.

EDWARDS, D.S., PRESTON, J.C., KENNARD, J.M., BOREHAM, C.J., VAN, AARSSEN, B.K.J., SUMMONS, R.E. AND ZUMBERGE, J. E., 2004—Geochemical Characteristics of Vulcan Sub-basin Hydrocarbons, western Bonaparte Basin. In Ellis, G.K., Baillie, P.W. & Munson, T.J. (Eds), Timor Sea Petroleum Geoscience: Proceedings of the Timor Sea Symposium, Darwin. Northern Territory Geological Survey, Special Publication 1, 169-201.

EDWARDS, D.S., KENNARD, J.M., PRESTON, J.C., SUMMONS, R.E., BOREHAM, C.J. AND ZUMBERGE, J.E., 2000—Bonaparte Basin. Geochemical characteristics of hydrocarbon families and petroleum systems. Geoscience Australia Research Newsletter. December 2000, 33, 14-18.

GEORGE, S.C., GREENWOOD, P.F., LOGAN, G.A., QUEZADA, R.A., PANG, L.S.K., LISK, M., KRIEGER, F.W. AND EADINGTON, P.J., 1997—Comparison of palaeo oil charges with currently reservoired hydrocarbons using molecular and isotopic analyses of oil-bearing fluid inclusions: Jabiru Oil Field, Timor Sea. The APPEA

Journal, 37 (1), 490-503.

HANTSCHEL, T., ARMIN INGO KAUERAUFAND BJOÈRN WYGRALA, 2000—Finite element analysis and ray tracing modelling of petroleum migration, Marine and Petroleum Geology 17, 815-20.

HELANDER, D. P. 1983—Fundamentals of Formation Evaluation, Tulsa, OK: Oil and Gas Consultants International, Inc.

HORNER, D.R., 1951—Pressure Build-up in wells. In Proceedings of the Third World Petroleum Congress, The Hague, Section 2, Leiden, E.J. Brill, 503-21.

HOVLAND, M. AND A. G. Judd. 1988—Seabed pockmarks and seepages: Impact on geology, biology and the marine environment. London: Graham & Trotman. 293p.

HOVLAND, M., CROKER, P.F. and MARTIN, M., 1994—Fault-associated seabed mounds (carbonate knolls?) off western Ireland and north-west Australia. Marine and Petroleum Geology 1994, Vol.11 No.2, 232-46.

HUBBERT, M.K. 1953—Entrapment of petroleum under hydrodynamic conditions. AAPG Bulletin, 37, 1954-2026.

HUNT, J. M. 1996—Petroleum geochemistry and geology. 2nd ed. W. H. Freeman and Company, New York, 448-468.

HUYAKORN, P.S. and PINDER, G.F, 1983—Computational Methods in Subsurface Flow, Academic Press, Inc., San Diego, 473 p.

IES, 2002—Handout of PetroMod^{TM} 2D Training Course, Nov. 2002, 104.

KENNARD, J.M., DEIGHTON, I., EDWARDS, D.S., COLWELL, J.B., O'BRIEN, G.W. AND BOREHAM, C.J., 1999—Thermal History Modelling and Transient Heat Pulses: New Insights into Hydrocarbon Expulsion and `Hot Flushes` in the Vulcan sub-basin, Timor sea. APPEA Journal 39 (1), 177-207.

KENNARD, J.M. AND DEIGHTON, I., 2000—Vulcan Sub-basin geohistory modelling CD-ROM. AGSO Record 1999/40.

KIVIOR, T., KALDI, J.G. AND LANG, S.C., 2002—Seal Potential in Cretaceous and

Late Jurassic Rocks of the Vulcan Sub-basin, North West Shelf Australia. APPEA Journal 42 (1), 203-224.

LISK, M. AND EADINGTON, P., 1994—Oil Migration in the Cartier Trough, Vulcan Sub-basin. The sedimentary basins of Western Australia. Proceedings, Petroleum Exploration Society of Australia (PESA) Symposium, Perth, 301-12.

LISK, M., BRINCAT, M.P., EADINGTON, P.J. AND O'BRIEN G.W., 1998—Hydrocarbon Charge in the Vulcan Sub-basin. In: Purcell, P.G. and Purcell, R.R. (Eds), The Sedimentary Basins of Western Australia 2. Proceedings of the PESA Symposium, Perth, WA, 1998, 287-303.

LISK, M., BRINCAT, M.P., O'BRIEN G.W., EADINGTON, P.J. AND FAIZ, M., 1999—Palaeo-Hydrology on the Vulcan Sub-basin: Implications for Trap Integrity. APPEA Journal 39 (1), 208-26.

LOWRY, D., 1998—Inferring Kerogen Kinetics for Exploration in the Timor Sea Region. In: Purcell, P.G. and Purcell, R.R. (Eds), The Sedimentary Basins of Western Australia 2. Proceedings of the PESA Symposium, Perth, WA, 1998, 305-12.

MARSDEN, D., 1989—I; Layer cake depth conversion. Geophysics: The Leading Edge of Exploration. 8; 1, 10-14.

MCKENZIE, D.P., 1978—Some remarks on the development of sedimentary basins. Earth and Planetary Science Letters, 40, 25-32.

MILDREN, S. D. and HILLIS, R. R., 2000—In situ stresses in the southern Bonaparte Basin, Australia: Implications for first- and second-order controls on stress orientation. Geophysical Research Letters, Vol. 27, No. 20, 3413-3416.

O'BRIEN, G.W. AND WOODS, E.P., 1995—Hydrocarbon-related diagenetic zones (HRDZ's) in the Vulcan Sub-basin, Timor Sea: recognition and exploration implications. APEA Journal 35 (1), 220-52.

O'BRIEN, G.W., HIGGINS, R., SYMONDS, P.,QUAIFE, P., COLWELL, J. AND BLEVIN, J., 1996a—Basement control on the development of extensional systems in Australia's Timor Sea: an example of hybrid hard linked/soft linked faulting? APPEA Journal 36 (1), 161-201.

O'BRIEN, G.W., LISK, M., Duddy, I., EADINGTON, P.J., CADMAN, S. AND FELLOWS, M., 1996b—Late tertiary fluid migration in the Timor Sea: A key control on thermal and diagenetic histories? APPEA Journal 36 (1), 399-427.

O'BRIEN, G.W., LISK, M., DUDDY, I., HAMILTON, J., WOODS, P. AND COWLEY, R., 1999a—Plate convergence, foreland development and fault reactivation: primary controls on brine migration, thermal histories and trap breach in the Timor Sea, Australia. Marine and Petroleum Geology. 16, 533-60.

O'BRIEN, G.W., MORSE, M., WILSON, D., QUAIFE, P., COLWELL, J., HIGGINS, R. AND FOSTER, C.B., 1999b—Margin-scale, basement-involved compartmentalisation of Australia's North West Shelf: a primary control on basin-scale rift, depositional and reactivation histories.: APPEA Journal 39 (1), 40-63.

O'BRIEN, G.W., COWLEY, R., QUAIFE, P. AND MORSE, M., 2002—Characterising hydrocarbon migration and fault-seal integrity in Australia's Timor Sea via multiple, integrated remote sensing technologies. In: Applications of geochemistry, magnetics, and remote sensing, D. Schumacher and L. A. LeSchack, eds., AAPG Studies in Geology No. 48 and SEG Geophysical References Series No. 11, 393–413.

O'BRIEN, G.W., COWLEY, R., LAWRENCE, G., WILLIAMS, A.K., EDWARDS, D. AND BURNS, S., 2004—Margin to prospect scale controls on fluid flow within the Mesozoic and Tertiary sequences, offshore Bonaparte and northern Browse Basins, north-western Australia. In Ellis, G.K., Baillie, P.W. & Munson, T.J. (Eds), Timor Sea Petroleum Geoscience: Proceedings of the Timor Sea Symposium, Darwin. Northern Territory Geological Survey, Special Publication 1, 99-124.

OKUI, A., SIEBERT, R.M. AND MTSUBAYASHI, H., 1998—Simulation of oil expulsion by 1-D and 2-D basin modelling – saturation threshold and relative permeability of source rocks. Geological Society, London, Special Publications, 141, 45-72.

PATTILLO, J.,AND NICHOLLS, P.J., 1990—A tectonostratigraphic framework for the Vulcan Graben, Timor Sea region. APEA Journal, 30 (1), 27-51.

PEPPER, A.S. AND CORVI, P.J., 1995—Simple kinetic models of petroleum formation.Part III: Modelling an open system, Marine and Petroleum Geology, Vol. 12, No. 4, 417-52.

PETER, K.E. AND NELSON, D.A., 1992 —REESA – an expert system for

geochemical logging of wells. AAPG Annual Convention Abstract, Calgary, p.103.

RULLKOTTER, J., LEYTHAEUSER, D., HORSFIELD, B., LITTKE, R., MANN,U., MULLER, P.J., RADKE, M., SCHAEFER, R.G., SCHENK, H.J., SCHWOCHAU, K., WITTE, E.G. AND WELTE, D.H., 1988—Organic matter maturation under the influence of a deep intrusive heat source : A natural experiment for quantitation of hydrocarbon generation and expulsion from a petroleum source rock. Org. Geochem. Vol.13, Nos. 4-6, 847-56.

SHUSTER, M.W., EATON, S., WAKEFIELD, L.L. AND KLOOSTERMAN, H.J., 1998—Neogene tectonics, greater Timor Sea, offshore Australia: implications for trap risk. APPEA Journal 38 (1), 351-379.

SWEENEY, J.J. AND BURNHAM, A.K., 1990—Evaluation of a simple model of vitrinite reflectance based on chemical kinetics. - American Association of Petroleum Geologists Bulletin, 74: 1559-70.

TISSOT, B.P. and WELTE, B.P. 1978—Petroleum Formation and Occurrence. New York: Springer-Verlag, pp. 500-521.

WAPLES, D.W., 1997—A manual for source rock evaluation using petroleum system concepts. Prepared by Douglas Waples for Japan National Oil Corporation, September, 1997, JNOC-TRC unpublished book.

WOODS, E.P., 1992—Vulcan Sub-basin fault styles – implications for hydrocarbon migration and entrapment. APEA Journal 32 (1), 138-58.